UNIVERSITEIT·STELLENBOSCH·UNIVERSITY
jou kennisvennoot · your knowledge partner

Computational Investigation of a Crossed Slot Cavity-Backed Array Antenna

by

Dewald Voigt

Thesis presented in partial fulfilment of the requirements for the degree of

Master of Science in Electronic Engineering

in the Department of Electrical and Electronic Engineering at the University of Stellenbosch.

Department of Electronic Engineering
University of Stellenbosch
Private Bag X1, 7602 Matieland, South Africa

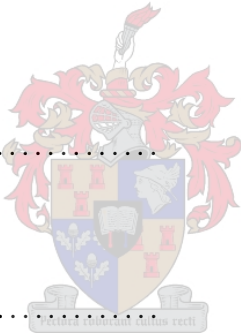Supervisor: Prof. K. Palmer

April 2006

Declaration

I, the undersigned, hereby declare that the work contained in this thesis is my own original work and that I have not previously in its entirety or in part submitted it at any university for a degree.

Signature: . . . .

D. Voigt

Date: . . . .

Abstract

This thesis investigates a computational model of an electronically steered antenna array. It focuses on a simple element comprising an S-shaped, crossed, cylindrical cavity-backed slot antenna. An unusual aspect of the element is the addition of a top hat, which contributes to the low scanning ability of the array. The objective was to confirm this contribution of the top hat.

During the investigation, the computation code Feko was validated for slot analysis through consideration of the basic properties of a dipole and slot and how they related to each other.

Various alternative models were evaluated, before a final accurate model was modelled in Feko, to find possible equivalent models. The final model, which implemented the use of Feko as release 5, was the only one that achieved successful results.

The results showed that the top hat does play an important role in the steering of the beam. The mechanism through which this occurs was identified. The results that where obtained indicated that there may be more effective elements than the cylindrical element and the identification of this is proposed as a field for further study.

Opsomming

Hierdie tesis ondersoek 'n numeriese model van 'n elektronies gestuurde antenna matriks. Dit fokus op 'n enkele element wat bestaan uit 'n dubbele S-vormige, oorkruisde, holte-gesteunde gleuf antenna. 'n Ongewone aspek van die element is die byvoeging van 'n hoed, wat grootliks bydra tot die lae stuurrigting van die matriks. Die doel van die tesis was om die bydrae wat die hoed lewer te bepaal.

Die numeriese kode Feko is gedurende die ondersoek bevestig deur evaluering van die basiese eienskapppe van 'n dipool en 'n gleuf en hoe dit betrekking het op mekaar.

Alvorens 'n akkurate model finaal in Feko gemoduleer kon word, is verskeie alternatiewe modelle geëvalueer om moontlike ekwivalente modelle te vind. Sukses met 'n finale model is eers met die vrystelling van Feko weergawe 5 behaal.

Die resultate toon dat die hoed wel 'n belangrike rol speel in die stuur van die straal, soos geïdentifiseer. Die resultate wys daarop dat daar selfs 'n effektiewer element as die silindriese element mag bestaan, en navorsing hiervan word as 'n veld vir verdere studie aanbeveel.
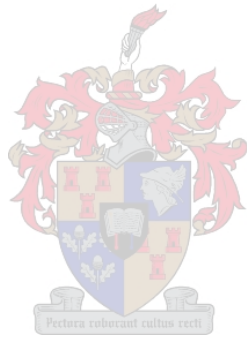
Acknowledgements

I should like to express my sincere gratitude to the following people and organisations for their contribution to making this work possible:

- Cornell van Niekerk for the Matlab codes adapted for the thesis, and Hendrik de Villiers, (Hennie), for input on problems encountered while developing the code;

- The Feko development team for the development of CadFeko, which made the analysis of the array possible;

- The Feko support team for quick response to any error and to problems picked up, as well as the introductory course to CadFeko;

- Prof. Keith Palmer of Stellenbosch University, my supervisor;

- Anita van der Spuy, and Allen for editing of the thesis;

- My friends and family for their support and sacrifices through the last months.

Contents

List of Figures

List of Tables

Chapter 1

Introduction

In this thesis, an existing antenna array that complies with the exacting requirements set for aeronautical satellite communications will be investigated. In a world of fast developing electronic communication, with the increasing pace of the business world, people all over the world need to be connected electronically. The company that can produce a means of communication that can do this most cheaply and effectively will prosper, and the work presented here is aimed at developing an understanding of this aspect of communication technology.

The antenna that is presented in this thesis is used for satellite communications in the aeronautical industry and is regarded as a leading product in the market. Modelling of the antenna has not previously been conducted on the scale that is attempted in this thesis. The product is believed to have been developed with the use of an experimental technique, which means that not all the elements of the array could be evaluated simultaneously. This thesis aims not only to evaluate the existing array but also to produce a model which would be easy to adapt, and in so doing to move away from the time-consuming experimental process. This would cut down on manpower requirements for further development of the array.

The proposed antenna for the investigation was the Chelton Areo Satcom High Gain Antenna, which comprised a thirty-six element array, and was found compliant with INMARSAT requirements. The antenna was primarily designed for aeronautical applications and is used for the transmission of voice and data communication, with a speed of 460kb/s per channel. The requirements with which the antenna has to comply are:

Frequency	L-Band RX$\sim 1.54GHz$, TX$\sim 1.64GHz$
Gain	$12dB_{ic}$ (RHCP)
Side lobe levels	$< 13dB$ at $45°$ from pointing
Axial Ratio	$< 6dB$

These requirements have to be valid for 75% of the hemisphere above $5°$ which can be interpreted as $85°$ from zenith as cited in [1].

Additional Requirements cited are:

Inter modulation products	$< 180dB_c$(2 Carriers of 22.5W)
Operating Temperature	$-70° - 70°$

Low gain below horizon to reduce multi path interference.

As it is a manufactured product availible on the market it is possible to cite the performance specifications of the antenna. This is also availible in the appendix.

Frequency	$1.525GHz$-$1.6605GHz$
Coverage	Seamless coverage compliant with Inmarsat SDM.
Gain	Between 12 and $16dB_{ic}$ over 90% of the Inmarsat hemisphere
	10 dBiC over 100% of Inmarsat hemisphere.
Multi path rejection	Exceeds 10dB at 5 degrees and 12dB at 20 degrees elevation.
Side lobe levels	$13dB$ and better over coverage region.
Power requirements	$28VDC@1.6amps$

As far as physical and mechanical restrictions go, the structure should not interfere with the drag factor of the craft it will be mounted on, therefore the structure needs to be small, affecting the aerodynamics of the craft as little as possible. This is a key factor to be looked at when purchasing and installing the antenna on a high-speed craft. The antenna should furthermore be kept as light as possible, to not add significant weight to the aircraft. Reference to these properties can be found in [2] and [3]. Investigation of the physical dimensions of the antenna, which is about half the length of the antennas that competitors in the market have to offer, and not as high or wide as the competing antennas, indicates that the dimensions were addressed in the development of the antenna. What adds to the success of the antenna is that its dimensions are suitable for use on smaller aircraft, whereas the models produced by the competition were to large too be mounted on smaller craft.

1.1 Chapter Layout

In point form, the chapter content is as follows.

- Chapter 1 - Introduction

- Chapter 2 - Slot

    - Validation of the computational accuracy of Feko for slot analysis
    - Study of slot with non-zero sheet thicknesses
    - Study of the effect of a dielectric substrate on a slot
    - Study of input impedances based on feeding a slot by transmission line

- Chapter 3 - Element

    - Study of two models considered to be equivalent to the existing element
    - Study of the effect of the top hat
    - Study of a more accurate model, modelled in CadFeko
    - Quick glance at cavity properties

- Chapter 4 - Array

    - Presentation of the array layouts for computational purposes
    - Computation of the impedance matrix and active impedances
    - Study of the coupling between the elements

Chapter 1 introduces the topic. In the second chapter, the Feko computational accuracy was evaluated by criteria presented in the Babinet Principle and Booker's extension. This is followed by analysis performed on slots with varying sheet thicknesses and slots manufactured on dielectric substrates, with the response of the impedances being investigated for a possible technique for passively matching to a specific system impedance. The only characteristic that is developed in this chapter and applied to the models of chapter 3 is the shifting of the feed pin for input impedance matching. The other characteristics are presented for general slot design. The dielectric substrate results, however, are applicable to the element under investigation. In the models of Chapter 3 the dielectric on which the slots would be manufactured is ignored as Chapter 2 presents the effects that would be expected and including the substrates would only increase computational time.

In the third chapter, a single element of the array is investigated to form an idea of the role the top hat plays in a single element, before evaluating it in an array. However, problems arose in the modelling of a precise single element due to limitations in the computational modelling code. Thus alternative models were devised for investigation until CadFeko was released,

which allowed for more accurate modelling of the element to be constructed. From the array analysis point of view, the feeding of each element should take place through a single feeding port, which in this case was done by modelling the port in MicroWave Office, using the data obtained from Feko. Investigation into the cavity yielded inconclusive results, as the cavity of the existing model had a cut-off frequency that was above the operating frequency of the element.

In the fourth chapter, the array is evaluated. In this evaluation, the feed network of chapter 3 was used to combine all the small feeds into the necessary ports, so that the coupling and active impedances of the array as presented in the existing model could be evaluated. This feed network made it possible to phase the array for steering of the beam and presented a way to evaluate the excitations of the separate small feeds in Feko, so that the far field of the steered beam could be calculated. Not only could the field be evaluated by the steering of the beam, but it was possible to compute the active impedances of the array through mathematical models as the beam is steered by performing simple calculations on the impedance matrix. The results could be used to show how the top hat contributes to the performance of the array.

In the last chapter, the conclusion from the results regarding the use of the top hat is presented, along with a possible recommendation. In the Appendices, the Babinet Principle and Booker extension are described, and the problems which were encountered in the modelling of the array are also stated, along with some useful Matlab functions that have been developed as aids in processing the results.
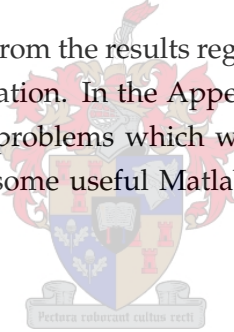
Chapter 2

Properties of a Single Radiating Slot

2.1 Introduction

- Paragraph objective

  - Validation of Feko computational code based on the Babinet Principle
  - Introduction of the NRP (Normalised Root of the Product)
  - Evaluating the NRP for various sheet thicknesses
  - Introduction of dielectric substrate in the presence of a slot
  - Evaluation of the self-impedance of a slot

- Purpose of the above objectives

  - Using a knowledge of dipoles to evaluate slots
  - Validation of the accuracy for analysis of slots
  - Finding reasonable sheet thicknesses, with the assistance of the NRP, for slot application
  - Finding the effective dielectric constant of a substrate in the presence of a slot
  - Searching for a good match with the slot feed
  - Revealing feed edge effects of a slot

- Method adopted to attain objectives

  - Validation of the computational code is done by evaluation of an ideal dipole-slot complementary pair
  - The NRP is introduced by evaluating non-ideal dipole-slot complementary pairs of various sheet thicknesses
  - Evaluating NRP for broader ideal slot

5

– The self impedance of a dipole is used to calculate self impedance of a slot

– The self impedance of a slot is verified with Feko while showing the edge effects.

The Babinet Principle (see Appendix A) states that there is a relationship between the radiating properties of a complementary dipole-slot pair. This fact was used by Booker [4] who proved this also to be the case for the impedances of the complementary pair.

Using the criteria presented by Booker, slots were analysed in Feko to determine how they would respond if certain aspects of the slot, such as the sheet thickness, were no longer ideal. Due to the computational nature of Feko, it was necessary to first prove the computational accuracy of Feko in using an ideal dipole-slot pair.

With the validation of Feko's accuracy in computing of a radiating slot, a handle was obtained that could be used for the investigation of the accuracy of non-ideal slots by evaluating a non-ideal complementary pair. The tool that was developed is the NRP, which represents the root of the product of the two impedances normalised to $\frac{\eta}{2}$ as obtained by Booker's extension.

The NRP not only presented an evaluation technique for the analysis and design of non-ideal complementary dipole-slot pairs, but also a useful method for evaluating the use of a dielectric substrate in the search for a technique for the calculation of the effective dielectric constant.

In the last part of this chapter, the impedance response of a slot over the length of the slot was considered as a possible feeding technique and as a means to determine what the effect would be of feeding close to the edge of the slot.

The work reported in this chapter was expected to make it possible to simplify the model of a single element. With the results gathered through this, it became be possible to gain an understanding of how these simplifications would affect the array model in the end.

a) Dipole   b) Slot
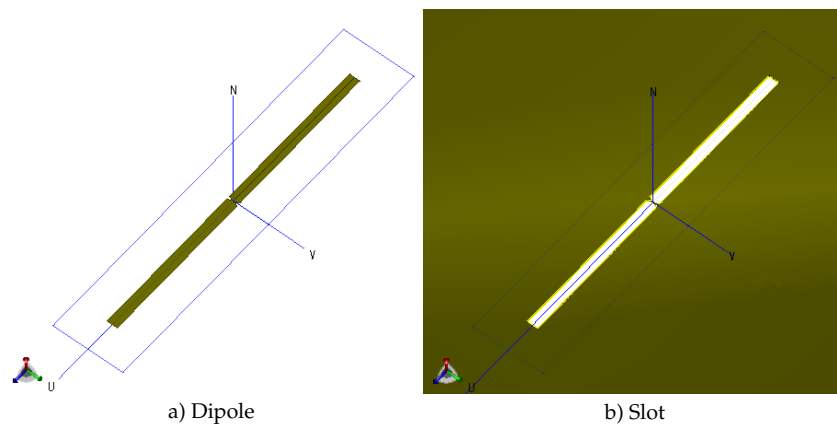
Figure 2.1: Complementary Slot-Dipole pair

2.2 Validation for the computational code Feko of the Babinet Principle

- Paragraph objective

    - Validation of Feko computational code

- Purpose of the above objectives

    - To Evaluate the computational accuracy of Feko for further investigation into slots

- Method adopted to attain objectives

    - Analysis of an ideal dipole-slot complementary pair designed with effective width and zero sheet thickness

This section deals with an analysis that was performed on a complementary dipole-slot pair to verify the computational accuracy with which Feko can solve the analysis of a radiating slot. The problem, which was presented with the computation of a slot on an infinite ground plane, can be solved in certain computational codes which allow for a slot to be defined on an infinite ground plane. In Feko, however, the ground plane cannot be of infinite size, as Green's function, which computes the ground plane, does not comprise any algorithms that support a hole or slot being defined on a ground plane. Therefore the problem needed to be approached differently. A large sheet was defined in free space, with a slot that would be defined in the centre of the ground plane. In Appendix B, the initial problems of the analysis are stated in detail. These indicated finding a meshing for the slot area and an effective size that could be considered as an infinitely large ground plane for the problem at hand. This meant that various inaccurate and misleading results were obtained before accurate results could finally be obtained and replicated repeatedly.

However, before the solution of Feko could be validated, a criterion was required to act as a measure in validating the Feko results.

The criterion was presented through the Babinet Principle, which was originally adopted from the study of optics, and is presented in Appendix A. The Babinet Principle allows for the analysis of a slot through the general understanding of a dipole. This is a useful technique as it uses the knowledge that has been obtained in all undergraduate studies, combined with text on the analysis of a dipole, to show the properties of a slot by describing the relationship that exists between the two. From the Babinet Principle, which is worked through in Appendix A, the relationship was found to be in the components of the electric and magnetic fields, when the the slot and dipole form a complementary pair. A complementary pair implies that it should be understood that the the dimensions of the height, length and thickness should all be the same for the dipole and the slot. Returning to the Babinet Principle, it was shown that a constant
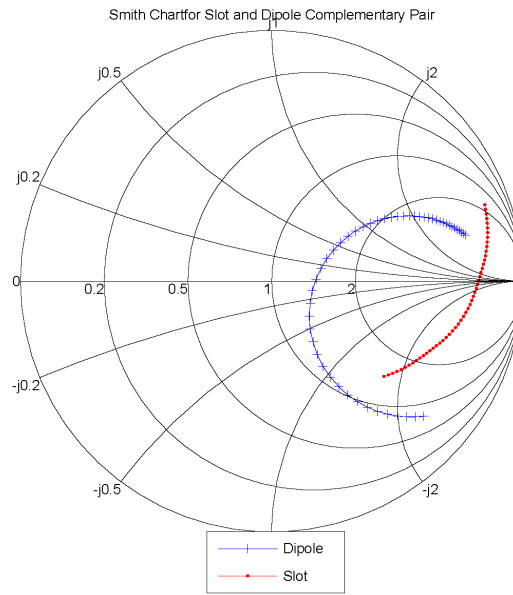
Figure 2.2: Complementary slot and dipole impedance on Smith Chart

relationship between the components of the radiated field can be found and that it is derived in equation A.1.21 as:

$$\mathbf{E}_1 = \kappa \mathbf{H}_2 \quad \mathbf{H}_1 = \frac{-\kappa}{\eta^2} \mathbf{E}_2 \tag{2.2.1}$$

This could form the basis of the criterion that would lead to the validation of the Feko code by first evaluating the fields of a dipole and then using the calculated fields of the dipole, together with the relationship presented in equation 2.2.1, to verify the fields which will be computed when an analysis on a slot is done by means of Feko. By comparing the difference between the expected field values, and the calculated field values it would be possible to verify the accuracy of Feko for the analysis of a slot. This technique, however, was not used due to a criterion presented by HG Booker [4] for the relationship between a complementary dipole-slot pair. In his extension of the Babinet Principle, he proved that the relationship for the fields of a complementary dipole-slot pair can be extended to the input impedance of the complementary pair. This relationship was preferred for the validation of the Feko code, as it is easier to evaluate from Feko results. If the fields were to be evaluated, it would have been necessary to divide the fields into the various cartesian components they comprise.

The relationship that was presented by Booker states the following relationship, which is presented in Appendix A.2. It is given in the following equation:

$$Z_{slot} Z_{dipole} = \frac{\eta^2}{4} \tag{2.2.2}$$

where η is the intrinsic impedance of free space.

To validate the computational accuracy of the Feko code it was necessary to perform two computational analyses with an eye to the criterion that was presented. The dipole was designed by means of the criterion presented in [5] for the design of an effective cylindrical dipole. The dipole was then adapted to form a flat dipole, through the following relationship:

$$r = w + t \tag{2.2.3}$$

where r is the radius of the cylindrical dipole and w would be the width of the flat dipole, with t being the sheet thickness.

This was done to validate Feko for the perfect flat dipole, therefore the sheet thickness was taken as zero and the dipole was made to be the complement of the slot, with an operating frequency of $8.5GHz$. The analysis of the dipole in Feko presented quick, accurate results for the calculation of the impedances. However, a different scenario was created with the slot, where it was necessary to find a way to cut down on the computational time without loss of accuracy. Thus, when introducing the slot through Feko, certain techniques, such as the use of symmetry, were implemented to cut down on the computational time. Electrical symmetry could be established along the length of the slot, onto which the electrical fields could terminate and be mirrored, while the magnetic symmetry could be established along the width of the slot for mirroring the magnetic fields, terminated onto it. This improved the time taken for the calculations without any loss in accuracy, thus decreasing the painfully long wait when performing the integral equation for all the triangles that are used to represent the slot, as referred to in Appendix B.

Figure 2.2, displays the impedances of a complementary slot dipole pair, illustrating that no apparent relationship can be seen on the Smith Chart.

Figure 2.3 the imaginary part of the dipole's impedance response is illustrated as being quite linear over the requested frequency band and the real impedance can be approximated by a linear equation in the proximity of resonance when the dipole length is in the order of half a wavelength for the desired operating frequency. Due to this linear approximation of the separate impedance components of a dipole, it could easily and mistakenly be assumed that the approximation of a slot's impedance could be undertaken similarly. Unfortunatly the impedance of a regular slot cannot be approximated accurately enough over the frequency range as in the case of a dipole, as it is far from being linear and the mistake was realised.

The expected impedance could be calculated through use of the complex dipole impedance and equation 2.2.2 and is presented in Figure 2.4, which clearly illustrates that the impedance cannot be approximated by a set of linear equations across the evaluated frequency band. The same graph which presents the expected values of the slot also presents the results of the com-
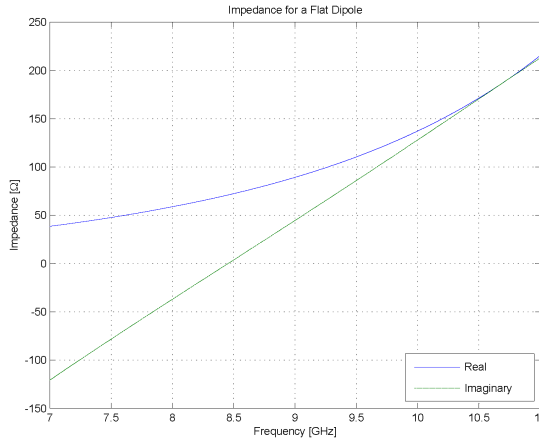
Figure 2.3: Impedance of flat dipole
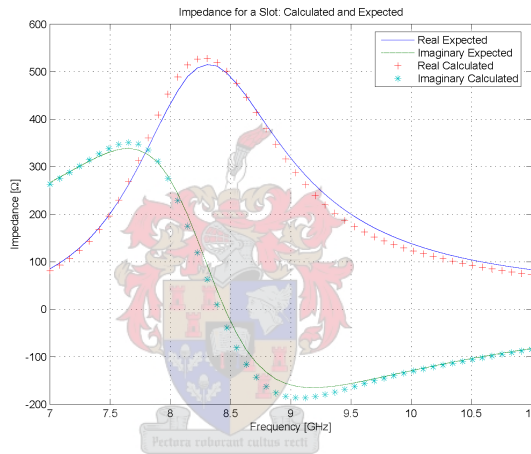
Figure 2.4: Impedance of slot: computed and expected value derived from a dipole's impedance

plementary slot obtained through Feko. It is clear that the two graphs follow each other very closely, except for a small deviation.

The deviation is further evaluated by the equation presented by Booker as the product of the impedances. Figure 2.5 shows that in the real part of the product the deviation is quite small, and that the deviation is greater in the imaginary values of the product. However, the error for which the deviation is responsible, for the most part is well below the 10% error margin, which is considered to be within a reasonable margin for validating the accuracy of the Feko computational slots.

A third approach for presenting the results for validation of the computational accuracy would involve evaluating the root of the product of the impedances, which is supposed to yield the following result if the analysis is accurate:

$$\sqrt{Z_{dipole}Z_{slot}} = \frac{\eta}{2} \tag{2.2.4}$$
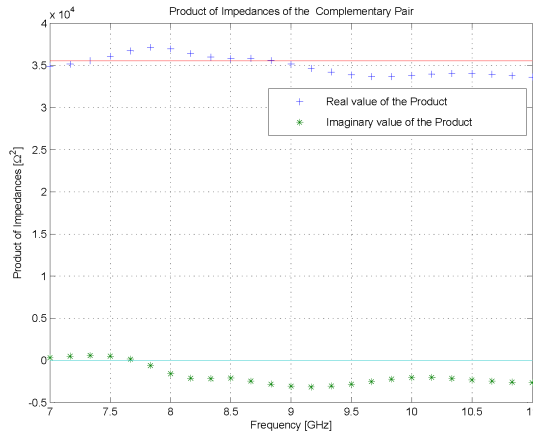
Figure 2.5: The product of the impedances for a dipole and its complementary slot in an ideal cases
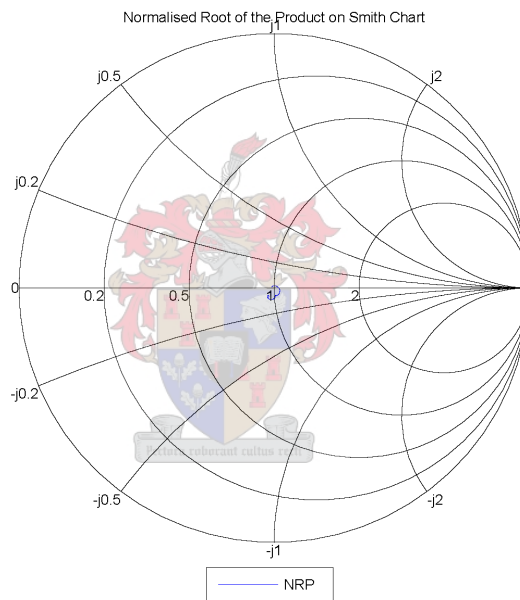
Figure 2.6: The normalised root of the product(NRP) for a slot and its complementary dipole on the Smith Chart

By normalising the results of the root of the product to $\frac{\eta}{2}$ accurate results would yield a single point on the Smith Chart, at the centre. In Figure 2.6, this is not exactly the case as the normalised root of the product of the complementary pair that was evaluated, instead of amounting to a single point, encircles the centre of the Smith Chart. This circle is the product of the deviation and is clearly illustrated to be well within reasonable range of what may be considered to be accurate.

It can thus be concluded that, if all the physical requirements presented in Appendix B are met, the computational accuracy of Feko can be shown to be sufficient for the analysis of slots.

2.3 Introduction to NRP (Normalised Root of the Product)

- Paragraph objective

  - Introduction to NRP (Normalised Root of the Product) for further validation and analysis

- Purpose of the above objectives

  - To have a single value complex variable that indicates the degree to which the Booker/ Babinet Principle is valid

  - To assist in designing slots for broadband applications

- Method adopted to attain objectives

  - Computing the NRP for an ideal broad dipole-slot complementary pair

In this section, the NRP (Normalised Root of the Product) will be introduced. The basic function was touched on in the previous section, on the validation of the computational accuracy of Feko. It was represented by a small circle around the centre of the Smith Chart, showing that no other conclusive data could be read from the graph except that the Feko code could be validated by means of the NRP, which is calculated in equation 2.3.1:

$$NRP = \frac{\sqrt{Z_{dipole}Z_{slot}} - \frac{\eta}{2}}{\sqrt{Z_{dipole}Z_{slot}} + \frac{\eta}{2}} \tag{2.3.1}$$

Because the root of the impedance product has ohm as a unit, it was assumed that the additional information could be gathered in the Booker extension, if the root of the product was handled like an impedance value and presented on a Smith Chart when normalised to $\frac{\eta}{2}$. This was not effective, as there was a very small distribution around the center of the Smith Chart. The expected result for a perfect dipole-slot pair would be a point at the center of the Smith Chart. Any distribution around this point indicates an error or, rather an aberration in the analysis, due to physical properties of the complementary pair. The thrust behind the development of the NRP is to find trends in the deviation to create an understanding of how slot models could be simplified and for which forms these simplifications would be valid.

As shown, the NRP was normalised around the value of $\frac{\eta}{2}$ therefore the variation seen in Figure 2.6 can be shown to be the degree of error that is present in both the design and the computational accuracy. In this section, a more practical model of a slot will be evaluated, with its complementary dipole, to determine the error of accuracy that is introduced in Feko when the sheet thickness is ideally regarded as zero. For the analysis, the dimensions of the dipole-slot complementary pair was: length 0.475λ and width $\frac{\lambda}{20}$, with an operating frequency of $8.5GHz$.

These dimensions were chosen as the arbitrary cross section for a flat dipole as it relates to a cylindrical dipole apparently only holds for slender dipoles, and there is a need to investigate slots which are broader and thus more practical.

According to Booker [4], the selectivity of antenna resonance for a slender complementary pair is considered good, and reduction of the selectivity of a slot will occur when the slot is widened. This reduction in selectivity due to the widening of the slot is found to be similar to the effect of lengthening a dipole and is discussed in [6], where non-uniform slot widths were investigated. This results from the fact that the model for a slot is a transmission line terminated on short and the length to the short is increased slightly when the slot is widened. The reduction in the selectivity was witnessed and the Antenna Vector Effective Length [7], was reduced accordingly, to 0.475λ.
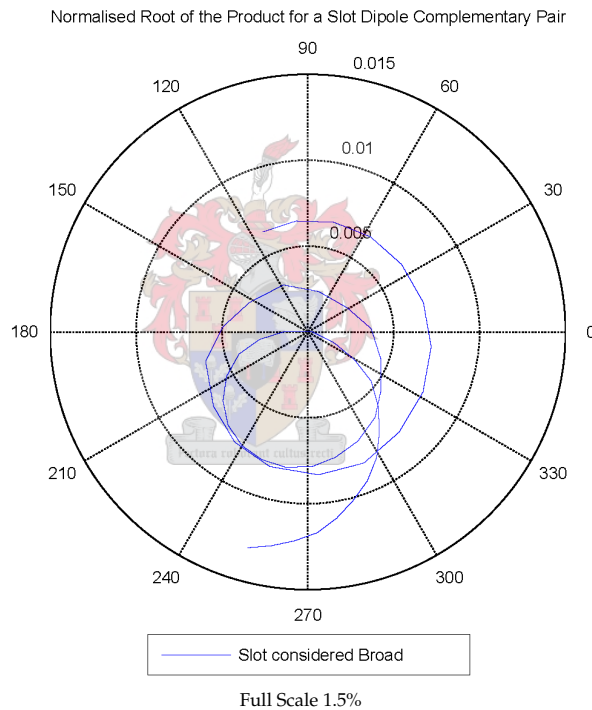
Figure 2.7: NRP for a complementary dipole-slot pair

Figure 2.3 clearly illustrates the error that is presented by Feko when the NRP is presented on a polar graph. It can be shown from the graph that the largest error introduced by Feko is below 1.5% and that it passes through the centre of the graph at the frequency of resonancy. Therefore verifying the computational accuracy of Feko for the problem is related to the analysis of slots.

With the NRP, this new tool that has been developed, a new criterium has been found that makes it possible to find trends relating to the properties of the materials used in the manufacture slots. In the following two sections, the NRP will be used to find trends in the sheet thickness used to manufacture slots and the effects of a dielectric substrate placed under the slot.

2.4 Evaluating the NRP for Effective Sheet Thickness Design for Ground Planes

- Paragraph objective

  - Evaluating the NRP for different sheet thicknesses

- Purpose of the above objectives

  - To assist in designing slots with 'reasonable' sheet thicknesses

- Method adopted to attain objectives

  - Computing the NRP for non-ideal dipole-slot complementary pairs by varying the sheet thicknesses

    * Sheet thickness $\frac{\lambda}{1500}$
    * Sheet thickness $\frac{\lambda}{500}$
    * Sheet thickness $\frac{\lambda}{250}$
    * Sheet thickness $\frac{\lambda}{100}$
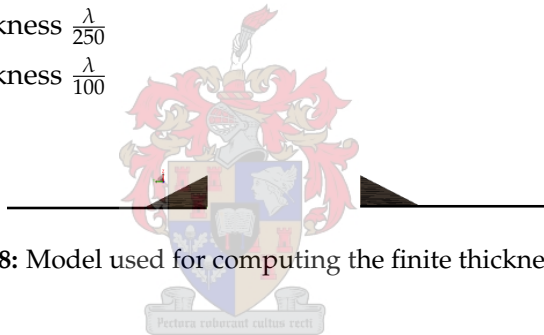
Figure 2.8: Model used for computing the finite thickness of a slot

In this section, the influence of the thickness of the sheet from which the slot is manufactured will be evaluated by means of the NRP. In most cases, slots are cut from cavity wave guides which vary in thickness according to the applications they are designed for or the manufacturing process that is used. Consideration therefore was given to evaluating how a practical slot would differ from the ideal model when the Babinet Principle was considered for designing a slot antenna based on dipole properties. Diffraction of the edges of the non-zero thickness sheet was expected to influence the complementary dipole-slot pair in a negative way, rendering the Babinet Principle inaccurate for thick ground planes. In evaluating the problem, there was also an attempt to establish the ground plane thickness for which the Babinet Principle could be used. Not only was it possible that diffraction of the slot's edges could influence the complementary pair's properties, but that a large current would also be found flowing at the edges of the slot. The model depicted in Figure 2.8 was used for the computation to minimise the number of triangles required.

To accomplish the above, four different sheet thicknesses were used: $\frac{\lambda}{1500}$, $\frac{\lambda}{500}$, $\frac{\lambda}{250}$ and $\frac{\lambda}{100}$. The operating frequency was $8.5GHZ$, similar to the operating frequency used in the previous sections. For these slots, the complementary dipoles concerned were given the same sheet

thickness as the slot. If a cylindrical dipole were to be used with the Babinet Principle to evaluate a slot, it should be realised immediately that the effective radius of the cylindrical dipole relates to a flat dipole.
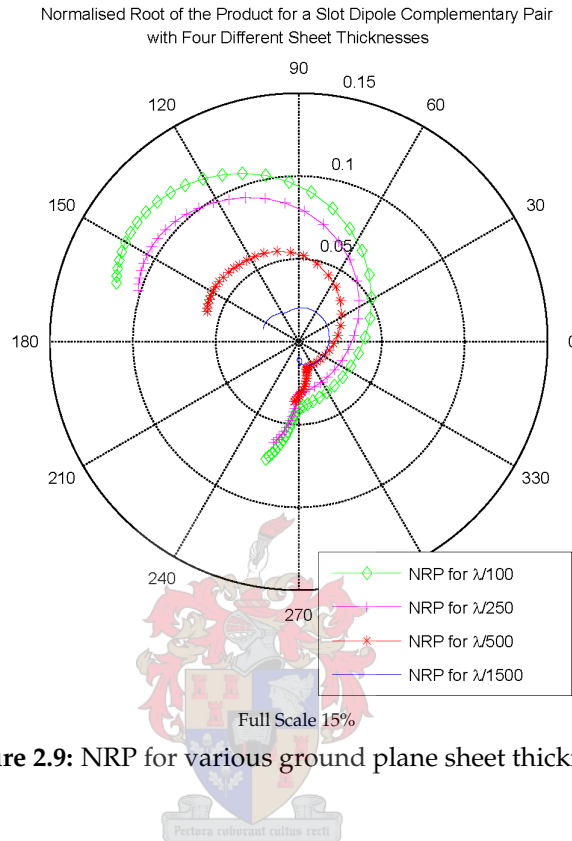
Figure 2.9: NRP for various ground plane sheet thicknesses

The results from the calculated NRP for the various sheet thicknesses are illustrated in Figure 2.4, which clearly indicates the circular distribution around a point, with the error margin in the distribution increasing for various values of sheet thickness. It will be shown, later, that the fact that the point around which the circular distribution is found is not in the centre is due to the inductance of feed that has been introduced. This was seen more clearly on a Smith Chart. By ignoring the feed's influence on the problem, each circle of the NRP could conceivably be shifted to lie around the centre of the polar graph and the variation of magnitude around the centre would then indicate the amount of error. It can be seen from the figure that the error for a sheet thickness of $\frac{\lambda}{1500}$ is only slightly larger than for the ideal case illustrated in Figure 2.4, which presents an error of roughly 2%. By increasing the thickness to $\frac{\lambda}{500}$, the error that is introduced is just below 5%, clearly illustrating that the error becomes greater with increase in sheet thickness. These two thicknesses indicated that the slot area should be meshed much more finely than for other computations performed on the slot, and this resulted in far longer simulation time. It is therefore recommended that the ideal case should rather be considered for these thicknesses and that a 5% error should be ignored. Normal slot meshing could be used in the case of sheet thicknesses of $\frac{\lambda}{250}$ and $\frac{\lambda}{100}$ and the difference in calculation time was not as great. The error margins for these two cases were in the order of 6.5% and 8% respectively. A

Sheet Thickness	Error introduced
0	1.5%
$\frac{\lambda}{100}$	2.2%
$\frac{\lambda}{250}$	4.8%
$\frac{\lambda}{500}$	6.4%
$\frac{\lambda}{1500}$	7.9%

Table 2.1: Margin of error presented by sheet thickness

6.5% error was establised for a sheet thickness of $\frac{\lambda}{250}$ and an 8% error was found for a $\frac{\lambda}{100}$ sheet thickness. Though both are still marginally below 10% error, steering clear of these thicknesses, and rather using a sheet that is as thin as possible for the design is recommended. The table below gives the error margins for the different sheet thicknesses that were evaluated.

It should be possible to estimate the error that diffraction off the edges of the slot will contribute by using the results in the table as a reference. Another factor to be considered is that the diffraction and the error both play a role in the selectivity of the operating frequency of the antenna, and that this should therefore also be considered before a thick sheet is used for the slot.
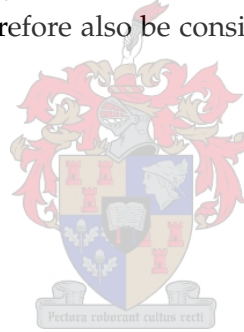
2.5   Investigating NRP for Slots with Dielectric Substrate

- Paragraph objective

  - Investigating the effect that a substrate will have on a slot

- Purpose of the above objectives

  - To establish whether it is possible to calculate the effective dielectric by using the RP (Root of the Product)

- Method adopted to attain objectives

  - Calculating the NRP and RP for a dipole-slot complementary pair having a dielectric substrate present

The idea of evaluating a slot over a dielectric substrate comes from an existing model where the slot is etched from a PC board. Manufacturing a slot from a PC board allows for using thin sheet thicknesses, while the slot still has structural integrity. However, it is evident that the dielectric of the substrate contributes more than just structural integrity.

It becomes clear that the electric fields excited by the magnetic dipole that exists in the slot differ in the regions below and above the slot because of the introduction of the substrate [8], and it was this property that led to the analysis of the dielectric substrate. The idea was to evaluate the problem and determine whether the effective dielectric constant could be computed from the results that would be presented. For this purpose two substrates with different dielectric constants were used: $\epsilon_r = 2.5, 5$. It was also thought to be relevant to include different substrate heights and to evaluate how much this would affect the effective dielectric constant. Furthermore the setup required the substrate to be present on the analysis of the dipole as well.

From Figure 2.5, it it can be shown that the same circular error distribution as in the case where the different sheet thicknesses where investigated is presented by the NRP. However, the shift away from the centre appears to be of a capacitive nature, which is believed to be because of a large field being excited in the slot, which might have to do with limited fringing. It can furthermore be shown that the substrate with dielectric constant $\epsilon_r = 2.5$ introduces an error of nearly 10%, while the substrate with the dielectric constant $\epsilon_r = 5$ introduces an error of roughly 15%, with the heights of the substrates causing only a slight difference in the error. Therefore it is claimed that the height does not play an important role in computing the effective dielectric constant. It was considered possible that the NRP could shed light on properties resulting from the use of a dielectric substrate. This was presented in spite of the fact [9] that the impedance of a substrate through which a wave propagates differs from that of freespace and knowing that equation A.2.4 would no longer hold true. A new relationship is considered to exists between the individual slots of a complementary dipole-slot pair that includes the properties of the substrate, and this can be given in the following equation:
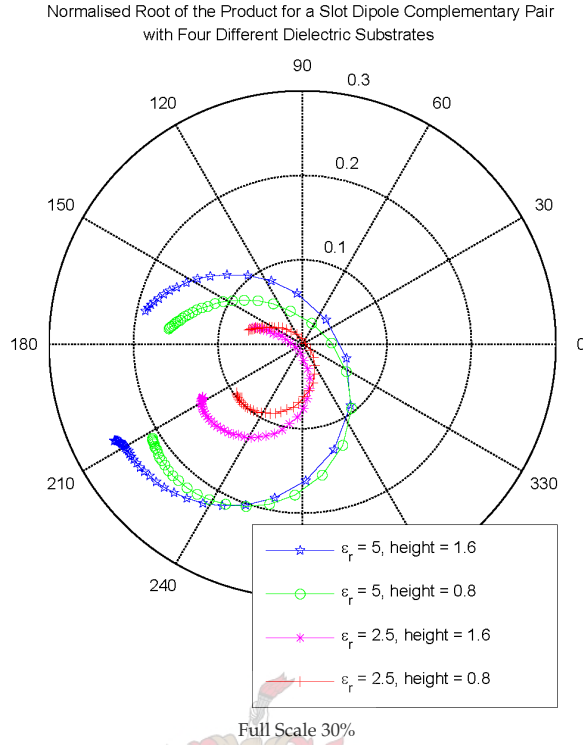
Figure 2.10: NRP for various dielectric substrates

$$
\begin{aligned}
\frac{\eta^2}{4X} &= Z_s Z_d \\
\frac{\eta}{2\sqrt{X}} &= \sqrt{Z_s Z_d}
\end{aligned}
\tag{2.5.1}
$$
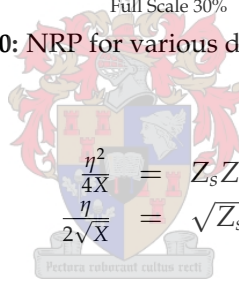
From the plots presented in Figure 2.5, it is established that two significant values are present on the plot of the Root of the Products, in the real part. The first part is a value to which the real part converges, and this is considered to hold a connection to the effective dielectric constant. The relationship between the complementary dipole-slot pair is therefore considered to be contained in the equation

$$
\frac{\eta}{2\sqrt{\epsilon_{reff}}} = \sqrt{Z_d Z_s}
\tag{2.5.2}
$$

where ϵ_{reff} is considered to be the effective dielectric constant with the values that are calculated for the above-mentioned substrates, as presented in Table 2.2

As the case is presented in microstrip patch antennas where the effective dielectric constant affects the effective length of the patch, it can be shown that the slot is affected in a similar way due to the presence of the substrate. In the case of a patch, the effective length of the slot is adapted by a factor $\sqrt{\epsilon_{reff}}$, so that the correct resonance can be achieved. To prove the above-mentioned effect, the slot length is kept constant for the operating frequency of $8.5 GHz$ and the properties of the substrate is varied. The second value that is presented from the Root of the

a)$\epsilon_r = 2.5\ height = 0.8$ b)$\epsilon_r = 2.5\ height = 1.6$

c)$\epsilon_r = 5\ height = 0.8$ d)$\epsilon_r = 5\ height = 1.6$
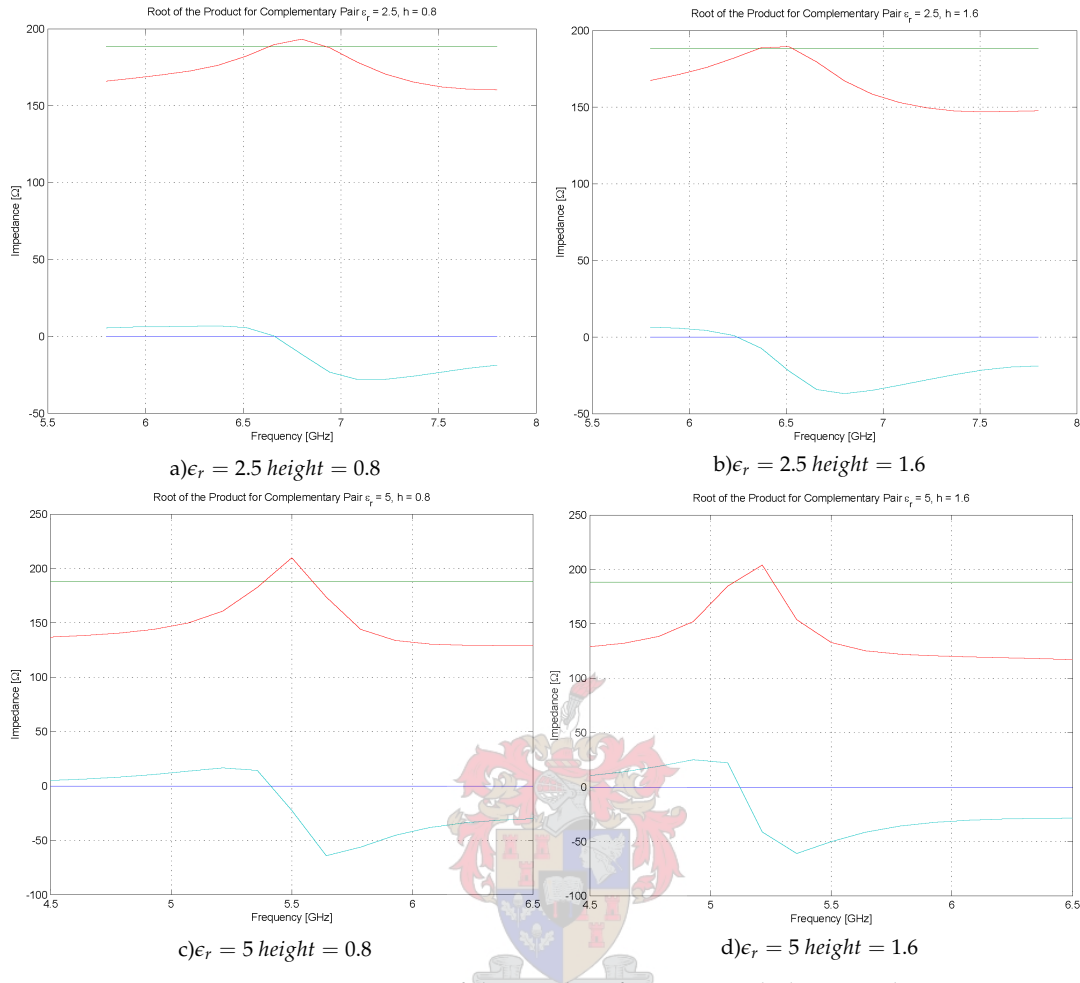
Figure 2.11: Root of the Product for various dielectric substrates

Dielectric Constant ϵ_r	Height [mm]	Effective Dielectric Constant ϵ_{reff}
2.5	0.8	1.495
2.5	1.6	1.699
5	0.8	2.3802
5	1.6	2.5841

Table 2.2: Effective dielectric constants calculated from the root of the product

Product is a peak that is found in the new resonating frequency of the slot. These frequency changes were taken and the effective dielectric constants were calculated, using equation 2.5.3, which is based on the effective length of a microstrip patch. The results are presented in Table 2.3

$$f_{eff} = \frac{f_r}{\sqrt{\epsilon_r}} \tag{2.5.3}$$

Dielectric Constant ϵ_r	Height [mm]	Frequency [GHz]	Effective Dielectric Constant ϵ_{reff}
2.5	0.8	6.86	1.55
2.5	1.6	6.55	1.684
5	0.8	5.5	2.388
5	1.6	5.15	2.774

Table 2.3: Effective dielectric constants calculated from the Frequency Response

The values of the effective dielectric constants that are presented in Tables 2.2 and 2.3 can be used to show that they compare well, and thus that either one can be used to determine the effective dielectric constant of a substrate. The peak that is present at the resonant frequency can furthermore be accounted for through the model of the radiating slot, based on the analysis of impedances of cavity-backed slots. In these cases, the slot would radiate into only half of the free space, which would relate to half the admittances and conductances being dropped, which would double the slot impedance. In the case of a slot over a substrate, the radiated field does not extend only just half in free space, but altogether over free space, although with lesser field strength in the half where the substrate is located. Due to the losses, the impedance will increase over the band where the slot is resonant.
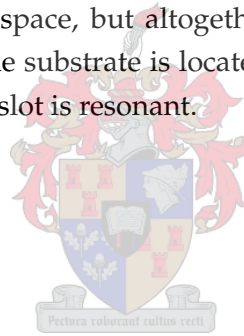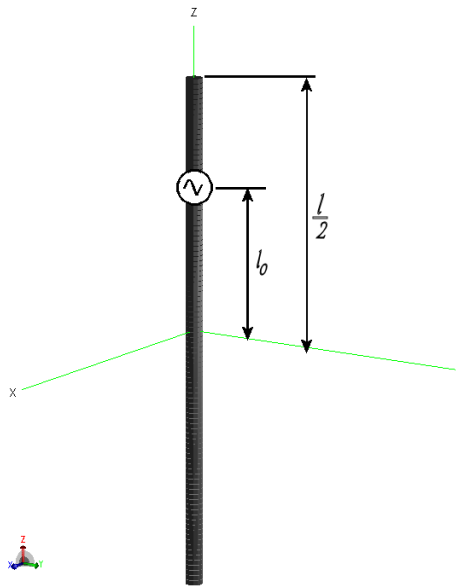
Figure 2.12: Calculation of input impedance of off-center fed dipole

2.6   Self-Impedance of Slot

It is a given assumption that the current flow distribution found on a dipole will be approximately of a sinusoidal distribution over the dipole, as derived from Hallen and Pocklington's integral equation in [7]. For a half-wave dipole, were it is to be directed along the z-axis, the current distribution would lie on the z-axis and, since the dipole would consist of a perfect conductor, the tangential electric field would be zero and therefore no electric field will be found on the dipole, except between the arms of the dipole, where the dipole is fed. Thus there has to be an investigation into how the current is distributed on the dipole in order to determine the input impedances along the length of the dipole. What is to be expected is that maximum current will be in the centre, so the input impedance will be at a minimum there and that the current at the ends will be much lower, and a maximum input impedance will be found on the edges. Assuming that the current distribution will not deform too seriously when shifting the point of excitation, the expected impedance will be an inverted sinusoidal function. Since the excitation of the current on the dipole is of a sinusodial source, it may be expected that the input impedance along the dipole length will be an inverse sinusoidal distribution. However, the above assumption is incorrect, it holds only for the symmetric dipole fed at the centre, whereas the current on the asymmetric dipole is given as:

$$I(l) \quad \begin{cases} = I_1 \sin(k(l/2 - z)) & z > l_0 \\ I_2 \sin(k(l/2 + z)) & z < l_0 \end{cases} \tag{2.6.1}$$

maintaining the sinusoidal current distribution on the dipole and l_0 being the location of the

feed found in [10]. The current flowing in towards the source and the current flowing from the source should be equal, yielding the equation 2.6.2

$$I_1 \sin(k(l/2 - l_0)) = I_2 \sin(k(l/2 + l_0)) \tag{2.6.2}$$

resulting in current flow that can be related to the source current as:

$$I(h) = I_s \sin(k(l/2 - l_0)) \sin(k(l/2 - z)) \tag{2.6.3}$$

For a half wavelength dipole this equation, being manipulated with trigonometric equations, becomes

$$I(l_0) = I_s \sin^2(\frac{\pi l_0}{l}) \tag{2.6.4}$$

from the centre of the dipole.

With a constant voltage driving the dipole, the input impedance along the length of the dipole will yield a $\frac{1}{sin^2}$ normalised impedance graph, if taken from the edge of a dipole to the other end. However, the dipole impedance is of no significance (other than for Booker's extension) when the dipole impedance is evaluated when fed at the centre, since this gives a handle to enable evaluation of the input impedance at the centre of the slot. The current distribution on a slot, though sinusoidal, differs from that of a dipole in that maximum current is found at the ends of the slot, and that the current is distributed along two edges towards the ends of the slot. In [7] one of the equivalent current density techniques for analysis on a microstrip patch antenna refers to the fringing fields as having a similar electric distribution to that found on slots. Therefore the analysis of a patch can be done on the assumption that there are two radiating slots along the width of the patch. In the impedance analysis of the microstrip antenna, the input impedance is calculated from the cosine squared rule, as depicted in Figure 2.13, where maximum impedance occurs at the edges of the patch where the electric field is at its maximum and where the current is at a minimum.

Because the patch antenna can be modelled with the use of a slot approximation as presented in [7], the principle thought to be drawn from this is that the impedance along the length of a slot might be similar to that of a microstrip patch antenna. Analysis with FEKO was done to determine the input impedance along the length of the slot and it gave the results present in Figure 2.14.

The analysis conducted through FEKO encountered pitfalls that are described in Appendix B. The results of the single feed analysis for the input impedance, for example, yielded very strange values, and only after the second analysis was it determined that the symmetry that
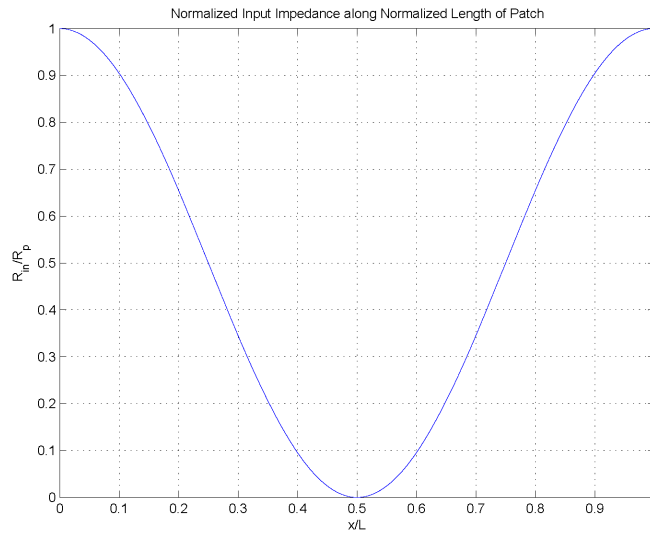
Figure 2.13: Input impedance along the length of a patch antenna
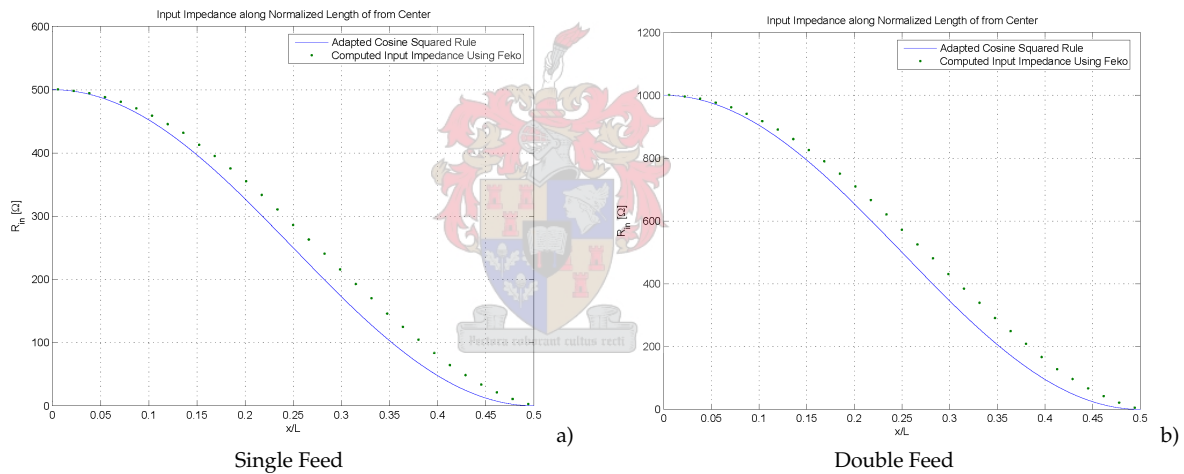
Figure 2.14: The input impedance along the length of a slot

was the setup for the slot analysis in the above sections no longer held. This lengthened computational and the meshing of the slot was made coarser to save time. However, the symmetry was sufficient for the double fed slot, since the fields in the slot had the necessary symmetry.

Figure 2.14 presents the results of an analysis done on a slot with a resonant frequency of $1.6 GHz$. The figure depicts the impedance as a cosine squared rule, however, this was taken from the centre of the slot. Thus the impedance will be similar towards $-x/L$, which, in this case, would be sine squared function, with the relationship to the cosine squared rule given as $1 - cos^2(x/L)$ when starting at an edge and going along the full length of the slot. However, the slot that was investigated in the project was a quadrature-fed crossed slot and the input impedance of a slot with two feeds was investigated. Each slot of the quadrature-fed crossed slot was fed at two points, with a phase shift in the feed of around $180°$, due to the feed location, so that the two feeds would complement each other and the fields generated by each feed

would add up. From the slot antenna model shown in Figure 3.18, an estimation could be made to determine what effect the double feed would have on the input impedance of the slot. From the model, it was possible to split each element into two elements in parallel, but the values of these new elements needed to be adapted. The electric and magnetic fields of the slot did not change, therefore the fact that two feeds were used did not really influence the excitation of the slot and therefore the current delivered to the slot to produce the electric field remained unchanged from that delivered to the single feed. Thus the impedance observed with one feed would in effect be doubled, since only half the current from the feed was needed to establish the field. Figure 2.14b shows the impedance obtained from computation, revealing that the maximum impedance was doubled from that of figure 2.14a and that the impedance change along the length remained similar to the sine squared rule.

With both of the above systems it is known that the feed has an inductive contribution to the impedance of the slots, which can cause unwanted effects on the input impedance of the slot. Finding the input impedance of the slot along the length of the slot at a set frequency made it possible to explore the inductive effect of the impedance on both the single and double feed slots. Figures 2.15a and 2.15b show that the real part of the impedance starts to decay along a constant line of imaginary value, as the feed moves towards the edge of the slot, indicating a steady inductive value. This inductive line on which the impedance decays relates to the inductive value of the inductor found in the model of the slot. Since the feed, which is inductive by nature, is moved closer to the edge, the imaginary value also starts to decay, holding to the definition that two inductors in parallel reduce the total inductance. As the feed is at the edge of the slot, it is easily shorted by the edge of the slot and the total impedance shorted out. The impedance on the Smith Chart shows how the impedance is striving towards the location of a short, when the feed is moved towards the edge of the slot.
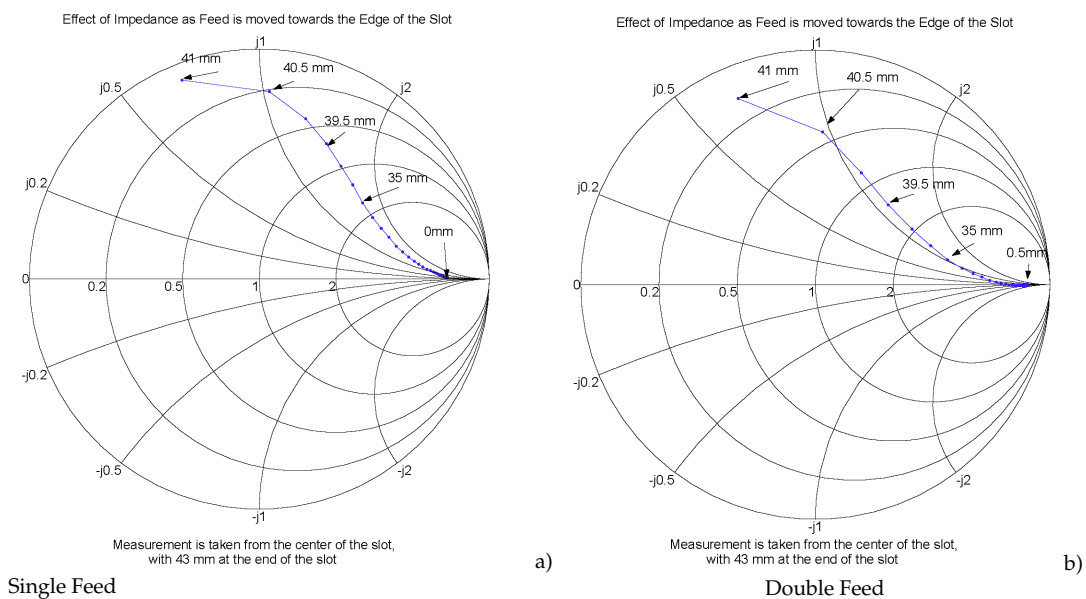
Figure 2.15: The inductive effect of the feed wires

2.7 Conclusion

A couple of conclusions can be drawn from the results reported in this chapter .

The first conclusion that can be drawn is that Feko is a powerful enough tool to evaluate the problem of a slot, although it will be a time-consuming process compared to that of a dipole. The results can be considered relevant and accurate as long as all the basic requirements that have been addressed here and in Appendix B are met.

Secondly, a useful tool that was developed and discussed in this chapter was the NRP. The NRP is used as a measure for evaluating the accuracy of a slot-based problem by evaluating the dual of the slot, which would be a flat dipole with the same dimensions or a cylindrical dipole that would relate to a flat dipole with the slot dimensions.

Thirdly, it was shown that Booker's extension, and therefore the Babinet Principle, cannot be evaluated accurately. The NRP illustrated an error that increased as the sheet thickness of the complementary dipole-slot was increased. It is very likely that diffraction off the edges of the slot could have been responsible for the error which was produced, as the computational code was considered accurate. Therefore it could be established that good slot analysis would lie in determining an effective sheet thickness for the slot.

The fourth point that was established also relates to the NRP. However, it happened to be useful before it was normalised to compute the effective dielectric constant of a dielectric that was found to be present when the slot was above a substrate. Thus another useful technique sprouted from the Booker extension of the Babinet Principle, proving the computational value of these two principles.

These principles were taken further in the computational analysis of the impedance of a slot. This approach was taken to evaluate, according to transmission line theory, where the feed of a slot should be located for the best possible impedance match. From this work it was established that there is no good feed location for good passive matching on the slot. What did become evident, however, is that the inductance of the feed could contribute significantly in the analysis of a slot if the feed were to be located close to the edge of the slot.

Chapter 3

Development of a Computational Model of a Dual Slot

3.1 Introduction

a) I-Slot Model   b) Z-Slot Model   c) Circular Modal
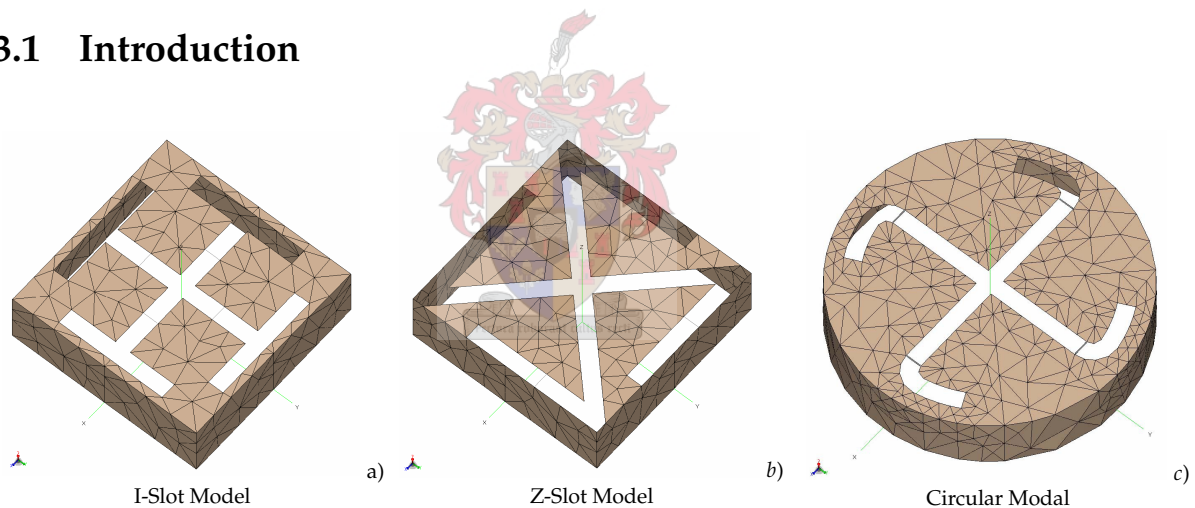
Figure 3.1: Models used for investigation

- Paragraph objective:
    - Shortcomings of the computational modelling code have previously prevented accurate modelling of an existing element
    - Search for equivalent models
    - Study input impedance of equivalent models
    - Study the far field pattern of equivalent models
    - Investigate the effect of a top hat
    - Study an accurate model
    - Take a brief glance at cavity properties

- Purpose of the above objectives

  - To evaluation of the impedances for purposes of effective design

  - To model the combined feeds of an element in MicroWave Office

  - To evaluate of far fields for calculation of low angle gain

  - To building a simple model of a top hat

  - To evaluate an accurate model of the existing element for further investigation of arrays

- Method adopted to attain objectives

  - Equivalent models were defined on the basis of slot length and cavity size

  - The input impedances and far field patterns of the equivalent models were evaluated with Feko

  - Far field patterns and impedance responses were evaluated for a range of top hats varying in size and height

  - A new computational modelling code made it possible to model the existing element, which then made it possible to evaluate the problem

The first problem that was presented in moving forward to the analysis of an array with the existing elements, was the modelling of the existing elements. The EditFeko modelling code prevented the modelling of the element, and this is described in Appendix B. Other models that could be of some equivalent form were therefore considered. These equivalent models are presented in Figures 3.1 *a* and *b*. The first model was more representative of a design consideration (see Section 3.2.1).

The responses of the impedances were evaluated against the criterion presented in Section 2.6, for the purpose of passively matching the feeds to a system impedance of 50Ω. When this could not be achieved, the values were taken from the Feko analysis and used for the combined feed in MicroWave Office (see Section 3.3.1.2). The far fields were evaluated for the different models with the purpose of establishing how they might contribute to the low scanning capacity of the array.

As part of the far field analysis, the top hat was presented (see Section 3.2.3) to establish the role it plays in the low scanning capacity of the array. It was found to be responsible for this. The top hat, however, not only changed the far field pattern but also changed the frequency response of the impedances of the elements. Therefore it was decided that the top hat should be presented as a basic model that consisted of lumped elements.

For the last analysis presented in the chapter, an accurate model was evaluated. The modelling of the accurate model was made possible by the release of the CadFeko tools, which offered

solutions to all the problems that the other CAD tools had presented. In this analysis it was also possible to evaluate the top hat more accurately, as well as to determine how it contributes to the efficient performance of a single element.

The last section of this chapter supplies a quick overview of cavities. The properties of cavities were not investigated as this was not considered of great importance, as the cavity of the existing model has a cut-off frequency that is above the operating frequency of an element.

3.1.1 Literature Study Regarding Crossed-Slot Cavity-Backed Elements

Before the modelling of the elements of the array, a background study was made of early crossed-slot cavity-backed elements used for satellite communications as presented in [6], [2] and [3]. The operating frequency in [6] and [2] was low, to the order of 240 and $400MHz$, that is in the UHF band, whilst the element in [3] was in the L-Band. One thing that was known of the UHF-band was that the radiators are large, and arrays would be out of the question. This meant that the radiating element to be used had to be able to utilise low angle elevation. With most conventional radiating elements failing the mechanical and electrical requirements, slots were given a favourable consideration. It presented low elevation gain towards the horizon, without presenting any significant drag factor change to a craft and a crossed configuration also makes it possible to obtain the necessary circularised polarisation required for satellite communication. As only the upper hemisphere requires coverage, the slot is boxed in by a cavity. It is shown in [11] that a cavity causes the slot to radiate only into the hemispherical region above the cavity; it is also shown that a cavity adds susceptance and increases the impedance of the slot. However, if the cavity depth was a quarter wavelength long, given the waveguide properties, zero susceptance would be added to the slot, and the impedance effectively would be doubled. The cavity presented a problem in that it increased the size of the element considerably, creating a large drag factor to the craft, unless sunk into the craft, which has its own disadvantages. Thus Lindenberg [2] proposed to reduce the cavity, by dividing the cavity in half along the H-plane, thus not influencing the field within the cavity and parting the two halves, to each lie 90 degrees from their original position. The result was a shallow cavity that brought down the height of the element, and is still used in size reduction. In addition to [2], [6] shows how the Voltage Standing Wave Ratio (VSWR) was influenced by the addition of ridges in the cavity and how this improved the bandwidth, alternatively the influence of the cavity depth and the slot dimensions were investigated and it was noted that this changed the resonant frequency, by either lowering it or increasing it.

In [3] Manshadi makes reference to some interesting methods for reducing the physical size of the element. The argument for this is that the large element structures presented in [2] and [6] are not suitable for phased-array applications. In producing smaller elements, non-uniform slots are used, which are based on results from non-uniform slots in [6]. These slots were broadened at the end and this is said to have an effective longer length than uniform slots, thus

reducing the resonant frequency and even improving the bandwidth. However, effectively the element that was presented as part of the array that was required to be investigated did not make use of any end loading, as the curve on the slot remains uniform. Thus, when it came to developing a simplified model, the end-loaded technique was not used with the Z-slot, it was considered necessary to keep the slot uniform, and bending it when it reached the confines of the cavity walls in order to lengthen the slots.

Utilisation of long slots in a small cavity resulted from the physical model. With a radius of $35mm$, the circular cavity required a cut-off frequency of $2.51GHz$ for the lowest order mode, the TE_{11}, with the simplified structures it therefore had small cavities for the slots to operate below cut-off frequency of the cavities, as is the case with the element within the array.

The second simplified model that was used also showed a resemblance to the end-loaded slots, but the design of these slots came from the single folded slot as presented in [12]. With two of these slots an I-shaped slot was obtained fed by a coplanar waveguide (CPW) transmission line. The CPW was removed and replaced with the conventional transmission line feed, that was to be utilised throughout this investigation. Because of the physical design of th I-shaped slot, the properties described in [3] were found to be present in the I-shaped slot. These included achieving a lower resonant frequency with considerably shorter slots.
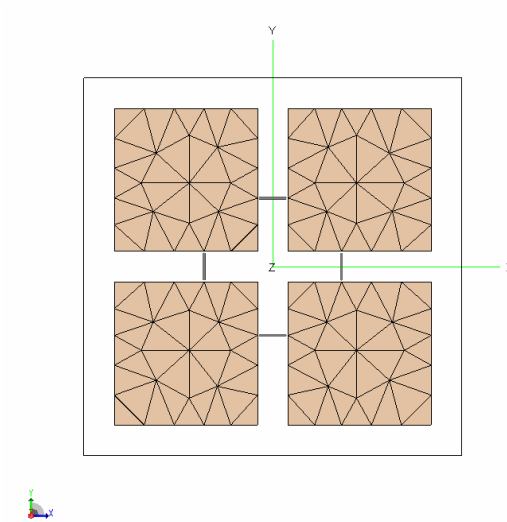
Figure 3.2: Annular slot model layout

3.2 Possible Geometries

3.2.1 Annular Slots

The first approximation was an I-shaped slot, though the geometry took on a shape that was more of an H, since the branches were extended at the ends in order to reduce the overall cavity size and maybe even find an equivalent square geometry that might replace the circular cavity, since manufacturing of square tubing apparently is much more economical and it is simpler to work with. Reducing the cavity and changing the slot geometry, while including the second slot for the crossed slot configuration, yielded an antenna configuration similar to that of an annular slot antenna. In the first annular design the calculation analysis was performed on a cavity above which were four 'patches', thus forming annular slots between the patches and the cavity walls. Figure 3.2 illlustrates the layout of the annular slot as seen from the top, with the feed wires present. This is a simple design that looks like a microstrip patch array of four elements contained in a cavity. The physical dimensions are as follows:

Dimension	Measurement [mm]
Cavity Size	50
Cavity Height	15
Slot Width	4

Table 3.1: Physical dimensions of annular slot model
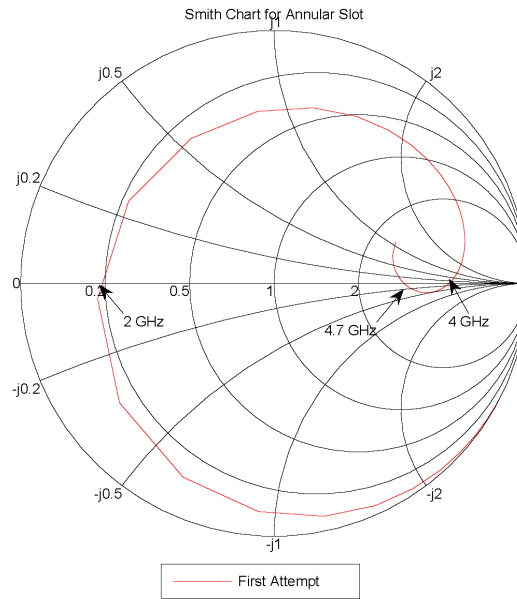
Figure 3.3: First annular calculation

3.2.1.1 Results

In the following section it should be noted that, for the next three equivalent designs, the active impedance referred to is the active impedance of a single feeding wire that is used to excite the geometry from the four feeding wires as calculated by the OS card in Feko, which takes into account coupling of the feeds. It was not necessary to consider all the feeds as all the feeds exhibited the same results, and thus a single feed was considered for the active impedances.

3.2.1.2 Results: Input Impedance of feed section

The analysis of the annular slot proved much more troublesome than had at first been expected. Instead of the expected frequency that it was designed for, $2GHz$, the computation yielded a resonant frequency of $1GHz$. At $1GHz$ there was a significant high impedance that lay so close to the edge of the Smith Chart that it could be interpreted as a open circuit, which is not a good starting point to work from.

The fact that the resonant frequency lies at half the designed frequency can be explained on the grounds of the fields that were excited in the slots. In the case of an annular slot the frequency of the field that is excited in the slot can be calculated by the slot length, as a full wave length field will be supported. On close investigation of the fields excited in the slots it was possible to prove that the effective length of the slots was not the length it had been designed for during the modelling process. A cursory look at the model reveals the four routes along the fields that are excited, but the results forced a closer look at the details.

The results indicated a resonance at half the designed frequency, which meant that the fields excited in the slots should be analysed more closely. An annular slot supports an electric field of full wave length within the confines of the slot. Thus the effective length of an annular slot would be the length of a full wave of the natural resonant frequency that will be excited and the annular model was designed on this basis. However, the fields excited in the slot model were not following the rules dictated by a simple annular slot, but had literally found some loopholes around it. It is not correct to state that the excited field did not obey the rules, as this would be impossible, but it should be made clear that the model was responsible for the bad performance of the excited field. Rather than supporting the full wave field that it is expected to be excited along the patches, which form the annular slots, fields of other frequencies are also supported. The field that was excited in the slots had enough freedom and a variety of routes of various lengths in which it could be excited, which supported the excitation of other frequencies. This is why the natural frequency was different to that for which it had been designed. When evaluating these results against the model it became clear from the layout of the model that annular slots of various lengths could be extracted from the model, which proved the presence of low frequency resonance in the model, and the presence of the designed frequency. To make the model more acceptable for use as a possible equivalent model to the original element, required that the resonance at $2GHz$ be improved. In improving the resonance at $2GHz$, the effective length of the annular slots were required to have the effective length of a $2GHz$ wave. There were two possible ways in which this reduction of the effective slot lengths could be achieved. Firstly, by reducing the physical size of the element or else by just shorting out the unwanted routes along which the field could be excited. The latter technique was used because of the simplicity of implementation and because the first technique was not considered as one of the options as the dimensions of the model were tried as true as possible to the original element.

In order to shorten the effective length of the slots, shorting pins were introduced in the model. The shorting pins were introduced at the corners of the cavity, for the simple reason that the cavity walls were an extension of the ground plane, thus connecting a patch to the cavity wall with a pin would produce the necessary effect of a short and locating the pin in the corners gave a large degree of freedom on the feed location, for reasons indicated in Section 2.6 regarding the input impedance of a slot. The primary purpose of the shorting pin was to to force a null in the field excited in the slot, which would in effect shorten the routes so that the field would have to conform to the restriction that the shorting pins placed on the effective slot lengths of the model.

The impedances of the $2GHz$ resonant frequency improved, as is shown in Figure 3.5 and the input impedance has improved even for the low frequency. It was thought that the input impedance could be improved by shifting the location of the feed by using the technique introduced in Section 2.6, which is indicated in Figure 3.4. For the purpose of the analysis, three different feeding locations were decided on (indicated as A,B and C), while the other wires in Figure 3.4 illustrate the shorting pins. Figure 3.5 gives an indication of how the active
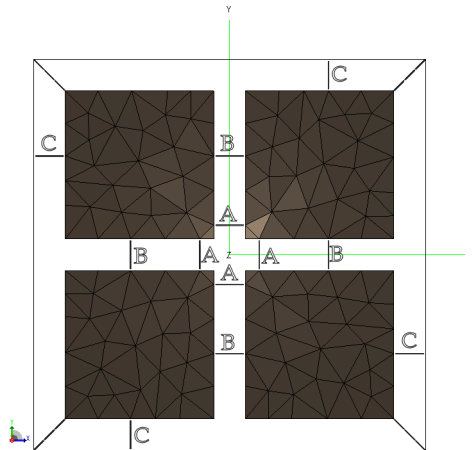
Figure 3.4: Feeding points used to establish better performance

Feed Point	Distance from short [mm]
A	45.5
B	37.5
C	12.5

Table 3.2: Feed locations on annular slot model
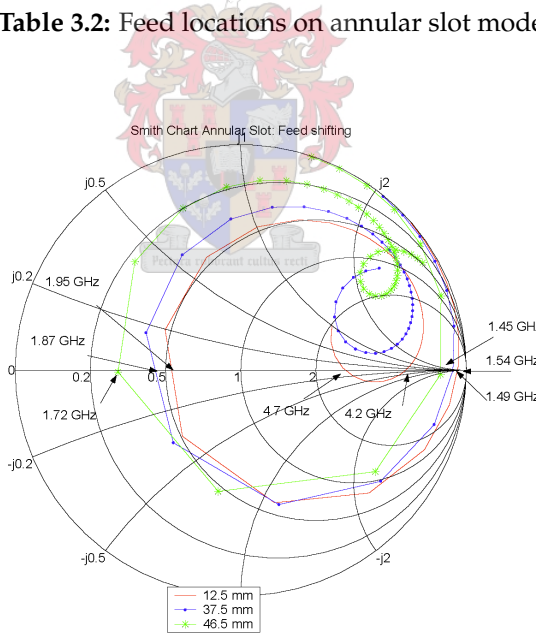
Figure 3.5: Finding good match for feed location

impedances of the feed wires are changed when the feed is moved closer to the shorting pins. The values on the graph legend indicate the distance of the feed from the shorting pin.

It is clear, from the location of the feeding pin, and shorting pin that a sufficiently low input impedance could not be realised for the low frequency of resonance, as the feed would have needed to be very close to the short and the bottom line would have been that the feed would in effect be shorted out. The investigation was taken right to the end where the short was located.

Nor could a high enough input impedance be realised for the $2GHz$ frequency (for which it had been designed) by moving the feeds towards the centre of the slot. From an impedance point of view, the geometry of annular slots is thus not a good equivalent design to work with.

The resonance found at $4GHz$ was the most incomprehensible as resonance shifts as the feed is relocated, or, for this specific case, as the feed is moved away from the centre of the slot. This is not unique as it was first recorded by F. Manshandi in [3], when he noticed that the resonant frequency increased as the feeding probes were brought closer to the centre of the cavity. It was also indicated in the changes of the frequency that changed where S_{11} passed through the real axis of the Smith Chart of Figure 3.5.

3.2.1.3   Results: Far Field Pattern

As the far field pattern was to be evaluated later in the project, it was decidedthat the effect of the shorting pins on the far field pattern of the annular slot element would be investigated and to get a feel for the field pattern that would be involved. Therefore the far field pattern was computed both for the case where the shorting pins were present and for the case where the original annular slot model was used.

When the shorting pins are introduced the field pattern changed remarkably at the low frequencies. The shorting pins passed current on to the cavity side walls, causing them to radiate as well. All the power that was radiated was no longer vertical to the cavity, but spread more in the azimuth plain, with four peaks, each peak lying in line with the centre slots and perpendicular to the cavity walls. Figures 3.6*a* and 3.6*b* show the change that took place by comparing the directivity of both the shorted and unshorted annular slot fields at the same frequency, which would be the frequency where the annular slot would have to operate.

With shorts present in the slots   a)   Without shorts present in the slots   b)
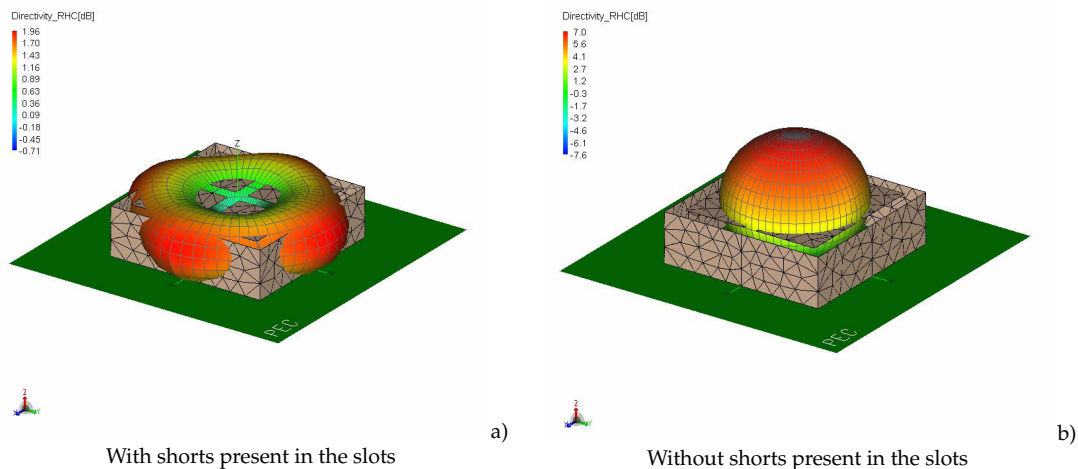
Figure 3.6: Far field pattern of annular slot at $2GHz$

The far field patterns are illustrated in figure 3.6, as these field patterns might form the basis for the expectations of how the far field might radiate for a given structure.

a)At $1GHz$ b)At $4GHz$
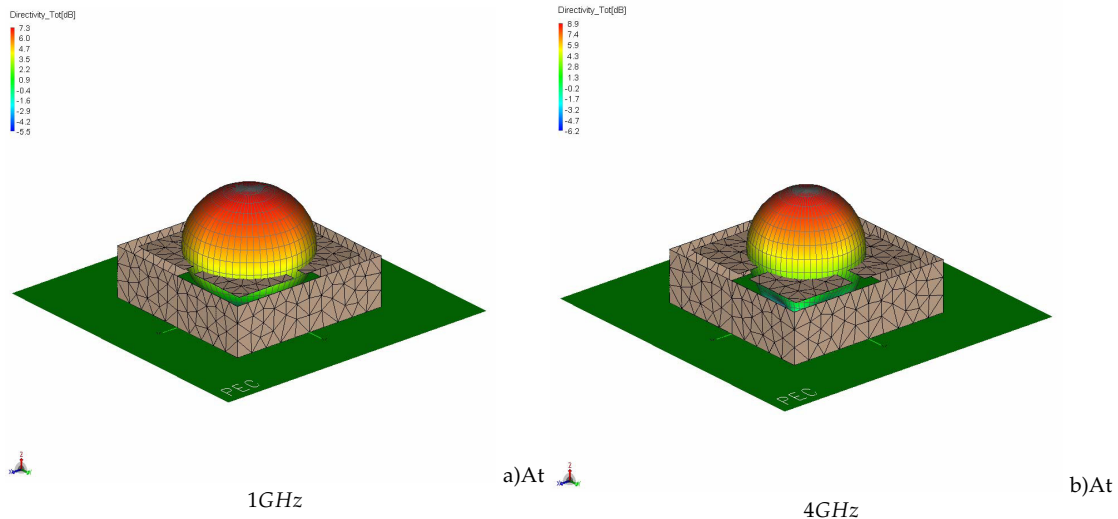
Figure 3.7: Far field pattern at other frequencies

In Figure 3.7*a*, the dominant frequency field is presented with the absence of the shorting pins, just to indicate the potential of high gain that the element has at the low frequency end of $1GHZ$. In Figure 3.7*b*, an intriguing result prevails that was included in the impedance result of the annular slot. The high directivity for this frequency, $4GHz$, desired from in the presence of the feed so close to the centre of the slot. A strong field was excited between the feeding ports, because the field at that frequency dropped when the locations of the feeds were shifted, thus the feeds contributed to the manner in which certain frequencies were supported in the slots.
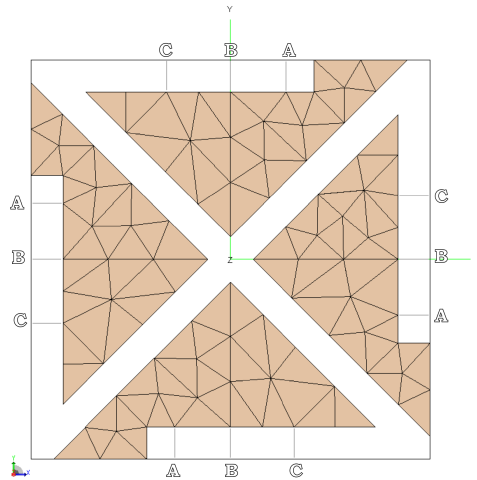
Figure 3.8: Z-Slot model layout

3.2.2 Z-Slot

Due to the fact that the annular slot gave so poor a performance and because of the unpredictiveness of the excited fields in the slots, a new geometrical model was needed to act as an equivalent model for the manufactured element. The geometry was changed, as it was thought that the annular design represented more of a model microstrip patch array than the annular slots. The idea of a new model was guided towards a model that might have the necessary effect on the active impedance of the slot, and slots that would resemble the basic form of the original slot layout. The model that was developed was a crossed double Z-slot geometry. The geometry of the Z-Slot is described as a slot running toward opposite corners of a rectangular cavity, 'connecting' the two corners and turning at the corners to run along the cavity wall, forming a Z. Figure 3.8 illustrates the visual layout of the geometry.

Dimension	Measurement [mm]
Cavity Size	50
Cavity Height	15
Slot Width	4
Slot Length $\ll$ to Cavity Walls	33.5

Table 3.3: Physical dimensions of Z-Slot model

Results obtained from the input impedance on a slot as discussed in section 2.6 suggested that finding a good active impedance might pose a problem. This had also come forward in the results of the investigation into the annular slot model. However, the investigation was continued in the hope that a good impedance match would be found.
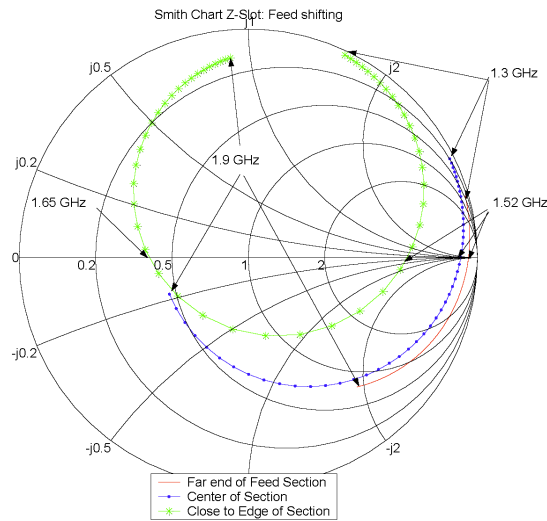
Figure 3.9: Active input impedance of crossed Z-Slot

3.2.2.1   Results: Input Impedance of feed section

To illustrate the results for the crossed Z-slot, the impedance of the model was calculated using three feeding locations along the length of the slot. These feeding locations were placed along the section of the slot that runs parallel to the cavity walls. This was a logical choice: results concerning the impedance of a slot have indicated that the input impedance close to the centre is high, because of the large electric field in the slot at this region. The original design also had the feed towards the end of the slot to match it to the feed wires. The calculated results are illustrated in Figure 3.9. The natural resonant frequency for which the design was developedwas $1.5GHz$. It yielded the first positive result so far for an equivalent model. The three plots show the input impedance of the structure with the zero crossing of all feed locations at the designed frequency, except for the feed located close to the slot's end, which was another zero point crossing at a higher frequency with low input impedance. The result of the feed close to the end of the slot end could be predicted from the analysis performed on the added induction of the feed, as presented in Section 2.6. Moving the feed towards the slot's end led to the reduction of the input impedance, but there was an effect of increased inductance on the input impedance, governed by the inductivity of the feed and that of the slot's edge, as the feed becomes closer as demonstrated in Section 2.6. This supported the validation on the impedance close to the slot's short, and showed where the resonance of the higher frequency was introduced.

Another principle that was worth considering was the effect on the model's properties when the slot length is adjusted. With the Babinet Principle being used as a handle for analysis, in other words, by evaluating dipole properties and predicting what would take place, it was gathered from the complementary pair equivalence that the effective length of a slot would increase by the same measure as the increase in effective length of a complementary dipole,
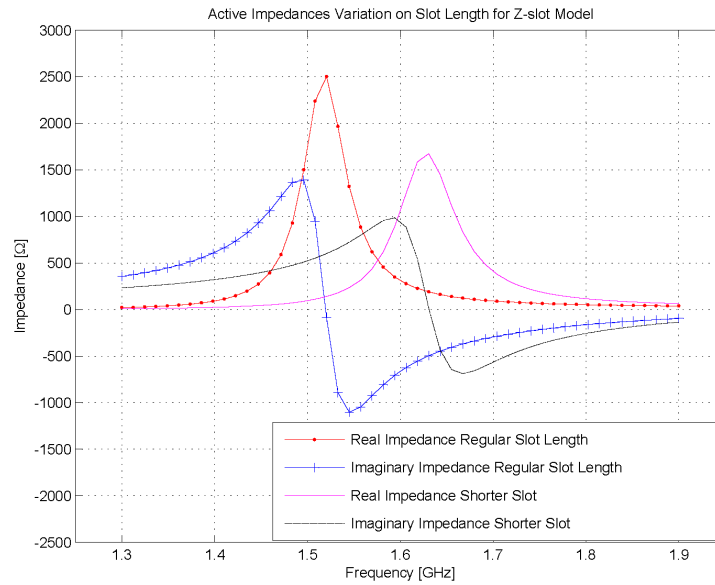
Figure 3.10: Length reduction of slot

when that is increased. The effect it has on the natural resonant frequency of a dipole, which is established fact, is that an increase in length of the dipole reduces the natural frequency of resonance for a dipole. This consideration was validated by a reduction of the slot length as illustrated in Figure 3.10, which clearly shows an increase of natural resonance, as was expected, this is also mentioned in [6]. The graph indicates that the input impedance was also reduced with the reduction of the cavity. However, the location of the feed was kept constant and thus the feed was in effect brought closer to the edge of the slot, which explains the lower input impedance. The Z-Slot can be tuned just like the End-Load Crossed-Slot that is presented in [3] which is easy to tune for a frequency well within its range. this raises on the possibility that the Z-slot could be used as a variation of the End-Loaded slot, but further investigation of this would be required.

3.2.2.2 Results: Far Field Pattern

The far field results of the design highlight aN interesting aspect, which points out a very interesting result when compared to the results from the annular slot discussed in Section 3.2.1.3. It was shown in the previous section that the gain of the total, as well as the circular polarised gain in the far field pattern, comprises four beams, spaced in a 90 degree rotation from one another around the Z-axis, in the case where the shorting pins are present. The total field for the annular design displayed the same field distribution, with the only difference being the direction in which it radiated to the horizon. The total gain is illustrated in Figure 3.11, and displays the same far field pattern as that of the annular slot.

A greater difference, however, was found in the directivity of the circular polarised far field
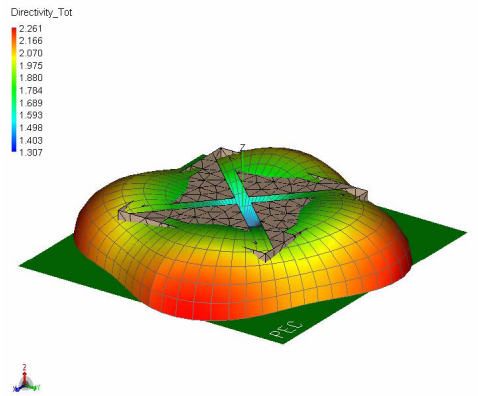
Figure 3.11: Total far field directivity for Z-Slot
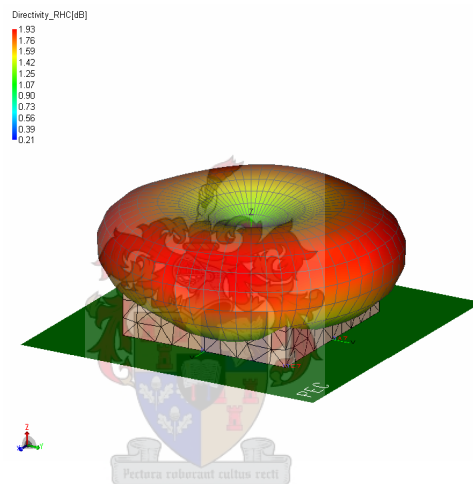
Figure 3.12: Right hand circular polarised far field directivity for Z-Slot

pattern. Figure 3.12 displays this interesting characteristic in the pattern for a Z-slot model. It is thought to have the same beam-like functionality as the annular model or, put differently, it was considered to have four peaks in the azimuth pattern. Instead, the circular polarisation far field pattern is more representative of a beam, though not entirely like a beam, directed more vertically with evenly distributed gain in the azimuth where the maximum gain is found, and lower gain looking straight up towards the sky.

To conclude, the annular model led to useful results for the analysis of the far field pattern, even though it was a weak model to work with. Together with the Z-Slot model, it led to a basic understanding of the far field pattern. This investigation has indicated that the far field pattern could be predicted by the layout of the slots on a geometry, from possible currents on the cavity walls.

3.2.3 Top Hat

It is known from [1] that the top hat substantialy improves the low-angle performance of the array, while it has a counter-intuitive effect on a single element in that the element becomes more directive with gain towards the zenith instead of the low angle gain. It does not seem possible, though, that the top hat will contribute to the low-angle performance of the array, as the top hat is smaller than the element. For the top hat to improve the low scanning elevation, it has to be a parasitic patch that is larger than the wavelength, in which case it would establish a wave that would creep towards the edges of the surface, as cited in [13]. This is what is puzzling: the top hat acts like a parasitic patch, but, due to its size, which is much smaller than a wavelength, does not create a creeping wave, which might explain the directivity that it brings on to a single element. Another aspect that has not been addressed is that the top hat can also improve the bandwidth of a single element in an array configuration. Reference to this is found in [14], [15], [16] and [17]. In [16] and [17], two parasitic disks are used. The first disk is there to improve the bandwidth and the second disk acts as a director to improve the gain of the radiating element. Extending from these aspects, the investigation that follows will be into the directivity brought about by a single patch and not so much into the bandwidth enhancements that it brings forth, which will be investigated with regard to the cylindrical model of Section 3.3.1.

The impedance change resulting from the presence of the top hat, was at first thought to be due to the following: Aa disc that is taken an infinite distance from the slot it does not couple with the slot feed and the impedance of the slot remains constant. If the top hat is brought into contact with the slot, for example by being introduced in the same plane as the slot, the slot will be shorted and the impedance reduced to zero ohm. Thus the top hat shorts out part of the electric field and this brings about a reduction in slot impedance. Another aspect that should not be overlooked is the possibility that the electric field is no longer just contained within the slot but that a field is established between the element and the top hat, creating a structure that supports a travelling wave along the length of the slot. It would then be found that the coupling between the feeds of the elements slot had increased.

The top hat is the most interesting part of the project design and is considered to be of great importance in the design. From what is known of the design, the array is not as effective without the top hats on the elements. Much thought therefore went into finding an effective way of analysing the top hat and noting the effect that it has on elements before considering a whole array both with and without the top hat. Therefore, in order to analyse what is considered to be the success factor in the design, the method decided upon was to analyse top hats of different sizes and in various height placements above the elements.

For analysis of the effect of the size of the top hat, three different sizes were chosen: a full area, half area and quarter area, with the area indicating the area of the cavity face. The height at these analyses was kept constant. For the analysis of the height of the top hat, a full area top

hat was used, the height of the top hat above the element being varied.

To adhere to the heart of the problem, the model of the geometry to be used was that of the double Z-Slot model. This model was chosen not only for its sound performance, as determined in the previous section, and for the geometrical shape of the slots, which resembled the element that existed already.

3.2.3.1 Results: top hat size

The effect of the top hat size will be addressed first to try and establish a relative model for the top hat. The Z-Slot without a top hat was used as a reference point, from where the properties of lumped elements by means of a Smith Chart were used to find a basic relevant lumped model for the top hat. When first investigated on the Smith Chart, the first factor that was visible indicated a drop in the input impedance of the model and it was thought that a part of impedance was being shorted out.

However, there were changes in the frequency, which cannot be considered an effect of the impedance being shorted out. That is why there was an investigation into a small model. The first top hat introduced in the model was the quarter area, which is shown in Figure 3.14. It did not have a great influence on the far field pattern and thus would not have much influence on the model. In Figure 3.13 the added effect of the small top hat seems to be similar to that of the addition of a shunt capacitor to the element model. With the introduction of the half area top hat, the field is just starting to be directed toward the vertical, but the gain is still considered low when Figures 3.15 and 3.16 are compared. The effect of the half area top hat, it can be deducted that a series inductor was added to the model, as the model is improved, as shown in Figure 3.13. By enlarging the top hat size still further the model changes by more than just the effect that a series inductor would have. Finding the frequency point from the previous values for the full area top hat by using the Smith Chart, will require the addition of an inductor in parallel to the problem.

However, the model is not yet complete, as there is another property of the top hat that influences the model, namely the height of the top hat above the element. This will be considered in the next section.

3.2.3.2 Results: top hat height

The height of the top hat did not have as great an influence on the frequency response, but it did influence the model enough for it to be considered an integral part of it. Lowering the top hat was seen to change the input impedance of the second natural resonance that was introduced by the full area top hat of the previous section, and this made for a good match. When the height of the top hat was increased, this resonance disappeared and the impedance increased.
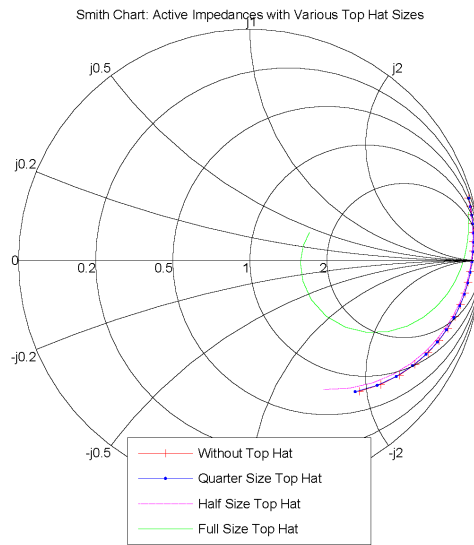
Figure 3.13: Varying top hat Size
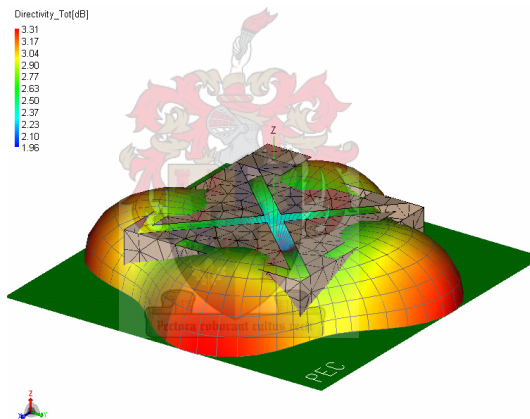
Figure 3.14: Far field pattern for quarter area top hat
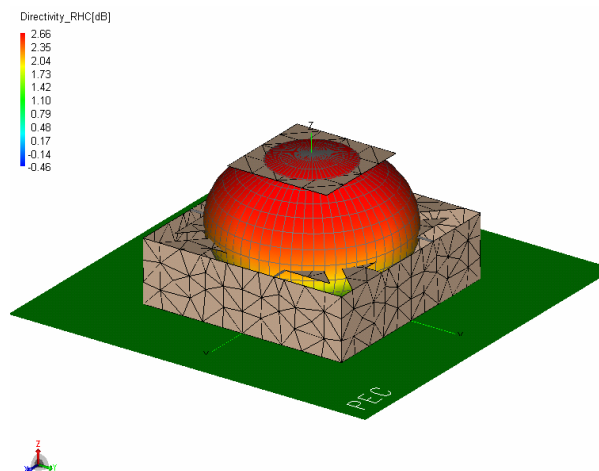
Figure 3.15: Far field pattern for half area top hat
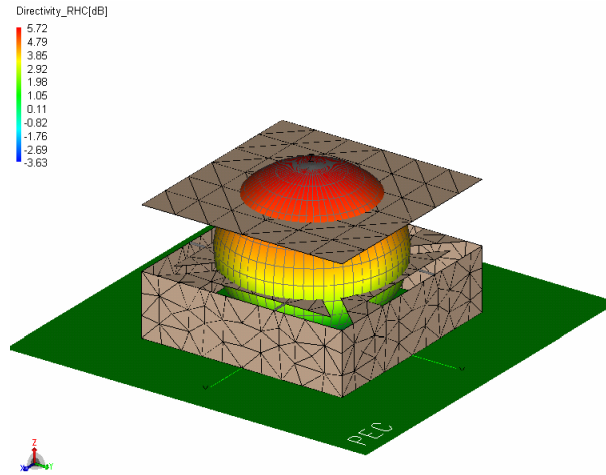
Figure 3.16: Far field pattern for full area top hat
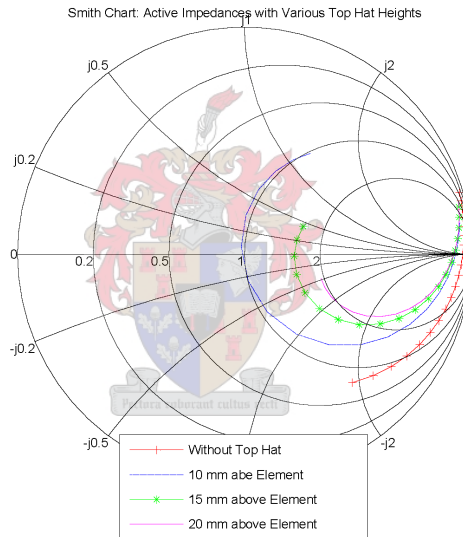
Figure 3.17: Varying top hat Height

This second natural frequency of resonance was found at a higher frequency, and changing the cavity height makes it possible that the impedance can be matched. Lowering of the top hat is expected to short out the impedances. This is a very basic model with regard to working with the top hat for design purposes. The results presented in Figure 3.17 indicate that the height of the top hat is better modelled as part of the shunt inductor that was introduced by the full area top hat. Thus a very simple first attempt at creating a model for the top hat would look something like the model presented in Figure 3.18.

Furthermore, it was established that the top hat functioned like a director that varied the width of the beam by varying the size and height properties of the top hat. These properties of the top hat that directed a beam to the vertical verified the existence of an electric field between the element and the top hat.
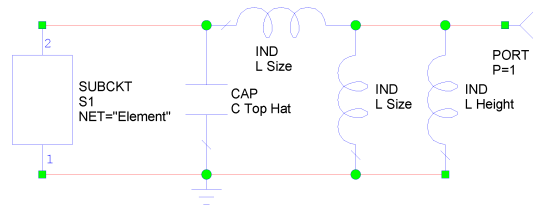
Figure 3.18: Model of top hat

On a single element the top hat certainly did not seen to contribute anything to the low scanning ability, as it directed the beam to the vertical. Thus it would seem that the top hat would be much more likely to improve the board side radiation of the array, rather than cause the low scanning ability of the array, therefore it could be concluded that a third parasitic disc is not necessarily needed to improve the gain of antenna. It was shown that the parasitic disk contributed to improving the gain and thus acted as a director.
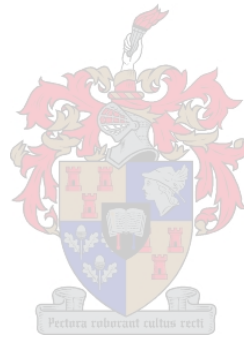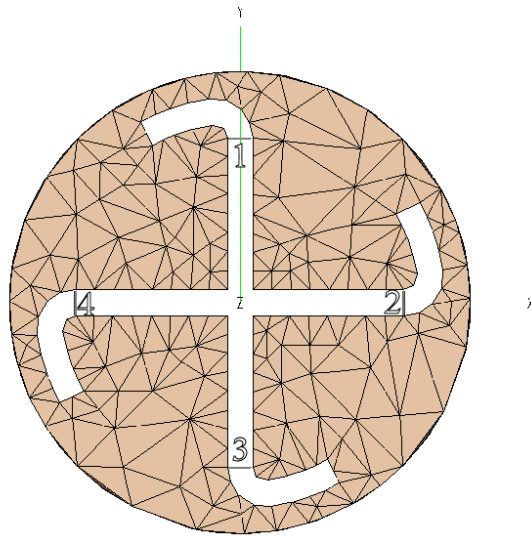
Figure 3.19: Circular model layout

3.3 Accurate Model

3.3.1 Circular Cavity

With the release of CadFeko, a means was found which made it possible to construct the complex circular cavity, including cutting away the S-shaped slots and meshing the geometry sufficiently to produce results from calculations that fit within the area of the design problem. The construction process that was used in Feko to produce an equivalent model is as follows here: The first step involved defining the cavity by using a cylinder. This was simple, as a card was includedon which only the cylinder position, the cylinder radius and the height of the cylinder s defined. After the cylinder is constructed, the properties of the cylinder need adjusting, as the default cylinder is of solid metal. The cavity, however, is known to have a non-air filling and a dielectric substrate, but for keeping the problem as simple as possible to keep the computational time to a minimum, the cavity's interior properties were set to free space. The second step was to make the cavity compliant with a perfect electrical conducting ground plane, to be introduced with the BO card in EditFeko. This was achieved by deleting the bottom face of the cylinder. Alternatively, a circular disc could be created and subtracted from the bottom of the cylinder. The third step was creating the slots at the top of the cavity. The first part of the slot was formed by the perpendicular slot crossing, by constructing a polygon from the centre of the cavity towards the edge. The second part of the slot consisted of a curved piece running tangential to the edge of the cavity wall. This part of the geometry could be constructed by using two elliptical discs that were subtracted from one another, with the one ellipse having a radius that formed the outer edge, and the second ellipse having a radius suitable to form the inner edge of the slot. Once subtracted, these elliptical discs formed a ring that was split in
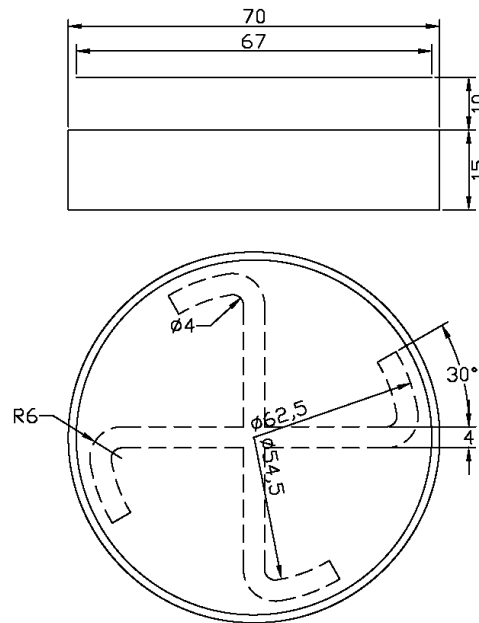
Figure 3.20: Dimensions of element modelled

two, and then another split of 30° was performed on one of the sections, so that only a small piece of the ring remained as part of the polygon while the unwanted parts of the ring are removed. The third part of the slot was the transition from the straight segment of the slot to the curved segment. A technique similar to that described for the curve edge was used, subtracting two elliptical discs. Copies of the all three parts of the slot were made and the transition area was subtracted from both the straight and curved segments of the slot, yielding truncated area. The truncated area is an unwanted area and needs to be removed from the desired slot area, however it also contained areas of the slot. Using the split, the area that formed part of the slot was removed, yielding only the truncated area which is then again subtracted from the original parts of the slots. The remaining wereas are then unioned together to form a quarter of the slot, which was then copied and rotated by 90° each time to form the complete crossed-slot geometry. Uniting the slot areas, this area was subtracted from the cavity so that the result was two slots which were backed by a cavity on an infinite ground plane. Figure 3.19 shows the geometry that was created in CadFeko and meshed. The figure was extracted with the use of PostFeko.

3.3.1.1 Results

As the model of section 3.3.1 yielded some segmentation violations, because the connection points on the areas of the slot did not line up perfectly and the meshing of the geometry yielded some illegal triangles, it was necessary to use a different method for creating the geometry In order to do the calculations on the circular cavity. Most of the geometry was retained, and only the way the slots were modelled in the geometry was changed, as well as the total construction
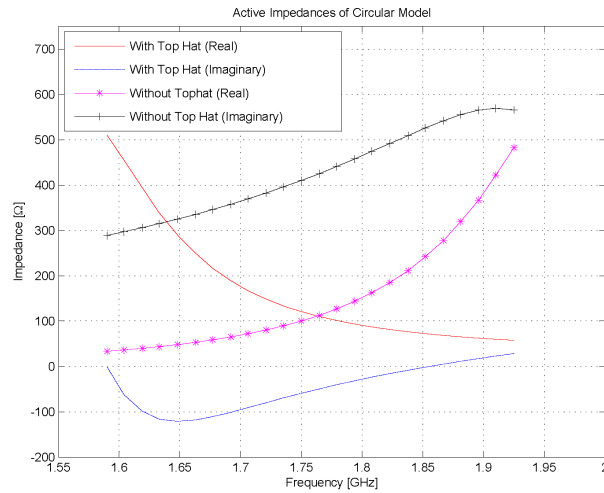
Figure 3.21: Active and passive input impedances

of the element. The straight segment of the arm stretched only to where it joined the transition segment, the curved segment also extended to where it would meet up with the transaction area. The transition curve was created as a circle at the end of the straight slot segment. This was then rotated around the centre of the cylinder. Simple trigonometric equations were used to calculate how much rotation would be required for the tangential points of the transition area to connect to the points of the other areas that formed part of the slot. By using this method it was possible to eliminate the small illegal triangles that were present on the first circular model. After the quarter of the slot had been subtracted from the cavity, the model was split into quarters. The quarter containing the quarter segment of the slot was kept and the others discarded. The total geometrical model was then created a quarter segment. The reason for cutting the cavity into quarter segments involved meshing purposes necessary for when the element would be contained in an array where the elements were close to each other. For this thesis, the elements in the array were to be spaced roughly 5 mm from each other. A general rule is that the closer the elements are to one another the finer the meshing should be in this area, as is shown in Appendix B in the evaluation of the use of the FM card. The general rule of thumb for the dimensions of meshing in such an area stipulates be a third of the distance between the elements. The reason for the spacing of 5 mm between the elements involves in the meshing of the problem and the existing array layout, which made it necessary for the elements to be spaced as near as possible to each other while not violating the meshing rules. A mesh size that did not produce too many triangles and thus also reduced the memory requirement of the problem and the amount of time spent on the calculation of the problem, was necessary.

For the circular element, two approaches were taken in considering the active impedance of each feed of the slot, due to coupling between the feeds. The first approach was to consider the absence of the top hat and the second approach was to look at the properties introduced by the top hat, to try and shed more light on the performance of the array in the end.

From Figure 3.21 it is clear that the active impedance with the top hat was in the order of $70 + 0i\Omega$. This indicated that there is resonance at the frequency of $1.9GHz$ in the slots with very low impedance, which made it attractive. However, the passive impedances also needed tobe investigated to determine whether the structure would have resonance in passive mode at any frequencies within range of the active mode, in order to establish how coupling influenced the impedances. In this case, the difference between the passive and active modes was that a single port was fed in the passive mode, while for all ports were fed simultaneously in the active mode, and thus each port was under the influence of the coupling of the other ports. In Chapter 4, the calculation of the active and passive impedance will be shown to explain how it is derived. The technique used to calculate the active impedances in this chapter is similar to that used for calculations of the active impedances of the array, with the only difference being that the element is not considered to be in the form of an array of slots, but as a single element. The feed of a single element was then recreated in MicroWave Office by combining the results of the four ports by which the element was fed. The feed network required matching to the active impedances of the ports, since it is known that a single element is resonant.

The impedances of the feeding ports were also investigated in the passive mode, as illustrated in Figure 3.22, to determine how the top hat influenced the impedances.

The figures indicate that there was no natural resonance in the nearby frequency range for the passive impedances of the feeds of both the element with the top hat and that without it. However, the effect of coupling produced by the top hat could be shown on the Smith Chart by evaluating the differences in the active and passive impedances of the different models. Through this approach it could be shown that, due to poor coupling between the ports the reflection coefficient of a single feed was not influenced by the other feeds of the element in the absence of the top hat. This is confirmed in Figure 3.23, where the coupling of the feeding ports are shown. However, there was a strong influence on the reflection coefficient of a single feed when the top hat is introduced in the active mode. The effect of the improvement on the reflection coefficient of a single port could be explained by considering the phasing of the coupling between opposite elements. It was shown that the phasing of the two ports found on the slot crossing the slot on which the investigated port lay was influenced little by the presence of top hat, and, from the size of the difference in magnitude that was presented in the results, it could be shown not to make any significant contribution to the impedance of the ports. There was a significant change in the phasing between the two opposite ports on the slot, at $1.9GHz$ the phasing was similar and contributed to constructive interference along the slot. From the phase differences of these ports, that is, the opposite ports, it could be shown that there was no natural resonance supported in the slot without the presence of the top hat, as the phase difference between the opposite ports droped by 90 degrees to become similar. This strong mutual coupling and the phasing clearly indicated the presence of resonance at a specific frequency within the slot. A fact that has to be made clear is that the slot had a length of roughly $80mm$, in which case it would have a resonant frequency at around $1.875GHz$, and
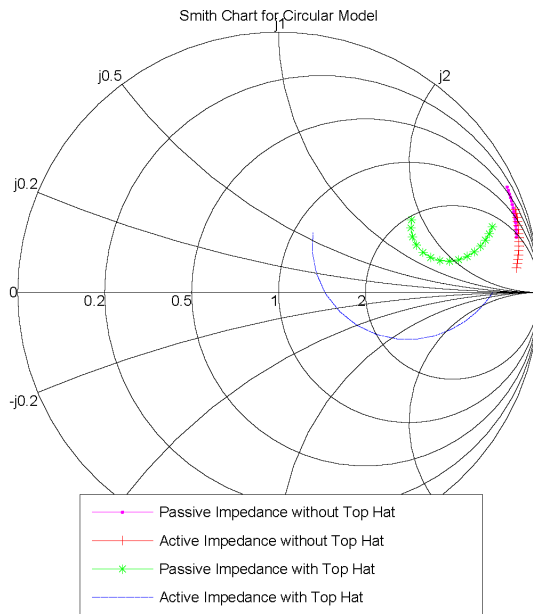
Figure 3.22: Impedance of single port of the model
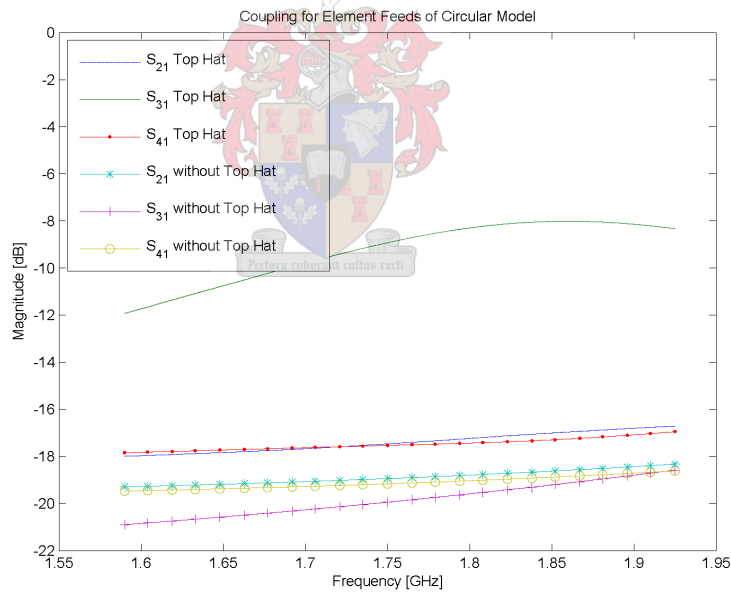
Figure 3.23: Coupling of ports on the element

therefore the top hat contributed to the tuning of the element. If the dielectric of $\epsilon_r = 2.5$ and thickness of approximately $0.8mm$ were used the resonance would occur at roughly $1.6GHz$, as desired, from the effective dielectric indicates in Section 2.5. Figure 3.22 indicates how the impedance of the active and passive modes was influenced by the presence of the top hat when the element was tuned to have natural resonance.

The coupling between the ports was investigated, but the coupling between the slots, that has not been addressed. To address the coupling between the slots a $180°$-Hybrid, together with
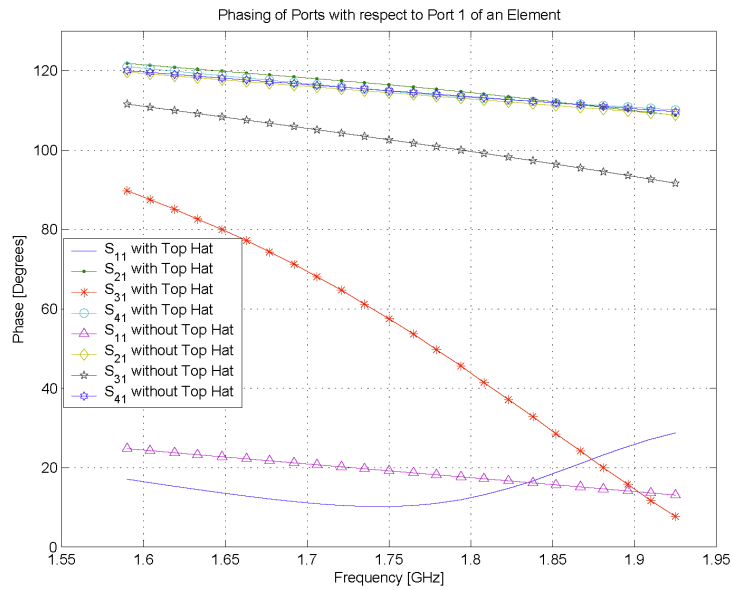
Figure 3.24: Phasing between port one and neighbouring ports
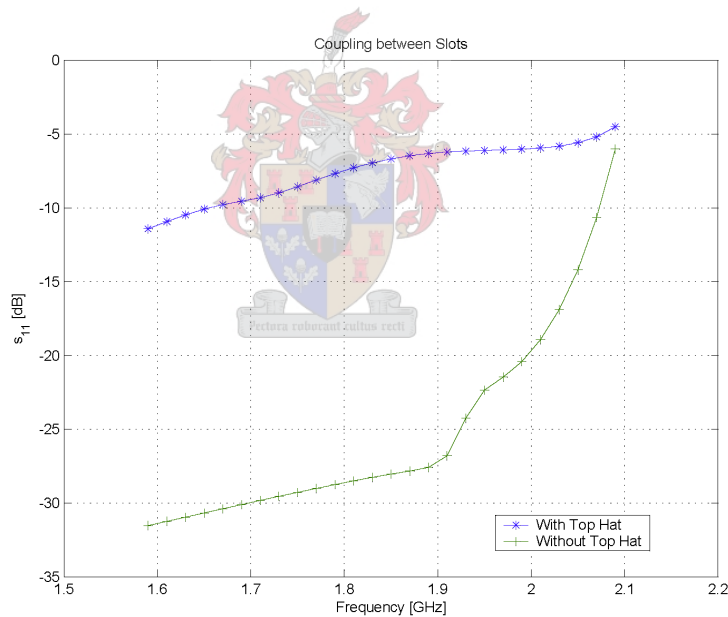
Figure 3.25: Coupling between slots

a 90°-Hybrid feed, as suggested in [2] and [6], has to be used to feed each slot. Figure 3.25 sketches a different picture to that of Figure 3.23. In Figure 3.23 little change is noted in the coupling between the ports of the slot crossing the slot with the port under investigation when the top hat is added. However, evaluation of the slots showed a 20*dB* change and a coupling far less than the coupling to the single ports of the element. It seemed that the top hat had a strong influence, not only on the opposite ports on a slot, but also on the coupling of the slots.
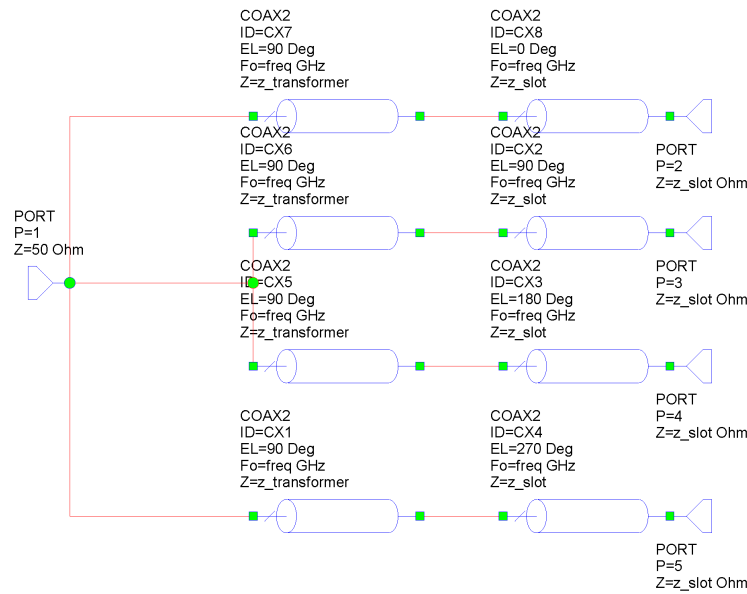
Figure 3.26: Feed 1: One port split

3.3.1.2   Results: Feed

Using the same principle, for the design to consider a single element, a feed network was required for combining the four separate feeds used in the Feko calculations into a single feed or port. The ports of the Feko results differed from the expected results for the design, because the input impedance was not 50Ω and therefore was not matched to the 50Ω wires of the design. According to the results, a shift in the feed would yield the desired feed impedance (as presented in Section 2.6). However, analysis through Feko showed thatsuch a shift created segmentation errors. By evaluating the results that had been obtained in Feko, the feed network was designed for the active input impedance of about 70Ω, to achieve a well-matched model. The problem of overcoming the single field was solved by using MicroWave Office, where the *S*-parameters generated in Feko were imported into MicroWave Office as a four-port network.

The two different techniques that were used to feed a single element were the one port split and the transmission line tap, illustrated in Figures 3.26 and 3.27 respectively.

The first feed network, illustrated in Figure 3.26, resembled the feed network found in the original problem, where the feed from the system was a 50Ω port which was then split into four by transmission lines that ran towards the feeding points of the slots. The impedance at the split was about 200Ω and this constituted the problem of the feed lines thickness. To overcome the problem, quarter wave transmission line transformers were introduced at the feed, which transforms the impedance to the value that was required at the feed location, $Z_{Transformer} = \sqrt{Z_0 Z_{slot}}$. Just behind the quarter wave transformer the phase shifting of the feeds was obtained by transmission lines of various lengths, each one being 90 degrees longer in electrical length than the previous line.
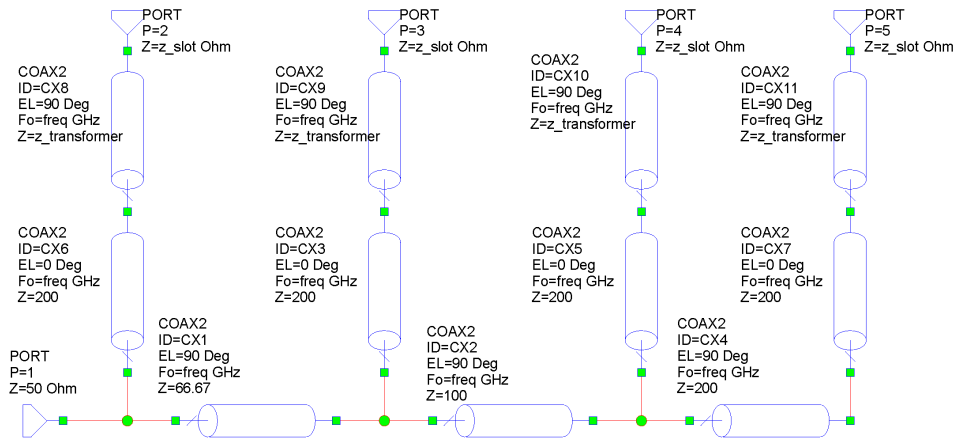
Figure 3.27: Feed 2: Transmission line taps
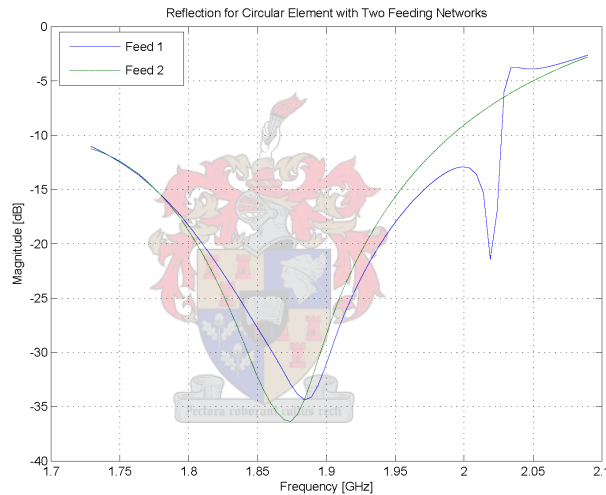
Figure 3.28: Reflection coefficient for a single element using the two feeding networks

In the second feed network, illustrated in Figure 3.27, a transmission line runs from the input port and the feed is tapped from the transmission line. At every tap the impedance of the tapping line was required to be of such an order that a quarter of the total input power was delivered to that line. After every tap, the impedance of the transmission line required adjusting. The phase shifting for the feeds was implemented in the transmission line itself, by tapping every 90 degrees of electrical length. Quarter wave transformers were used after every tap to transform the impedance at the tap to the correct impedance needed at the feed.

The results for the feeding network shows a $-30dB$ reflection coefficient, making both options perfect choices for feeding the element, with similar phasing of both designs indicated on a similar bandwidth. From the result of the feed network, and the fact that the feed was already designed to fit into the confines of the cavity, changing the feed was not considered as it was sufficient for the task. Thus the first feeding network is to be used when an element is being analysed, and also when the elements of the array are being evaluated.
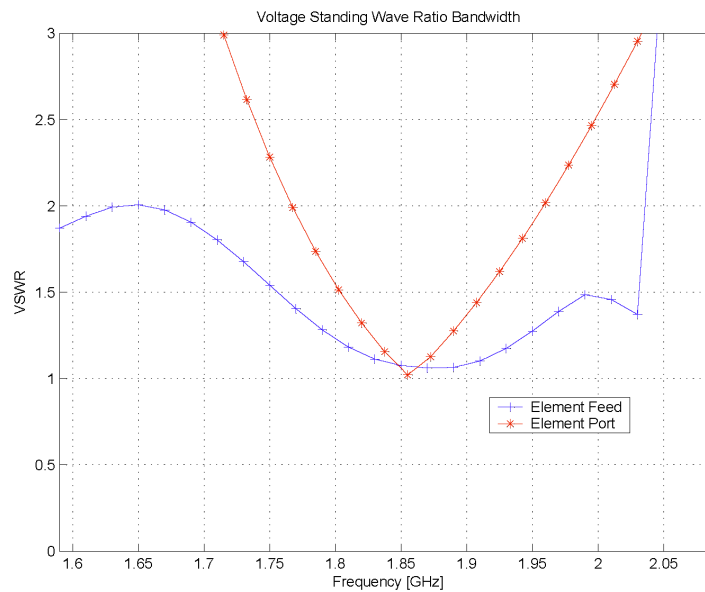
Figure 3.29: Bandwidth of feed and port of a single element

In Figure 3.29 the bandwidth of the element is defined as the frequency range where the Voltage Standing Wave Ratio is smaller than 2. First it was calculated for a single port of the element and for a port impedance of around 70Ω, as this was the input impedance of the port for which the feed network was calculated, in which case roughly a bandwidth of 10% was obtained. When the feed network is utilised on the element, the bandwidth would be increased to approximately 20%, which is an significant increase. The possibility of a larger bandwidth does emerge from Figure 3.29, with the inclusion of lower frequencies. This, however, is not accurate and roughly 2-5% of the bandwidth could be taken off for the absence of the dielectric substrate. Without the top hat the VSWR is far greater than 2 and was dismissed for bandwidth evaluation. Thus the characteristics of a parasitic disk as described in [14], [15], [16] and [17] for improving bandwidth holds true for the top hat.

3.3.1.3 Results: Far Field Pattern

When investigating the fields radiated by a single element it was found necessary to compare the different field patterns of the two different geometries of a single element. The field patterns of an element without and with a top hat were therefore compared. Figure 3.3.1.3 shows the two different geometries. In the previous section, where the effect of a top hat was introduced, how the top hat influences the field pattern of an element was explained. In this section the top hat size is similar to that in the problem of the height and the size of the disk, so that it is possible to clearly indicate how the top hat influences this specific design problem. The feed of the computational design was specified for left-hand circular polarisation, and further analysis introduced losses to investigate the scanning angle. Due to the fact that the dielectric was not considered in the design, the gain was not evaluated, but the directivity was evaluated instead.

Thus the left hand circular directivity will be evaluated throughout the project.

Geometry without top hat   a)   Geometry with top hat   b)
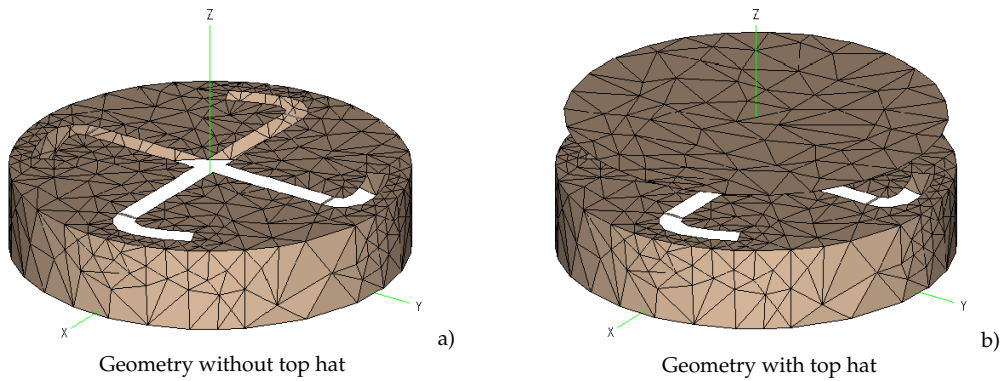
Figure 3.30: Geometrical model of circular elements used in the investigation

Without top hat

In the case where the top hat is absent the radiation field seems to bulge in the azimuth direction where the peak total gain lies at $\theta = 90°$. In satellite communications, however, the interest does not lie in the total gain but in the gain of the circular polarisation. In the case of the circular polarisation, the maximum gain is no longer to the horizon, but has shifted to $\theta = 66°$ from the vertical. A simple explanation for the maximum gain no longer being to the horizon is that of the ground being a perfect electrical conductor so that, the field is made to terminate on the ground, creating linear formulation.

The field terminating linearly on the ground plane is a common problem when scanning down to low angles with scanning array antenna. Attempting to achieve good gain of circular polarisation at low angles therefore is not a simple task.

Further consideration of the results in the half space above the ground, revealed that the maximum directivity is not found along the length of the slot. As in the case of the results established by the double Z-slot, the change in the slot shape shifted the field pattern from the direction of the slot length. In the case of the circular element design, the maximum directivity was found to have shifted by 10 degrees in the azimuth plane, achieving $2.21dB$, magnitude at the peaks.

Figure 3.32 shows a comparison between a measurement taken from [1] and the computational results taken of an element without the top hat. The simulated results do not show a sharp decline towards the horizon, although a sharper decline was to be expected from a practical point of view as the cavity walls have non-zero thickness. The higher peak gain was however not expected either, but could be contributed to the non-zero cavity wall as well. From $40°$ to $90°$ the measured results agree more or less with the simulated results although there are slight variations.
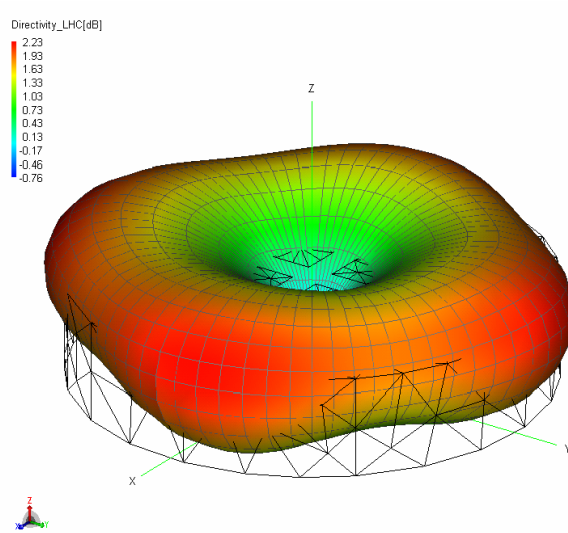
Figure 3.31: Directivity of radiation field for left-hand circular polarisation
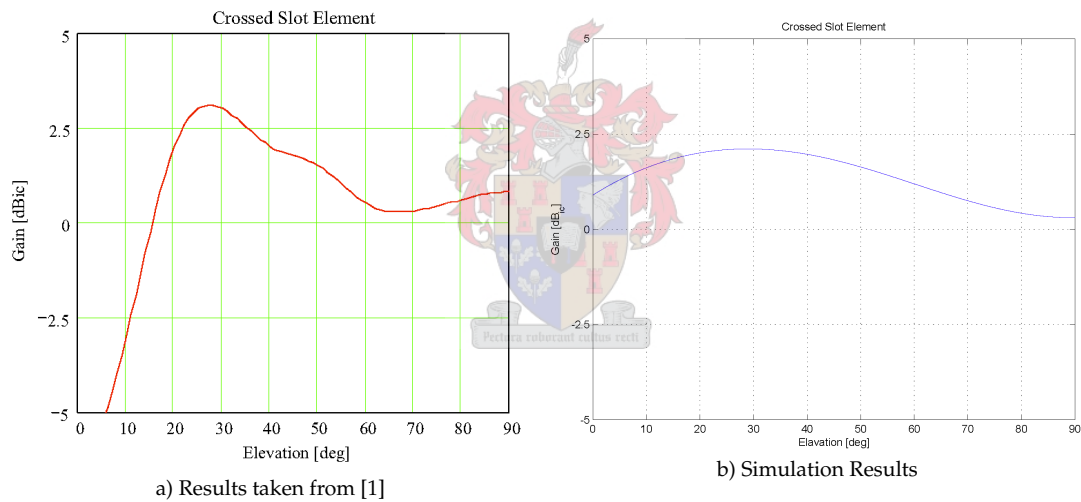
a) Results taken from [1]

b) Simulation Results

Figure 3.32: Geometrical model of circular elements used in the investigation

Without the top hat the element thus had an ideal field pattern to scan down to low elevation angles when used in arrays, a factor which will be considered later in this paper when the array analysis is introduced.

With top hat

In the case where the top hat is present and strong coupling between the feeds of the slot are found, the field pattern can be expected to radiate from the centre of the slots towards the vertical, as is to be expected from the results obtained from the analysis of a Z-Slot model with a top hat. The calculations that were performed on the circular model to yield results for calculating the far field clearly displayed in the results that the far field pattern comprised a primary beam being directed in the vertical, just as was predicted. The calculated directivity of the beam was
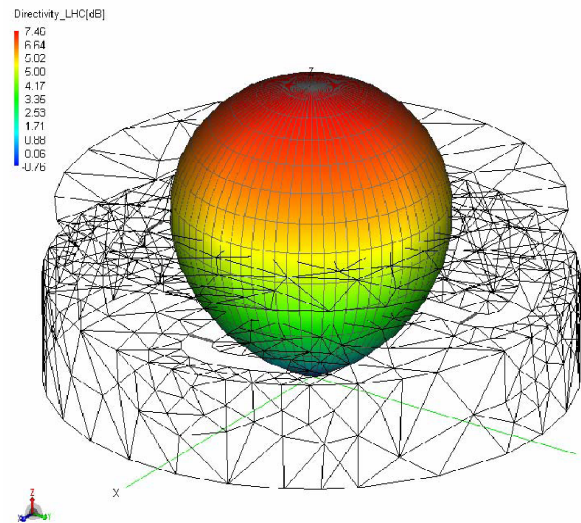
Figure 3.33: Directivity of radiation field for left hand circular polarisation without the top hat with the top hat

$7.46dB$, displaying sound improvement on the results obtained from the directivity calculated for the case where the top hat was not included in the model. It has therefore been established that more power will be radiated by the model within a resulting beam in the case of the model that includes the top hat and a field within the slots which supports the operating frequency.

To conclude: without the top hat, the model radiates to the azimuth plane, which is a good property for low angle scanning, while inclusion of the top hat in the model directs the field to the vertical, with more gain. From this it seems that the top hat model does not indicate good results for low scanning. When the top hat is introduced, the gain of the antenna is towards the zenith, and from the results of the coupling of the slots and ports, a mystery starts to unfold, as it would seem the top hat is gathering the field. However, it might be that the electric field that is established between the cavity and the top hat and couples to fields of other elements in an array is responsible for a wave travelling in the horizontal plane establishing the scanning capacity of the array.

3.4   Cavity Properties

The physical model of the existing element dictated that the cavity of the element could not be considered a true cavity, as the operating frequency of the slots, and thus of the element, was well below the cut-off frequency of the cavity. Thus normal cavity operation for the case of cavity-based slots was crossed off the list for cavity analysis. In the case of a slot backed by a cavity which has a cut-off frequency below that of the operating slot, the cavity functions as a tuning section of the slot, as impedance matching can be done with it [11]. This would be a good field to investigate for future work, as it is thought that the depth of the cavity of the existing model could have been derived from it. In cases where the slot's frequency is below the operating frequency of the slot, no real power will be propagated by the cavity. This, therefore, is the property that dictated the method of conventional transmission line feeding by which the slots are fed. The slots need conventional excitation with transmission line feed, as any attempt to excite the slot through the cavity will result in large losses in power, due to the cut-off frequency. Such useful properties pertaining to using cavities only becomes apparent in arrays, as shown in [18] were cavities are used to disrupt surface waves, so that power would not become trapped in the substrate, but would instead be forced to radiate into free space.

The fact that the cavity appeared to be in cut-off was a large hurdle overcame, as there was doubt about the cut-off of a shallow cavity. However, it was possible for the whole approach to the cavity to not be handled as a cylindrical waveguide. With reverse engineering of the cavity with certain aspects that are presented in [2], it was shown that the cavity was in cut-off. First, the cavity had to be regarded as a square cavity, instead of a cylindrical cavity with wall dimensions of $70mm$ by $15mm$. This provided a quarter wave waveguide length of $\frac{\lambda_g}{4} = 35mm$, which gave an imaginary cut-off wave number indicating that the slots, truly were operating below the cut-off frequency of the cavity. However, it is stated in [6] that the resonant frequency will be lowered when the cavity is made deeper.

3.5   Summary

It was established that the annular-slot design was a non-effective design as the frequency response was not easy to control: too many factors were acting on one another so that the model fell apart. With the Z-Slot model more stability was found in the analysis and the response could be predicted quite accurately. Then the top hat was brought in to the analysis upon which it became known as a director of the far field and a tuner to the impedance of the element.

Two methods are therefore presented in this chapter for tuning the element without changing the slot dimensions. These are the top hat and the cavity depth. Although the cavity properties were not shown, they are considered true. It was possible to show that adjusting the slot dimensions also changes the resonant frequency of the element. Thus we have the cavity, which provides maximum power radiation into free space, and a top hat which still presents a little uncertainty as to its contribution, other than its tuning ability, at this stage.
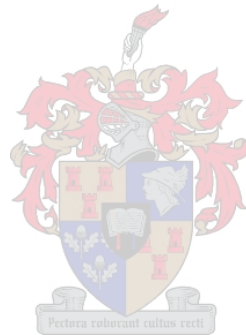
Chapter 4

Array of Dual Slot Elements

4.1 Introduction

- Paragraph objective

  - Feeding of the elements

  - Computation of the impedance matrix for an array of S-parameters

  - Study of the feed impedances of the array under various controlled circumstances

  - Study of the coupling between elements with and without the top hat

  - Study of the field pattern for passively excited elements

  - Study of the steering ability of the array.

- Purpose of the above objectives

  - To establish a feeding network to electronically steer the beam and to calculate the currents thereof

  - To find a method for calculating the active impedances from a set of S-parameters

  - To establish how strongly the elements couple and how this affects the steering

  - To determine how the array layout contributes to the steering

  - To determining how low the beam can be steered

- Method adopted to attain objectives

  - Feeding of a single element from Chapter 3

  - Calculation of a new set of S-parameters in MicroWave Office for the model with combined feeds

  - Calculating current for steering the beam is used in Feko to excite array, enabling steering of the beam.

The array was modelled around an existing array with the primary objective being to try to establish how the top hat improved the the low steering capacity of the array. To study the beam effectively, each port element was required to have a single feed port. This could be established by using the feed network which was presented in Section 3.3.1.2 and also presenting a technique for determining the excitation which is required to excite the array in Feko for beam steering.

The set of *S*-parameters generated in Microwave Office was generated from the *S*-parameters obtained in Feko, which meant that the ports of MicroWave Office had taken all the mutual couplings between the Feko feeds into consideration. Therefore the coupling between the elements could be computed with the accuracy that is obtained from the Feko computation. Both cases of the array were presented in the mutual coupling of the elements in the array, with cases where the top hat was included in the computation and, for the other case, where the top hat was excluded from the array analysis.

With the strong coupling present it was possible to illustrate, by means of the far field pattern of passively excited elements, how the coupling affected the radiation pattern. A passively excited element is a single element in the array which is being excited while all other feed ports are terminated in 50Ω load. These results were then compared with the results that had been calculated for an isolated element to determine the effect of the coupling on the radiating field.

The last aspect to be investigated for this chapter was the steering of the beam. In order to steer the beam, the necessary currents were first calculated in MicroWave Office by exciting the ports in MicroWave Office with the correct phasing. Using the currents on the Feko model which were calculated in MicroWave Office, the beam could be steered in Feko and the scanning angles could be evaluated.
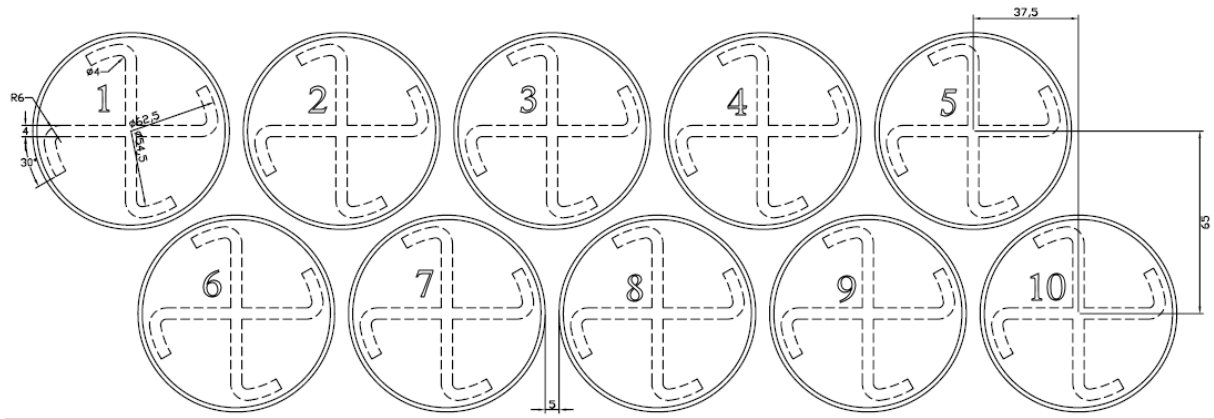
Figure 4.1: Array layout used

4.2 Array Model

Figure 4.1 illustrates the layout of the array that was used to analyse the ability to scan at a low scanning angle of the array to be analysed. This uses the same hexagonal packing of the elements that is found in [1] and shown in Figure 4.2. The smaller array was investigated as the time restriction prohibited the analysis of a 36-element array. The 10-element array is said to have a peak gain of $11dB$ against the 36-element array, which has a peak gain of $16dB$. Some of the techniques used in the measurements of the array, compared to the analysis that was performed for obtaining the required results in this thesis. Each element was approached as a four-port element, as the subset measurements of [1] suggests. Where it was possible to obtain S-parameters through measuring different subsets, directly from the element feed, a feeding network would be required for obtaining the S-parameters of the computational analysis. The advantages that the model presented were that the pattern could be computed without taking measurements, and the feed that was used could be changed without much trouble. Though this did not reduce the measurement time of two weeks, a computer could be used to compute the array characteristics and the necessary adjustments could be made and rerun a couple of times within the same amount of time that the measurements would have taken. This is not an absolute technique and it was only used as an aid to the designing process. In the end, measurements still need to be taken to characterise the product. As this was a phased array, a pin diode phase shifter was developed for the product. This was not part of the project, but considering that the S-parameters of the array were made available, it was possible to create a full model of the package.

There were, however, certain restrictions that prevented an accurate analysis of the existing array structure. One of the restrictions was a dielectric radome that covered the array, which was discarded. Discarding the dome yielded inaccurate computation results of the gain, as the radome will introduce losses into the problem. As will be shown, however, gain was not be considered for this thesis and directivity was the measure used in the investigation of all the
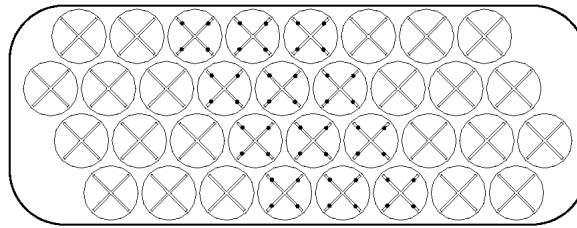
Taken from [1]

Figure 4.2: Hexagonal layout used for the array

fields in this thesis. With the absence of the radome, it was believed that the pattern of the far fields would be inaccurate to some degree. This inaccuracy could be taken into consideration in the sense that the angle at which the far field radiated would be changed when passing through the dielectric, similar to light being bent when it passes from one medium to another, as is known from optical physics. The second factor that played a role was the spacing, or rather the element placement, in the array. Due to the rough placement of the elements, element 6 was slightly closer to element 1 than to element two, but the difference in the distance was below 10% and was thus considered small enough to ignore. The third problem was that the elements could not be placed that close together, as convergence warnings were given by Feko using the Multilevel Fast Multipole Method (MLFMM), the FM card. For the method to work effectively, the mesh of the triangles on the edges of the cavities that were close to each other should have been about three times smaller than the distance between the elements. The latter limitation had to be considered with a great deal of thought, as it was responsible for the amount of time spent on the simulation. Implementing certain placements that differed slightly from the existing model was considered as results that COULD be considered accurate enough to demonstrate the properties of the existing array could still be obtained. After the element had been sufficiently spaced, the MLFMM technique was used, as it reduces the calculation time from 44 hours 24 minutes (when the normal calculation method for the smallest problem was used) to 4 hours 40 minutes, the longest time needed in using MLFMM for the same problem. Furthermore, the numbering of the elements is shown in Figure 4.1, as this will be referred to in the analysis of coupling and other properties throughout this chapter.

By using the feed network that was introduced in Section 3.3.1.2, it was possible to obtain the coupling between elements by simply importing results from Feko into MicroWave Office. This, however, meant rewriting the touchstone file containing the *S*-parameter that had been generated by Feko to the correct form that could be imported into MicroWave Office. A small Matlab code called FEKO2MWOStone.m was written for this purpose, because manipulating the *S*-parameter file by hand for a 40-port network to contain only 4-port measurements in a single line is very time consuming. Since the same problem existed for retrieving *S*-parameters from MicroWave Office and Feko, two other codes, called ldstoneMWO.m and ldstoneFEKO.m were adapted from ldstone.m, as ldstone.m was written for a 4-port network. The *S*-parameters, as retrieved, were placed in a three dimensional matrix, for the simple rea-
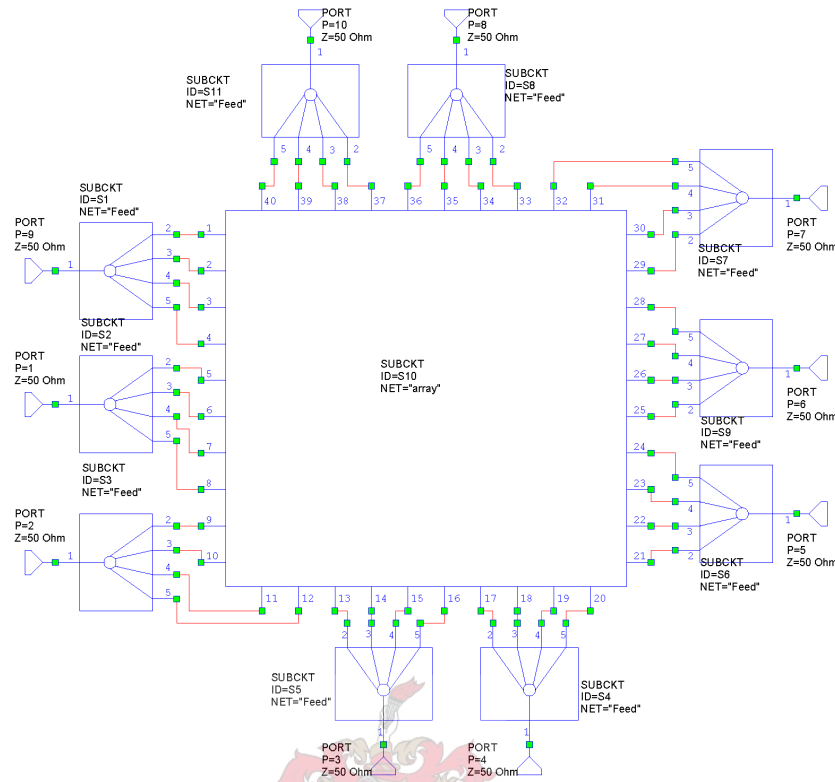
Figure 4.3: Model for evaluating the mutual coupling between elements

son that using a three dimensional matrix simplify the calculations of the active impedances, as one of the dimensions was the frequency, and because the *S*-parameters could then be presented in an NXN matrix.

Figure 4.3 illustrates the layout of the feed network and the array model, which was imported from Feko. The four ports from which a single element in Feko are combined into a single feeding port in MicroWave Office are shown. It is through this new port that the coupling between the elements could be investigated and the phasing of the array could possibly be calculated.

In Figure 4.4 the same type of layout as illustrated in Figure 4.3 was used to calculate the field while the array was being steered. It was used to calculate the currents that were required at every port of an element so that the array could be steered. The far field pattern could then be investigated while the beam was scanned through free space, by using the current values to excite the various feeds in Feko. Each port was driven with a voltage source with the same magnitude, constant for all ports, while the phase was incremented by the angle that constituted the correct degree of scanning.
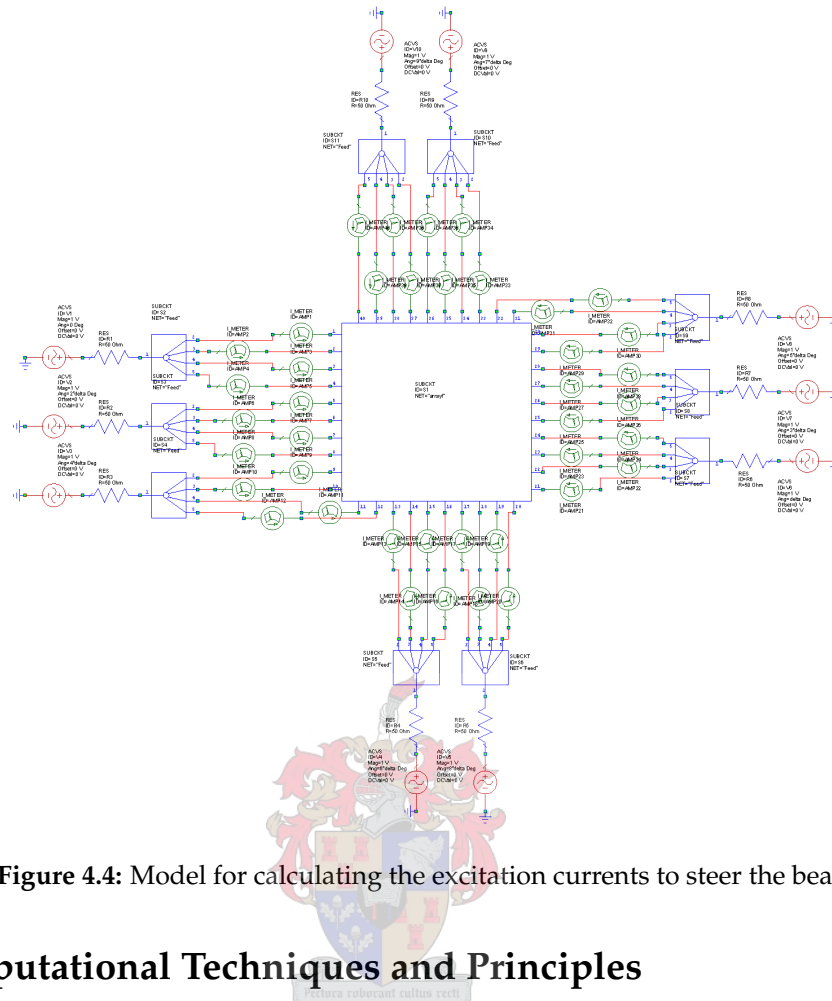
Figure 4.4: Model for calculating the excitation currents to steer the beam

4.3 Computational Techniques and Principles

In the analysis of an array antenna, the active impedances should be evaluated as part of the performance. The active impedance of an array antenna is a dynamic impedance that changes while the beam of the array is steered. Thus it would be necessary to compute the active impedances in order to evaluate the impedance response while the beam is steered.

Feko allows the user to compute the active impedances; however, on this model, this was impossible due to the feeding of the array. Not only was it problematic to extract the active impedances, but the computational analysis on the array mades it time consuming, since the active impedances needed to be calculated for various steering angles.

The active impedances could be computed faster by more efficient techniques. These techniques required the impedance matrix of the array for computation of the active impedances. To acquire the impedance matrix quickly and effectively, the Toeplitz technique was considered. There were, however, shortcomings in the model which did not meet the requirements for the calculation of the Toeplitz matrix. It was established, however, that it is possible to calculate the impedance matrix from the *S*-parameters and thus, ultimately, the active impedances.

4.3.1 The Impedance Matrix

In a multi port system, an impedance matrix can be expressed in the form of (4.3.1) and is denoted by [Z].

$$
\begin{bmatrix}
Z_{11} & Z_{12} & \cdots & Z_{1N} \\
Z_{21} & \ddots & & \vdots \\
\vdots & & \ddots & \vdots \\
Z_{N1} & \cdots & \cdots & Z_{NN}
\end{bmatrix}
\tag{4.3.1}
$$

Assuming that it is for a linear network, the relationship between the currents and voltages is:

$$
\begin{aligned}
V_1 &= Z_{11}I_1 + Z_{12}I_2 + \ldots + Z_{1N}I_N \\
V_2 &= Z_{21}I_1 + Z_{22}I_2 + \ldots + Z_{2N}I_N \\
\vdots &= \vdots \qquad\qquad\qquad\qquad\qquad \vdots \\
V_N &= Z_{N1}I_1 + Z_{1N}I_2 + \ldots + Z_{NN}I_N
\end{aligned}
\tag{4.3.2}
$$

This assumption leads to the calculation of either the voltages or the currents at each port, depending on the unknowns, using the general equation (4.3.3):

$$
[V] = [Z][I]
\tag{4.3.3}
$$

The equation (4.3.2) will hold true for an array, as calculation of the *S*-parameters of an array is approached as a linear network.

Thus, when calculating the impedance matrix, $[Z]$, of an array the impedances in the diagonal of the matrix represent the self-impedances of the feeds, while the off-diagonal impedances will be the mutual impedances of the feeds, as denoted by the subscripts.

These impedances are the starting point in the calculation of the active impedances and are known as the passive impedances of the array. The task now is to calculate the impedance matrix of an array.

4.3.2 Toeplitz

A general approach to array computations is to consider the array as infinitely large. However, as mentioned by A.E. Gera [19], the solution is only found to be practical for elements in the centre of the array, with the edge effects being ignored in the solution. This approach is, however, considered effective for large arrays. The technique was also considered for the accuracy

of the results when it came to the calculation of the active impedances when the array was electronically steered to a low angle.

The Toeplitz technique is an element-to-element approach that is implemented in the MOM techniques of most computational codes, where similar elements, spaced at similar distances from each other, would have similar coupling impedances. The Toeplitz technique is generally applied to a problem consisting of a large array of dipoles, where all the elements are uniformly spaced and where computational time is important when computing the impedance matrix.

The Toeplitz matrix makes it possible to calculate quite large impedance matrices by a greatly reduced number of calculations, for instance reducing the number of calculations of a *NXN* matrix from N^4 calculations to N^2 calculations. This is achieved by not solving the impedances at all the elements on the array, but calculating the impedances of only certain elements and using the symmetry of the Toeplitz matrix to fill in the uncomputed values of the impedance matrix. The reason why the array would be considered as of infinite size is that there are impedances which can be considered to be of similar value. This is what makes the Toeplitz such a formidable approach to the calculation of the active impedances of an array. Below is the form of the Toeplitz matrix with which the impedances were to be computed.

$$\begin{bmatrix} a_0 & a_1 & a_2 & \cdots & a_N \\ a_1 & a_0 & a_1 & \ddots & \vdots \\ a_2 & a_1 & \ddots & \ddots & a_2 \\ \vdots & \ddots & \ddots & \ddots & a_1 \\ a_N & \cdots & a_2 & a_1 & a_0 \end{bmatrix} \tag{4.3.4}$$

From the Toeplitz matrix layout it can be seen that not all the impedances of the impedance matrix need to be calculated, and how the values are filled in after the necessary impedance values of the array have been calculated.

The use of the Toeplitz matrix was discouraged by the technique which was used to feed the elements of the array. There was a point of symmetry in the array, but the Toeplitz matrix is defined for a line of symmetry, which was not only broken by the feeding of the elements but also by the layout of the array. The array was small, and could not be approached as an infinitely large problem, because the edge effects would contribute considerably to the active impedances of the array.

As the Toeplitz technique is an element-to-element approach, it is established that it takes the the mutual coupling of the elements in the array into consideration. Thus it would be possible to compute the impedance matrix from the S-parameters. This meant that the MicroWave Office results of the array, where the four feeds of an element were combined, could be used to calculate the active impedances.

4.3.3   Calculating the Impedances Matrix using S-parameters

When working with high frequency models, the information on the models is retrieved and stored in touchstone files. These touchstone files contain the S-parameters of a network or, in the case of this thesis, an array. The coupling between the elements can be directly extracted from the S-parameters, while the active and passive impedances are contained within the S-parameters. The passive impedance comprises the static impedances that are contained within the impedance matrix, while the active impedance would be the impedances as seen from the source, looking into a feeding port. The passive impedances are constant impedances that will only change if the array structure changes, while the active impedances will change as feeding is changed to steer the beam. The following steps aim to show how the impedance matrix can be computed with the use of the S-parameter, for the passive impedances.

$$[I] = [Z]^{-1}[V] \tag{4.3.5}$$

Using forward and reflected wave theory the equation (4.3.6) and (4.3.7) may be expressed as:

$$V_i = V_i^+ + V_i^- \tag{4.3.6}$$

$$I_i = \frac{1}{Z_0}(V_i^+ - V_i^-) = I_i^+ - I_i^- \tag{4.3.7}$$

With $Z_0 = 1\Omega$ it can be shown as in [20] that the S-parameters can be calculated from the impedance matrix, using

$$[S] = ([Z] + [U])^{-1}([Z] - [U]) \tag{4.3.8}$$

where [U] is an identity matrix with similar dimensions to that of the impedance matrix. Similarly it can be shown that it is possible to obtain the impedance matrix of an array by means of a set of S-parameters using (4.3.9)

$$[Z] = ([U] - [S])^{-1}([U] - [S]) \tag{4.3.9}$$

By using the technique described above, which is found in [20], the passive impedance matrix of an array can be computed from the S-parameters that are available. In having the passive impedance, the necessary handle has been obtained to compute the active impedances of an array through the coupling, which process will be pointed out in the following subsection.

4.3.4 Calculating the Active Impedances from S-Parameters Retrieved from Feko

With Feko, using the SP card which calculates the S-parameters of a network, the impedances which are calculated are all computed from the reflection S_{xx} found at the ports. Thus the SP card computes the passive self-impedance at each port. This is due to the fact that only one port is excited at a time and power being coupled to the port under investigation is therefore ignored. When using the OS card in Feko to compute the currents, all the ports are excited simultaneously. With this excitation the power couples to the ports governed by the S-parameters and the impedances calculated from these currents are known as the active impedances of the array.

The correct S-parameters from the ports of the array that is presented are not directly presentable through Feko, therefore it is not possible to compute the active impedances of the array with the OS card. To obtain the correct S-parameters of the feeding ports of the array, the SP card is used in the Feko computation of S-parameters of the array. This set of S-parameters is then combined in MicroWave Office into the correct array feed network. The active impedances, however, can not be effectively computed in MicroWave Office, as MicroWave Office can only compute the harmonics of the currents and voltages at a single frequency at the relevant ports. This method of computing the currents is used elsewhere in the thesis, where the beam is steered and evaluated at a single frequency. The active impedances, though, are calculated over a frequency band. In order to compute the active impedances, a study of the OS card of Feko is necessary. The calculations of the currents in MicroWave Office will be used later in the thesis for the steering of the beam.

Two Matlab codes were written, to aid the calculation of the active impedances of the array. This was done from the understanding of how the OS card in Feko behaves, to perform similar calculations from the results of MicroWave Office in order to compute the active impedances. The first function Zmatrix.m was derived from the previous subsection. It imports the S-parameters from a touchstone file generated in Microwave Office and computes the impedance matrix. The second function that was introduced was ActiveImpedance.m, which was used to compute the active impedances from the impedance matrix with imaginary defined voltage sources. The equations implemented in the technique are presented below:

The first step to be performed was a slight variation of equation (4.3.9), because the base impedance of the system was no longer 1Ω, but Z_0.

$$[Z_c] = Z_0[(U - S)^{-1}(U + S)] \tag{4.3.10}$$

The introduction of Z_0 was due to the fact that equation (4.3.9) is meant for a system normalised to 1Ω, while it was no longer normalised to 1Ω for the system under consideration but to the system impedance, Z_0. Using the normalisation of Z_o dictated that the all the ports of the

network were considered to have an impedance of Z_0.

The next step was to transform the coupling impedance matrix to find the excitation currents. Since the excitation voltages were known, the impedance matrix was transformed to an admittance matrix as the beam is steered,, for calculation of the currents from equation 4.3.5.

$$[Y] = [Z]^{-1} \tag{4.3.11}$$

As pointed out in [21], however, the impedances of the excitation ports needed to be considered before this transformation could be done since they also form part of the system's impedance. Therefore the impedance matrix that was to be inverted would be in the form of:

$$[Z_t] = [Z_c] + Z_0[U] \tag{4.3.12}$$

An inversion of this equation would yield an admittance matrix [Y] which would be used with the known excitation voltages, since the method of excitation in Feko is defined by voltage sources. This was to present a problem later in the project, which will be discussed duly. Using the voltages, made it possible to computethe currents flowing at the ports.

$$[I] = [Y][V] \tag{4.3.13}$$

Once the input currents at the ports were known, an element by element division could be done on the currents and voltages to find the total impedance at the ports.

$$Z_{in} + Z_0 = V_n/I_n \tag{4.3.14}$$

To find the true active input impedances at the input ports, the port impedances needed to be subtracted, since these impedances were added in serial to obtain the total impedance. Thus the active impedance of a port was:

$$Z_{in} = V_n/I_n - [Z_0] \tag{4.3.15}$$
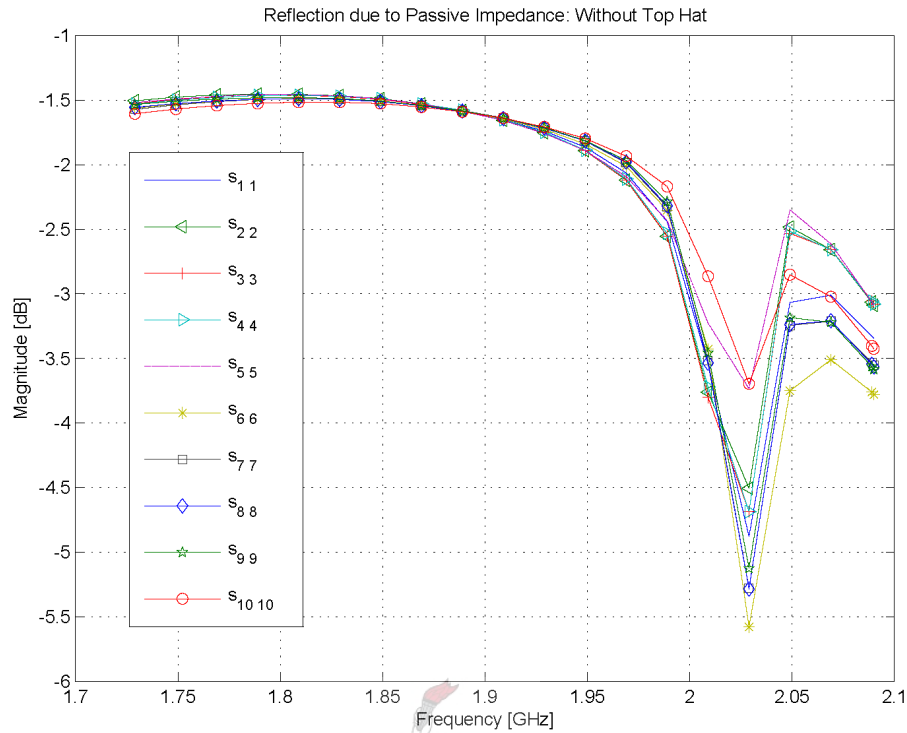
Figure 4.5: Reflection coefficient of elements in passive mode without top hat

4.4 Array Results

4.4.1 Results: Element Impedances

4.4.1.1 Results: Impedance of Passive Element

Firstly, the reflection coefficient of all the elements in their passive state in the array investigation was considered. By passive state it was understood that the element was considered within the array and is the only element being excited. The two cases that comprised considered were an analysis of an array where, in the first case, the top hats were present and, in the second case, the array was without the top hat. These will be evaluated. The analysis of the array without the top hat in Figure 4.5 shows that there was very poor reflection coefficient and this can be traced back to the analysis of a single element without a top hat, where there were extremely high input impedances. On the other hand, there was very good reflection coefficient on a single element with the top hat, as illustrated in Figure 3.28 of Section 3.3.1.2. When the element was introduced into the array, the reflection coefficient dropped by approximately $20dB$s, thus the active impedances would have changed. But at $-13dB$, as illustrated in Figure 4.6, this was sufficient to be considered an adequate match.

From the results of the passive impedances for the array with the top hat it could be seen why the Toeplitz technique could not be used for calculating the impedance matrix, as the central
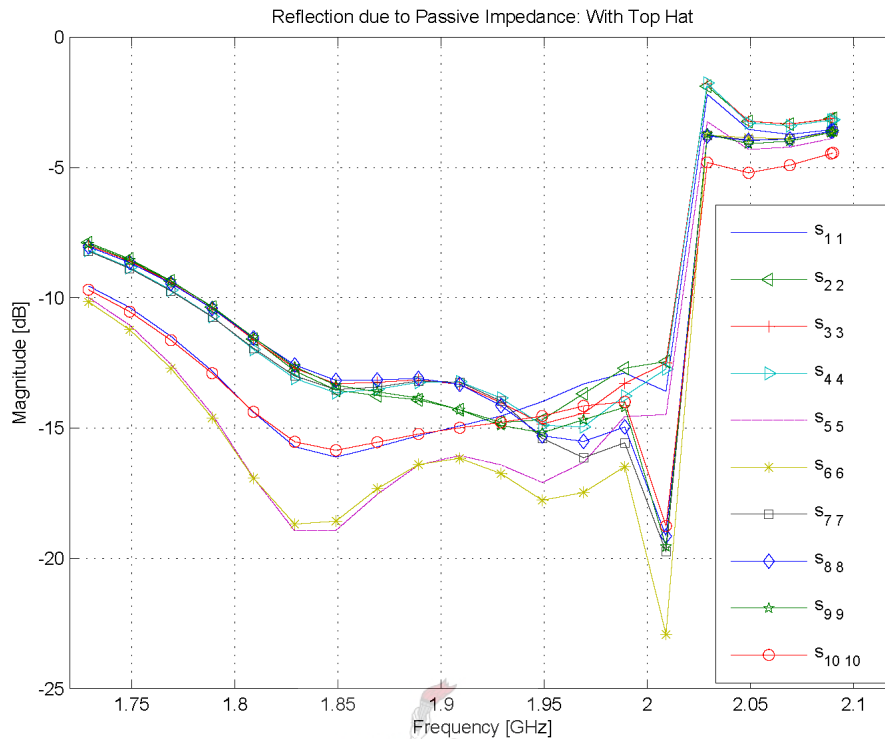
Figure 4.6: Reflection coefficient of the elements in passive mode with top hat

elements agreed, but the outer elements 1, 5, 6 and 10, clearly showed how the edge effects made the impedances of the elements differ from the the rest, by a significant amount.

4.4.1.2 Results: Impedance of Active Elements

Keeping to the basic concept of the array impedances with the top hat, it had to be possible, due to the good match that was achieved for the passive mode, to show how the active impedances changed as the beam was steered and the resulting impedances could then be compared with the passive impedances. To steer the beam, the elements were excited with voltage sources of similar magnitudes but with different phasing. While the beam was steered, the amount of power being radiated and coupled back at each element changed, and this affected the active impedance, while the passive input impedance remained the same. To compare these changes the *S*-parameters were driven by imaginary power through manipulation in Matlab. Using the the equations in Section 4.3.4 and an imaginary voltage source, the phasing of the sources were defined and used to calculate the active input impedance of the ports, as will be explained later in this chapter. These input impedances were used to compute the reflection coefficient of each element, to illustrate the difference through the reflection coefficients. For practical reasons, the difference was demonstrated by two different excitations which were used: the first excitation where the beam was directed vertically and where there would be no phasing differences between the feeds, while, in the second analysis, the scanning angle was steered 90
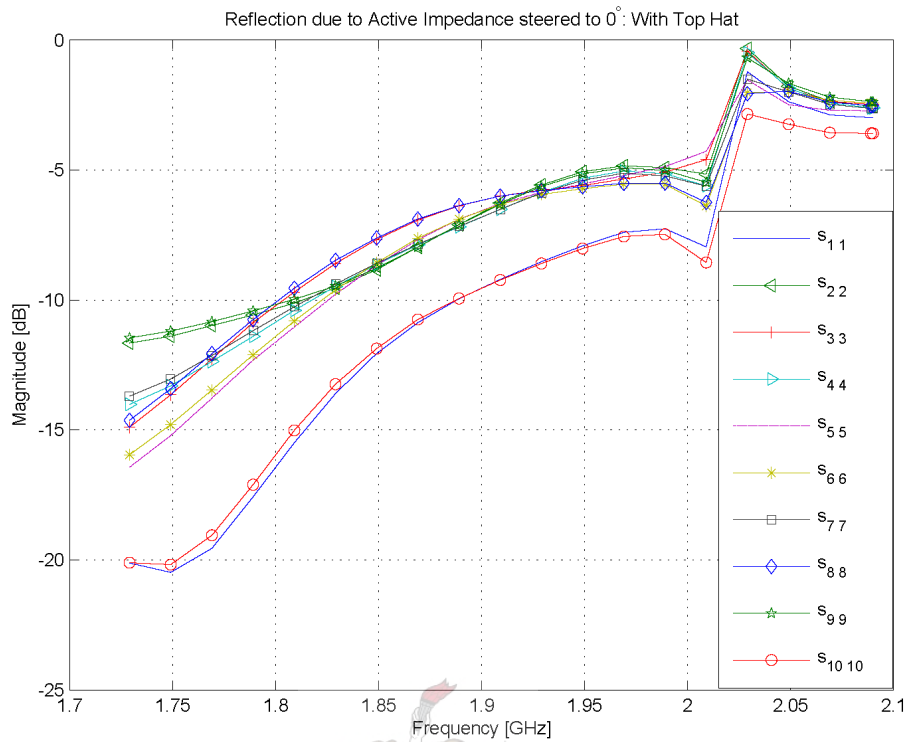
Figure 4.7: Reflection coefficient steering towards the vertical

degrees, directed at the horizon, and thus all the feeds were excited with a voltage source with a phase difference incrementing by multiples of 85.2750 degrees, which will also be discussed later.

Results from investigating the active and passive reflection coefficients presented some interesting indications, illustrating that, when pointing towards the sky, the two elements on the edge have better reflection coefficients than the rest of the elements, which all display similar reflection coefficients. This similarity changed when the beam was steered down to the horizon in the direction of element 1. When the beam was steered away from element 10, the reflection coefficients of the element at the operating frequency improved. This was the case for the reflection coefficients of all the elements, except for element 1, where the reflection coefficient remained constant. So, at first glance, it could be said that elements 1 and 10 could loosely be considered as being 'isolated' when looking straight up into the sky but, on the other hand, it becomes apparent that there is strong coupling when the beam is steered towards a low angle.

4.4.2 Results: Coupling of Active Elements

Two elements in the array were taken into consideration, as well as two different cases in the geometry, where one case involved the presence of the top hat and the other case dit not consider the top hat as part of the geometry.
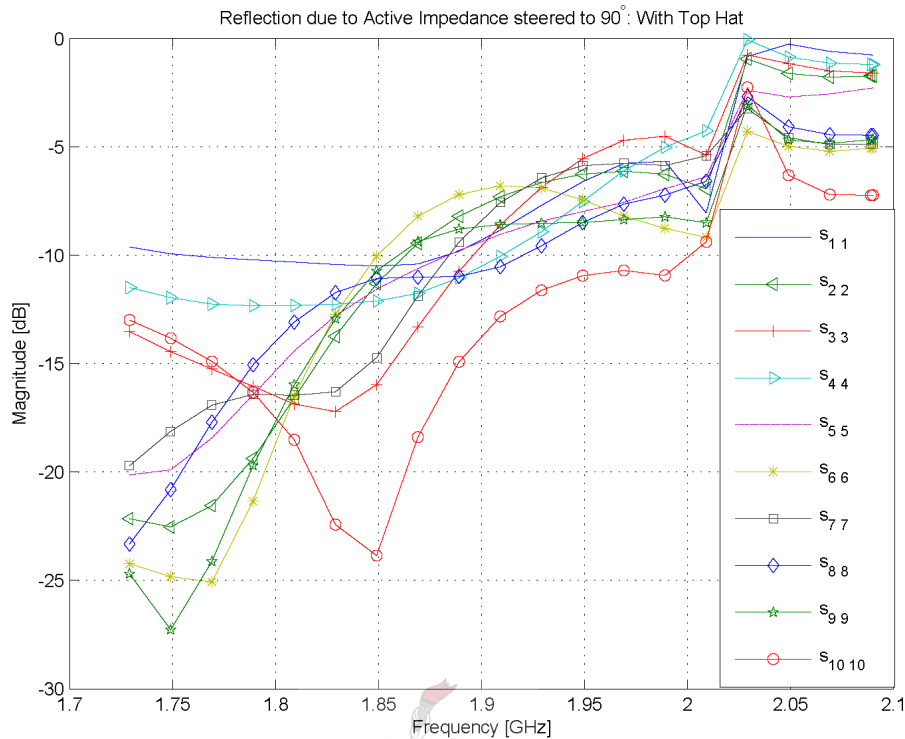
Figure 4.8: Reflection coefficient steering towards the horizon

4.4.2.1 Coupling of Edge Element to Neighbouring Elements

In the first sets of results obtained through the analysis, given here in Figures 4.9 and 4.10, element 1 and its coupling to the neighbouring elements was considered. For the case of the array where the top hats are neglected, the effect of the distance of the elements from each other form the basis for predicting the amount of coupling that is expected. It is a known fact that the remoter an element is from the one to which it couples, the weaker the coupling, and this is clearly illustrated in the first set of results. The results proving the reduction on the coupling are included in Figure 4.9, which indicates the amount of reduction in coupling when the elements are evaluated. The furthest elements were found to couple poorly. The effect of introducing the top hat is clearly illustrated in Figure 4.10 as not abiding by the rules. The largest visible influence was that the elements which were considered to be poorly coupled, now coupled much more strongly, such as element 10 which has now coupled $20dB$. Thus there seemed to be an interesting effect on the array. Generally the use of a cavity on this type of array is aimed to disrupt a travelling surface wave, where power would have become trapped. However, placing a top hat over the elements and having them so close to each other could cause a standing wave to arise, that is being excited between the elements and the cavity, and proof of this could be given later when the fields are evaluated.
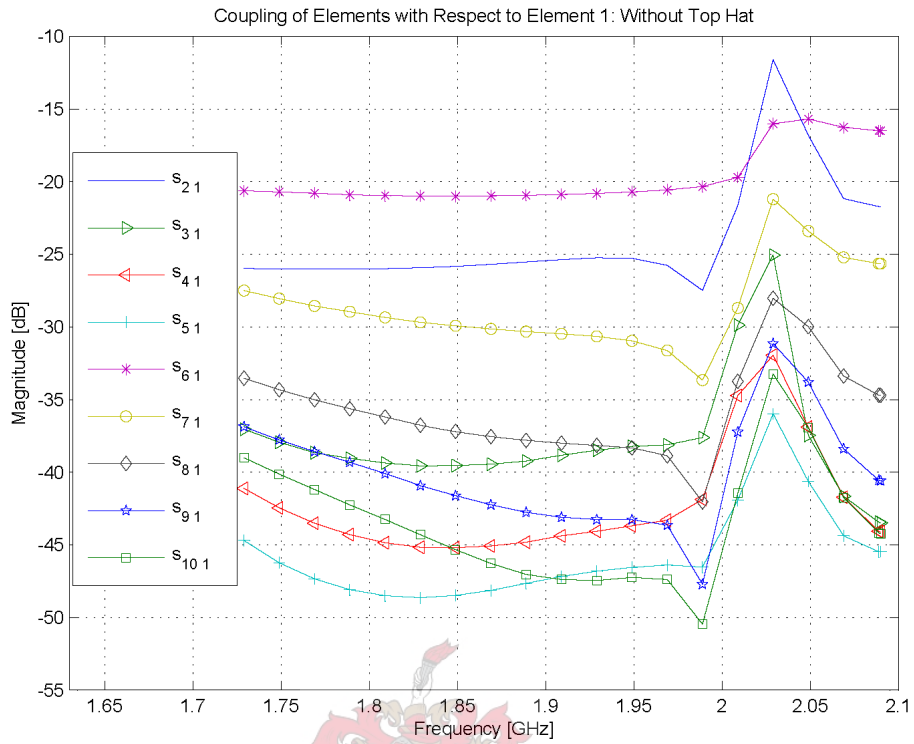
Figure 4.9: Coupling of neighbouring elements to edge element without top hats
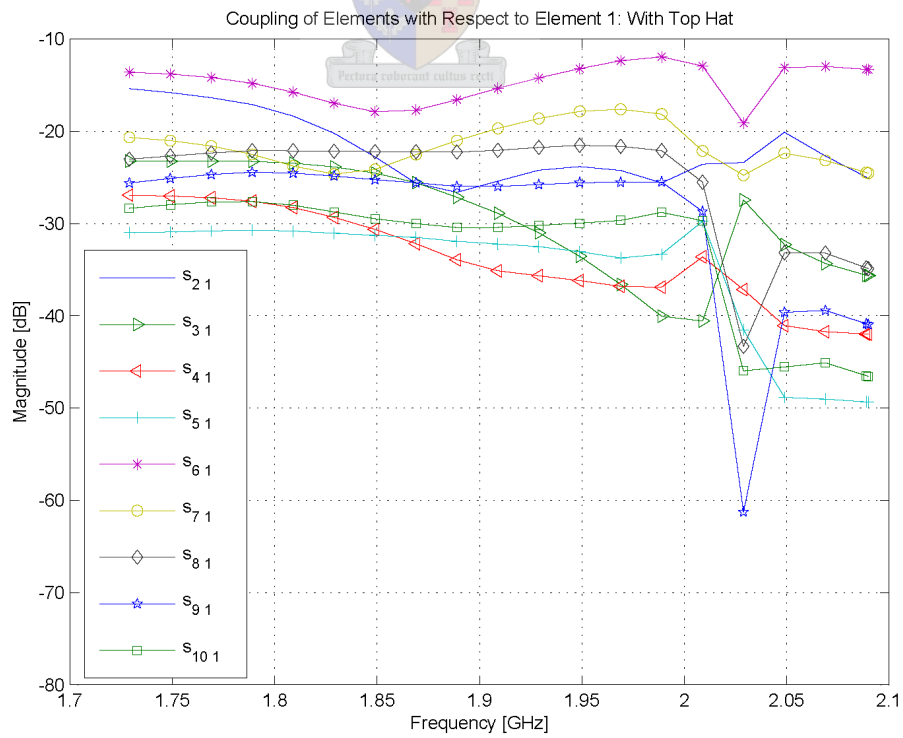
Figure 4.10: Coupling of neighbouring elements to edge element with top hats
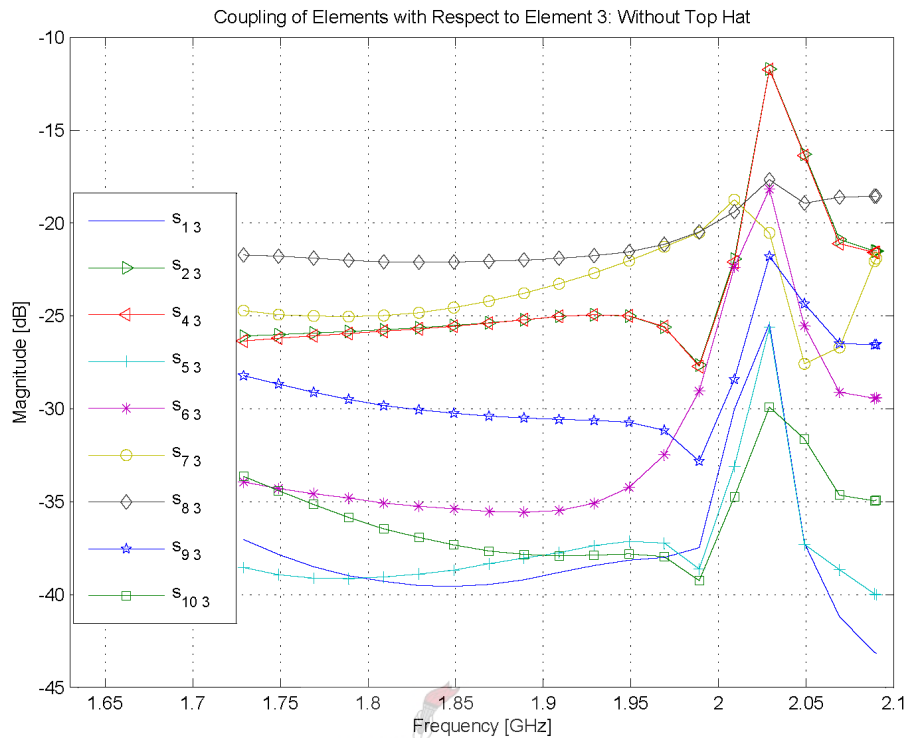
Figure 4.11: Coupling of neighbouring elements to central element with top hats

4.4.2.2   Coupling of Central Element to Neighbouring Elements

The results from the second set of analyses, where coupling of all the elements to a central element is evaluated, are illustrated in Figures 4.11 and 4.12. Some of the expectations were met, such as element 4 and element 2 having similar couplings with element 3, as these two elements lie on either side of element 3 at the same distance apart. Furthermore, element 7 and element 8 have a stronger coupling with element 3 than do elements 2 and 4, since the latter elements lie further from element 3. However, the coupling of elements 7 and 8 with element 3 is not similar, even though these elements lie at the same distance and even though element 9 is coupled more strongly than element 6. These results became apparent in the previous section when the top hat was introduced and was considered, the effect of the top hat being considered as tending to increase coupling. It appears that the coupling effect might have more to it than simply being the effect of a standing wave that is thought to contribute to stronger coupling.

4.4.3   Results: Coupling of the Slots

Twenty slots had to be evaluated for a 10-element array and a numbering system was required to distinguish between the slots.,The numbering involved assigning odd numbers to the slots lying along the length of the array and even numbers to slots that were perpendicular to the odd numbered slots. The slot number can be determined by the element on which it is posi-
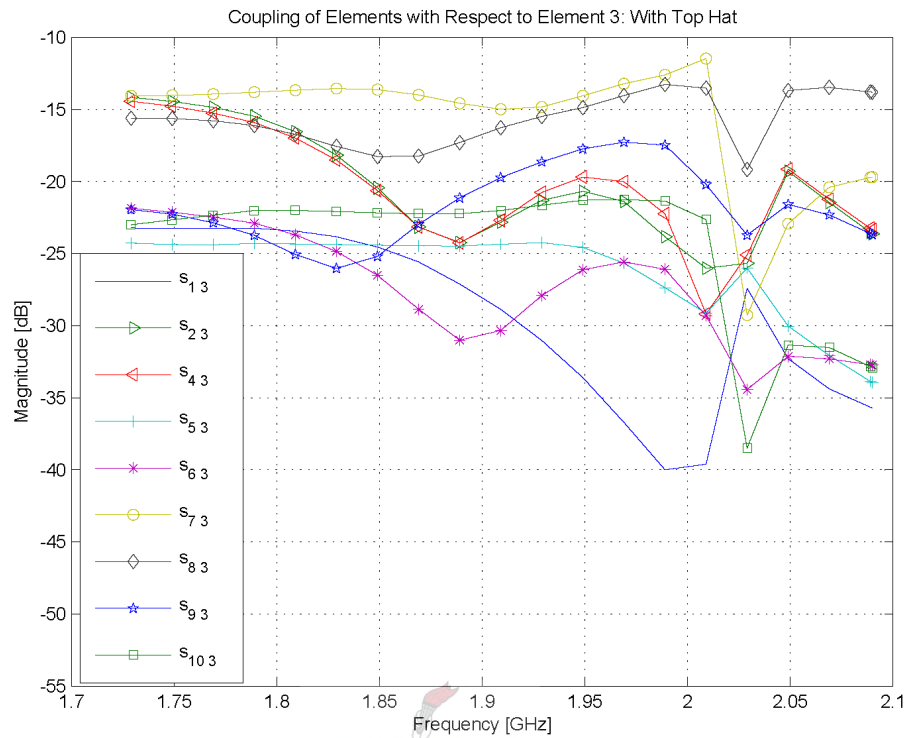
Figure 4.12: Coupling of neighbouring elements to central element without top hats

tioned, thus a slot can be calculated: 2*N-1, for the odd-number slots and 2*N for the even-number slots where N is the number of the element in the array, as labelled in Figure 4.1. These slot were fed at their ports by an 180°-Hybrid feed, with a 90°-Hybrid for phasing between the two feeds, for correct phasing when the element was fed. Only ten slots were evaluated here and these were the slots of elements 1 to 5. Thus there was mutual coupling between the slots that lay in line with each other and the slots that were parallel to each other, with results of the two different cases, one case including the analysis of the top hat and the other case excluding the top hat.

The results of the above analysis are presented in Figures 4.13 and 4.14. These figures clearly show the improvement of mutual coupling between the elements as stated in [1]. It clearly shows that the furthest slots are coupled quite strongly, just as with the elements that were coupled. It also indicates that the change in mutual coupling instigated by the top hat is more favourable towards the slots that lie along the length of the array than towards the slots that lie parallel to each other along the length of the array. There is, however, more to investigated under the topic of slot coupling, for instance the phasing between the slots and the coupling of elements 6 and 10, but this task is left for future work, as the models are easy to reproduce.
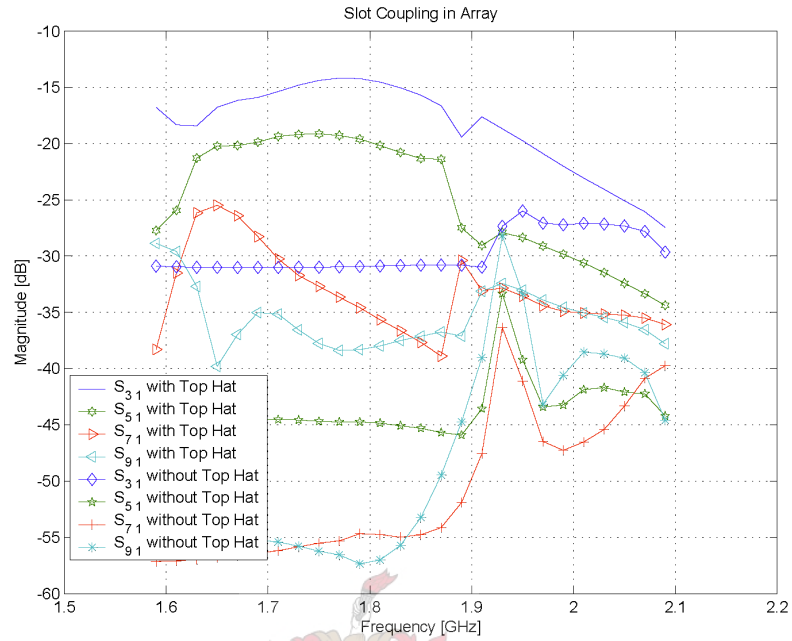
Figure 4.13: Slots that lie in line with each other
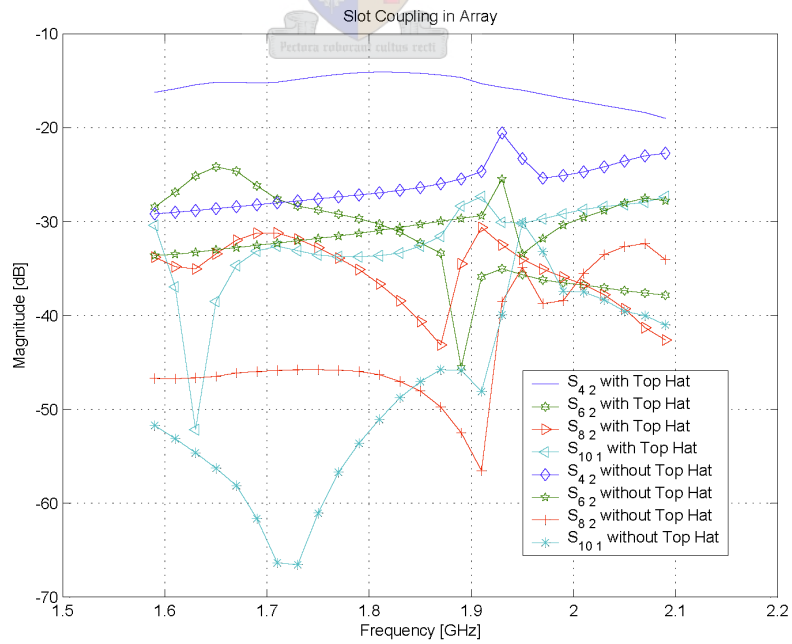
Figure 4.14: Slots in parallel with each other
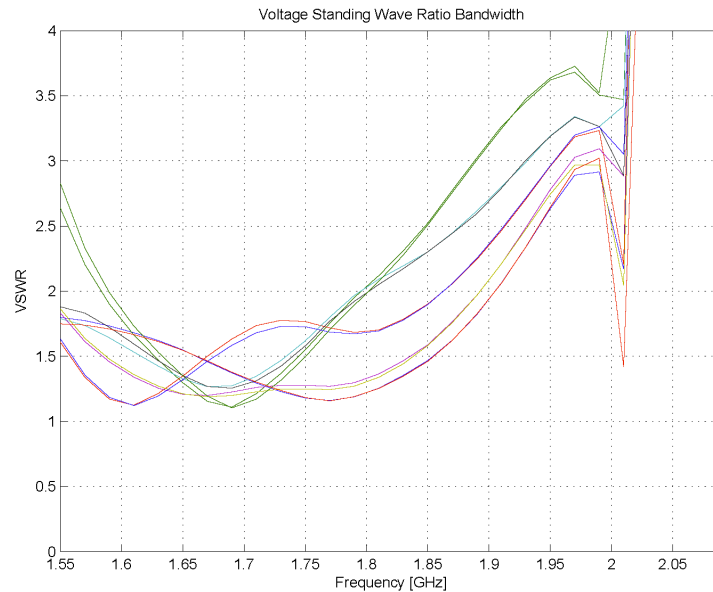
Figure 4.15: Bandwidth evaluation at zenith

4.4.4 Results: Bandwidth

The complete pin feed network was presented so the only evaluation to be done on the bandwidth of the array was to evaluate the bandwidth at each element in the array. It should be understood that the results presented in Figure 4.15 hold only for the beam steered to the zenith, as the steering of the beam influences the active impedances of the elements. The bandwidth results are well within the working specifications of the array, with the smallest bandwidth of an element roughly 12.8%. What is noteworthy is how the array structure has a favourable reaction in the low frequencies, which underlines the increase of bandwidth by the feeding network introduced in Section 3.3.1.2. It seems possible that the pin diode feeding network which controls the elevation angle of the array beam could have a positive effect on the bandwidth, if designed for optimal bandwidth.

4.4.5 Results: Fields

4.4.5.1 Results: Passive Element Field Pattern

The array effect that was mentioned in the above section will be demonstrated here, as to the effect of the array on the far field pattern. The technique that is introduced was originally known as an active element approach [22], in which a single element is excited and the pattern of the element is said to be directly proportional to the array pattern of an infinite dipole array. It would be possible to demonstrate how the strong coupling is achieved from the field pattern of a passively excited element, as it will be referred to in this project by evaluating how the far field pattern of a single element is influenced in the presence of the array when the array
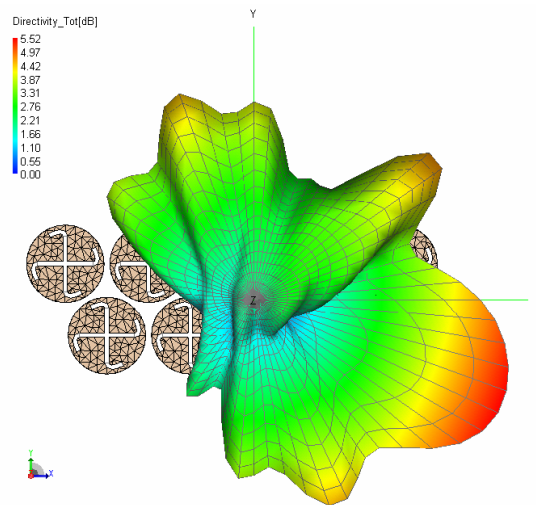
Figure 4.16: Far field of passive element 1 without top hat

feeds are terminated. The first observation of the field pattern was made without having the top hat, and with only element one being excited. This result is illustrated in Figure 4.16. The pattern shows that the field tends to have a large gain towards element ten, however the result is not that conclusive, since a single element radiates mostly towards the horizon and the array structure could therefore function as a director. Verification with a passively excited element, with top hats present in the array, was done to verify that the array was more than just a director and actually contribute to the coupling.. The result is displayed in figure 4.17, with the far field no longer in the vertical, but pulled to the horizon and the beam clearly directed towards element ten. Except for the beam being directed towards element ten, the gain was much higher than in the previous case of an isolated element, and it was also directed along the length of the array. This supports the idea, not only of a standing wave below the cavity, but also of a surface travelling wave between the elements and their top hats. The direction of the beam makes it possible to deduce why certain elements have higher coupling than others or higher than expected. The strong sense of coupling is clearly shown through the far field pattern of a passively excited element.

To verify the last statement, which claims that the strong coupling of the element could be predicted by the far field pattern, a passively excited central element was investigated. Figure 4.18 illustrates the far field with element three in the array excited and the far field being displayed showing the expected results. The far field that is excited radiating in two directions, and these directions were influenced by the coupling. It was shown in Figure 4.11 that elements seven and eight coupled most strongly with element three, with the resolve of the two beams being radiated in the general direction of elements seven and eight.

Thus the direction of the beam of a passively excited element is shown to be dependent on the strongest coupling or, put otherwise, the pattern is governed by the closest element to the passive elements and this leads to a chain reaction with regard to the coupling of the elements
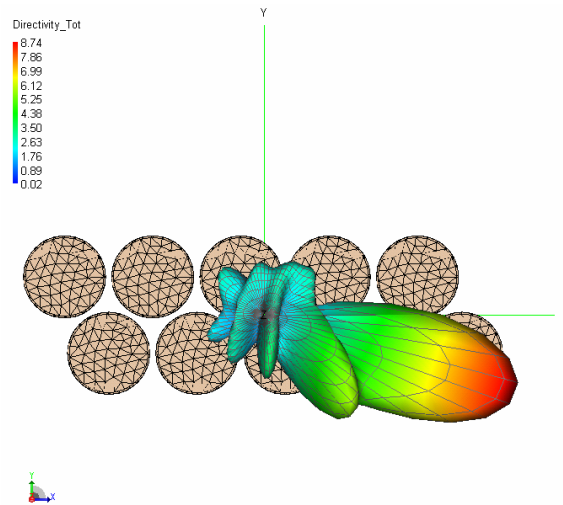
Figure 4.17: Far field of passive element 1 with top hat
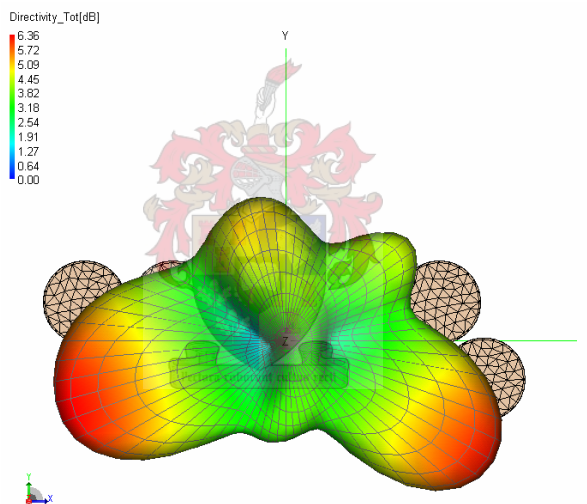
Figure 4.18: Far field of passive element 3 with top hat

further down the array.

In trying to understand the excitation of a surface travelling wave, reference was made to [23] and [13], where it is stated that a creeping wave will be established in the shadow region of the surface where the incident wave is intersected by the surface and thus energy starts to travel tangentially with the surface. For this to take place the surface needs to be larger than a wavelength. This is not the case with the top hat, however, due to the element spacing being far smaller than a wavelength the top hats forms a large surface that is interpreted as a large surface, with much larger dimensions than the frequency wavelength.
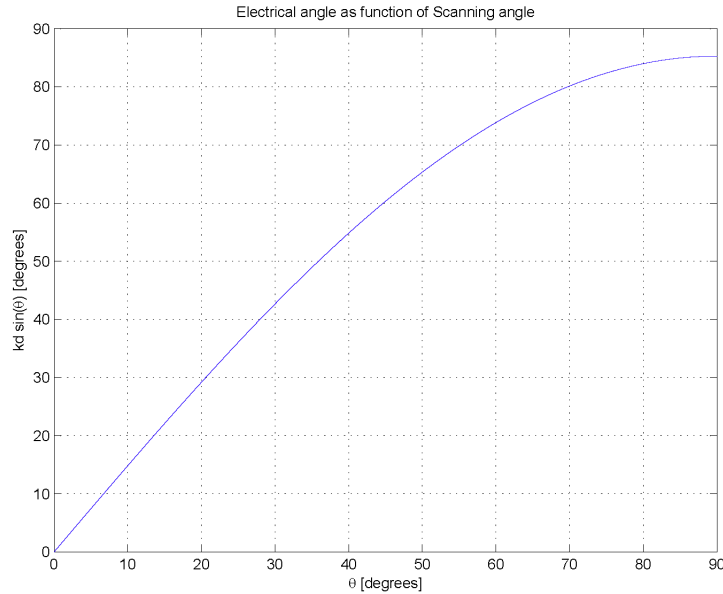
Figure 4.19: Phasing angle required to steer the beam

4.4.5.2   Results: Steering of the Array Beam

The steering of the array needed investigating for determining performance of the far field of the array. The elements first of all needed to be phased along the array through the feeding sources to provide the necessary phase difference to steer the main beam. The phasing at a specific point in the far field needed to be equivalent for constructive interference, for steering the beam. By using this relative point at an angle in free space, the phasing of the sources could be calculated, by means of equation (4.4.1),

$$V_\theta = kdsin(\theta) \tag{4.4.1}$$

where
- V_θ is the source phasing,
- k is $\frac{2*\pi}{\lambda}$,
- d is spacing between elements in wavelengths and
- θ is the angle along which the beam is steered.

Figure 4.19 shows the phasing angle that was required as a function of the angle to which the beam was steered. This was based on the spherical coordinate system and ϕ will be kept constant at 0 degrees, thus the steered beam will be evaluated in the X-Z plane, except where the 3-dimensional field is presented.

After the phasing was calculated, the problem was to excite the ports in Feko to obtain the correct phasing. There was a problem in that the phasing for the combined feed was calculated in MicroWave Office and not for the Feko model. Thus, using MicroWave Office, the ports

were excited with the necessary phasing of a voltage source, with a slight error in the sense that, instead of steering to positive angle, steering was done to negative angle. Thus, when it was mentioned that the beam is steered to positive, the results will be illustrated at negative angles. The currents were evaluated in MicroWave Office at the ports of the Feko model, to determine a feeding method in Feko to steer the beam. Since Feko uses the voltage sources for the excitation of the ports, the currents that were calculated in MicroWave Office needed to be manipulated, which was done using a Norton-Thevenin model. Each port in Feko is loaded with a $1M\Omega$ load and a source voltage, which is the product of the currents that were calculated in Microwave Office and the values of the loads used in Feko. For this reason, the gain of the Feko model was not considered in the project, since most of the power is lost in the loads, but the load needed to be of extremely high impedance. Since the passive impedance of the ports was high already, an extremely high input load was needed to govern the correct current for the excitation of an element to steer the array. A problem that took a lot of time on the project concerned retrieving the currents from Microwave Office, as this had to be done by hand, copying and pasting the values into Feko. This was done for a few steering angles, however only four were considered, $\theta = 0°, 15°, 30°, 85°$. For the validation of the steering angle and steering analysis, this phasing was considered on a finite ground plane only, for the case where the top hats are present, as this would be the more practical approach to the existing design. But first it will be shown why the array with the top hat is not considered further in the analysis.

a)Without top hats   b)With top hats
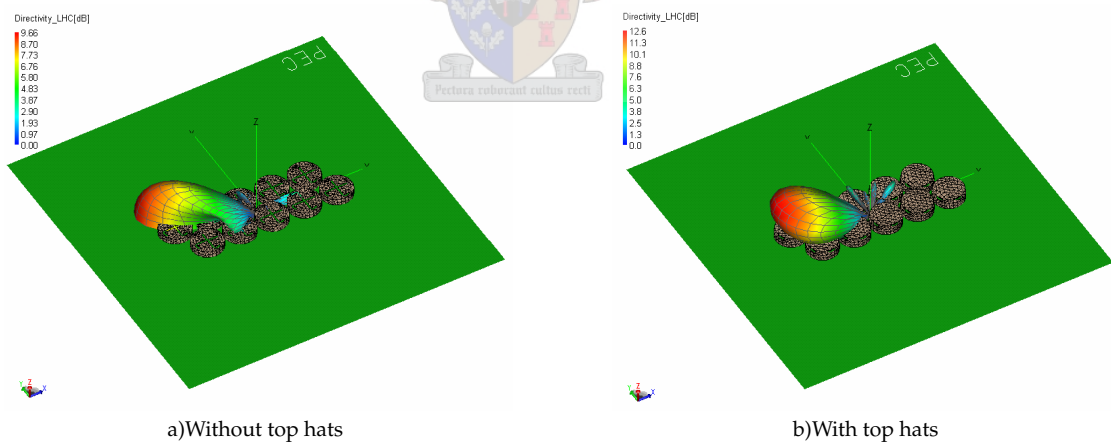
Figure 4.20: 3D far field pattern of beam steered towards the zenith

The 3-dimensional far field patterns of two array models are displayed in figures 4.20a and 4.20b. Here the elements of the array were modelled over an infinite ground plane and the beam was steered to a low angle. Regarding the two cases that were investigated and where the top hat was present the beam was steered down to 85 degrees from the vertical in one of the cases, as is seen in Figure 4.20*b*. The results of the two far field patterns illustrate that the beam can be steered to an extremely low angle without the top hat, but this is not the case when the top hat is present. With responce to Section 3.3.1.2, it is possible to demonstrate the possibility

of the low steering angle by evaluating the far field pattern of the element without the top hat. It is also shown that, for the array without the top hat, the beam is not directed 180 degrees in the ϕ direction, as would be expected, but rather more towards $\phi = 150°$. This is the result of the beams of a single element radiating in four beams into the azimuth. A total far field result would by a result of the array factor multiplied by the element pattern. At low angles the element pattern becomes dominant, and then starts to pull on the array pattern, exerting a powerful influence influence on the total far field being excited. Therefore the beam cannot be steered effectively without the top hat and the top hat will therefore not be excluded from the analysis from this point onwards.
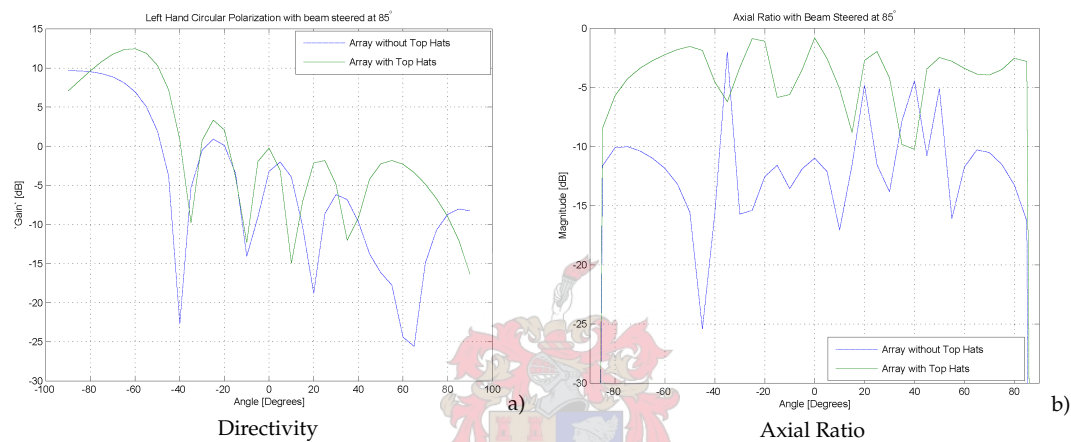
Figure 4.21: Steering of the beam to -85 degrees from zenith, along $\phi = 0$ degrees

From the directivity presented in Figure 4.21a, it is clear that the array containing the top hats has a peak gain of $12.4dB$, which is $2.8dB$ more than the peak gain of the top hatless array, which indicates that the E-field is doubled when the top hat is not present. This result is well within the region of the $11dB$ specification that was given for the 10-element array. The top hat array also has a better axial ratio than that of the top hatless array, which means there is more purity in the left-hand circular polarisation with the presence of the top hat, as illustrated in Figure 4.21b.

The analysis of the array with the top hat being steered down to 85 degrees from the vertical indicates that the peak gain lies at 60 degrees from the vertical. As this could be considered an error in the calculation of the phasing of the array, analysis was done on other scanning angles to verify the phasing. As part of the verification problem, the infinite ground plane was replaced with a more practical ground plane. This ground plane was finite and the extent was slightly longer and broader than the extent of the array, representing a more accurate and practical model.

In Figure 4.22, phasing is displayed for four angles to verify the phasing of the elements. The figure clearly illustrates that the phasing is calculated correctly, as the peak gain of all the steering angles is at the correct angle, with the exception of the 85- degree steered beam. It even
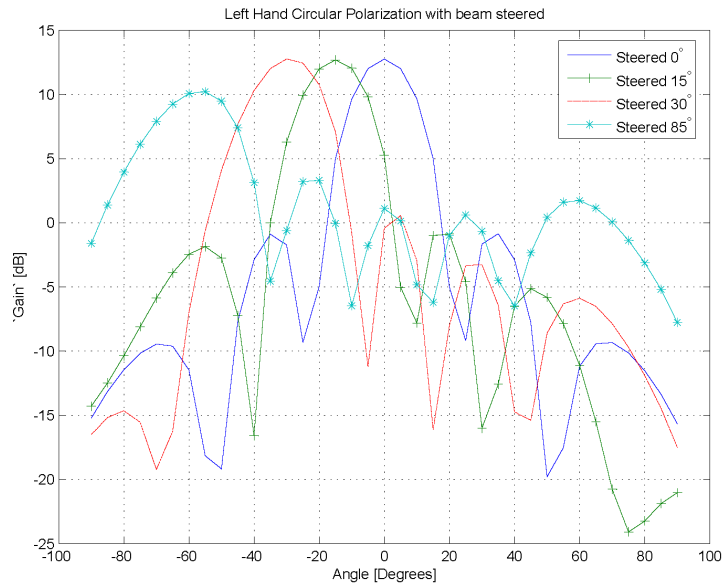
Figure 4.22: Verification on steering of the beam

becomes clear from the graph that the peak gain is reduced, which is quite possibly the effect of the far field that is becoming linearly polarised at the low scanning angle. Since the peak gain for a beam steered to 85 degrees is located at 60 degrees, the far field of a beam steered to 60 degrees is considered and compared with a beam steered to 85 degrees, as illustrated in figure 4.23.

a)Direcivity   b)Axial Ratio
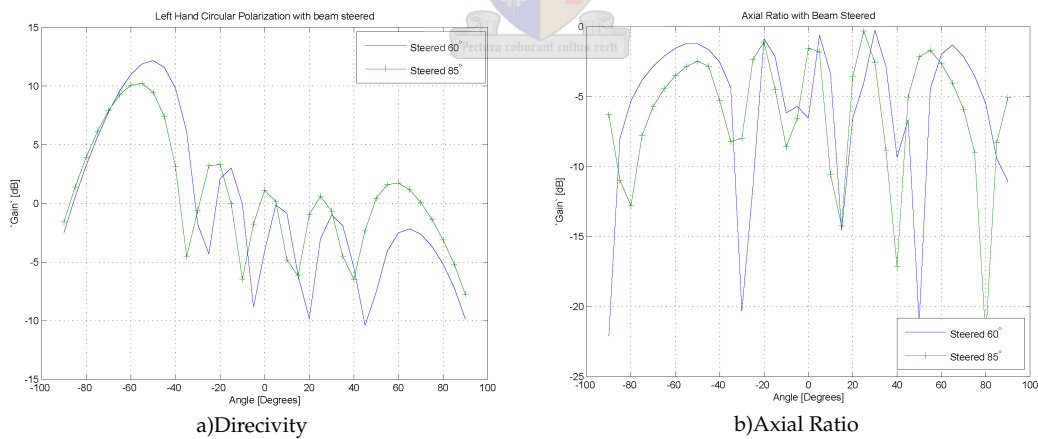
Figure 4.23: Maximum effective steering of the beam

In the comparison it becomes clear that the gain is considerably more when the beam is steered down to 60 degrees, than when the beam is steered down to 85 degrees. However, the circular polarisation should not be considered without the axial ratio of the beam that is steered down to 85 degrees, as it might be possible that the axial ratio at 85 degrees is larger than for a beam steered down to 60 degrees, but this seems very unlikely.

Figure 4.23 illustrates the fact that the axial ratio is worse when the beam is steered down to 85 degrees, except at an angle between -85 and -90 degrees. However, between -60 and -85 degrees the axial ratio is much smaller for the beam steered to 85 degrees.

The results in this section indicate clearly that the top hat reduces the range of angles in which steering can take place, as the top hatless array can be steered extremely low, and steering down further than 60 degrees for this problem would be totally unnecessary and ineffective, as this has worse gain and even worse axial ratio. Not only does the top hat play a part in the steering that effects the problem, but it also affects the ground plane. Even a small ground plane is linearly polarised at low angles. Thus it would be recommended to consider either not steering down lower than 60 degrees, or else adjusting the top hat and playing around with the properties of the top hat found in Section 3.2.3.1, to see if steering down to lower angles is possible.

Grating Lobes and Side Lobes

To avoid grating lobes in an array, the spaces between the elements are required to be less than λ from each other for an array. For this model, the spacing between the elements was less than $\frac{\lambda}{2}$ and therefore no grating lobes where present. However, when working with the scanning of the array, the beam was steered past 90 degrees, thus causing the formation of grating lobes. By claiming that the beam was steered past 90 degrees it is meant that the maximum scanning angle defined as 85.275 degrees for electrical steering was overstepped. The problem with the prediction of where the beam would be pointing was that the grating lobes did not lie on the same ϕ-angle, however, analysis of this was not required as steering is not normally done past the maximum defined steering angle.

Side lobes, on the other hand, are present. Nothing much can be done towards avoiding it, other than using different types of array excitation. Using Dolph Tschebyscheff excitation, could for example reduce the side lobes of the model. The side lobes are about $12dB$s down from the main beam when looking straight to the sky at present and become less as the beam is steered. The lobe that increases is the lobe next to the main beam, closest to $\theta = 0°$. When the main beam is steered to 60 degrees, there is only $8dB$s difference between the side lobe and the main beam, and this becomes even less when the beam are steered to angles lower than 60 degrees. Thus it seems that the side lobes of the model is more problematic than the possibility of grating lobes being present.

Chapter 5

Conclusion and Recommendations

5.1 Conclusion

The results of the computational analysis into the array antenna revealed properties were found with regard to the working of the array that made it possible to steer down to low angles, even though the model was not a completely accurate representation of the existing array.

The accuracy of the model was affected, as the exact dimensions were not used and results were taken from an element of the array that was supplied. When the element was modelled, the dielectric that formed part of the model was not considered. The inaccuracy could be calculated with reference to the results presented in Section 2.5, considering the effect of the dielectric in a slot. Firstly, the input impedance would decrease. This effect was not illustrated in the analysis of an element in Section 3.3.1, as the feed wire on the model was located more towards the centre of the slot than on the produced element in to adhere to segmentation rules in Feko. In Section 2.6 it is shown that moving the feed wire outwards reduces the input impedance that is seen from the driving port. indicating why the match of the model to input port is good, considering that the feed is further from the slot edge than in the manufactured element. Secondly, the natural frequency of resonance produced by the active impedance is higher on the model than on the manufactured element. This again is an effect that the dielectric adds to the model, which is shown in Section 2.5 and which is found on printed dipoles and on microstrip patch antennas. When a dielectric is used in printed antennas, including slots, the natural resonant frequency is reduced by roughly a root factor of the dielectric constant.

When the array was introduced, the spacing between the elements was not exactly as

in the product, the reason being that this would have violated the segmentation rules of Feko, unless certain areas were meshed finer, which would have increased the simulation time. Despite this problem, the model could be considered accurate enough to demonstrate certain key elements. In the array analysis, the primary requirement was to show that the top hat serves not only as a director, as illustrated in Section 3.2.3.1, but that it provides a very strong coupling to the electric field of the slots and that this coupling, together with the coupling of the nearby elements in an array, produces a path of propagation for the electric field. This field is supported between the elements and the top hats and is responsible for the capacity to achieve a low elevation scanning angle. The results recorded in Section 4.4.2 made it clear that there is a tighter coupling between the elements with the top hat, than without it, indicating that more energy is being coupled along the array. Furthermore, the evaluation of the far field pattern of a single element, only can be used toillustrate how the far field of an isolated element is radiated, compared to the far field radiated by a passively excited element in the array. It can be shown visually that the energy is directed along the length of the array while the field is travelling along the array. In the case of an isolated element, the far field pattern was radiateding in a vertical direction, as discussed in Section 3.3.1.3. When the element is placed in an array environment and excited passively, the far field pattern illustrates how the energy of the far field is no longer radiated vertically direction but now shifts and is directed along the array. Thus the far field now radiates more horizontally with a low angle beam as shown in Section 4.4.5.1. Even when steering the array, the top hat proves to be useful piece in solving the puzzle: when it comes to steering to low angles, the main beam stays on track and is directed reasonably well at a constant angle in the azimuth direction. However, when the top hat is removed, it is observed that, when the beam is steered to low angle, the pattern seems to be strongly influenced by the far field pattern of an isolated element without a top hat. The far field pattern of the array will be influenced by the remoter element along the line in which the array is scanned. This leads to the conclusion that the top hat supports a tuning of a resonant frequency where energy is propagated along the length of the array and provides low angle scanning capacity.

Computational results of the steered beam indicates that the beam has an optimal steering angle. Should the beam be steered to a lower angle than is established by computational results, the gain of the main beam will be reduced, as illustrated in Figure 4.22.

Model	Measurements
Slot Length	130mm
Slot Width	4mm
Cavity Height	15mm
Cavity Length	50mm
Cavity Width	50mm
top hat Height	10mm
top hat Dimension	50mm

Table 5.1: Measurements of a Z-Slot model

5.2 Recommendation

Evaluation of the results, suggests that this is a good system and it would prove challenging to improve on the design. However, it is always worthwhile to consider new techniques for solving old problems and to apply old techniques to new problems. When trying to find equivalent models to investigate the problem, the geometry of a Z-slot was developed. Now this geometry could be considered more cost effective, as the cavity could be manufactured from square tubing and no special tools are required for this. This, however, is not the main reason why the element would be functional and is presented as an alternative. The main reason why the Z-slot is considered worth mentioning is the fact that the geometry already has good circular gain in the vertical direction. More than that, the height of the top hat in the model was not quite as high as that of the original design. Having a lower top hat contributes to two practical effects, tighter coupling and reduced volume occupied by the antenna. The array was not considered seriously, but it is thought that the antenna could be broader and probably of similar length. The dimensions for possible further investigation are given in Table 5.1:

If excitation for minimum side lobes levels is not used in the array, it should be considered. This might even make it possible to steer a couple of degrees lower towards the horizon.

Appendices
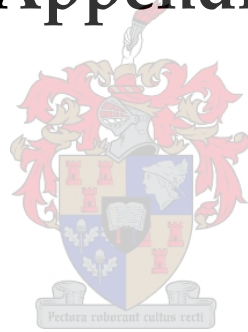
Appendix A

Introduction to Babinet's Principle

The best reference found in the literature is explained in [25], where an in detail discussion is given as to how the Babinet Principle is derived, most text just give a small explanation as to the origin of the Babinet Principle and as to how it is implemented. In this section of the appendix there will be looked as how the Babinet Principle is derived as the this Principle plays in intricate part in the development of the Booker Extension, which is the criterion for the validation of the computational code in Chapter 2.

A.1 Babinet Principal
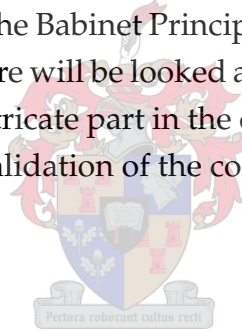
Babinet's principle which is derived for the study of optics and extended and the work of H.G Booker [4], (as shown in the following section) to study the behaviour of the electromagnetic fields of a radiating slot by using properties of a radiating dipole. Babinet's principle states that if a screen containing a hole of arbitrary size is placed
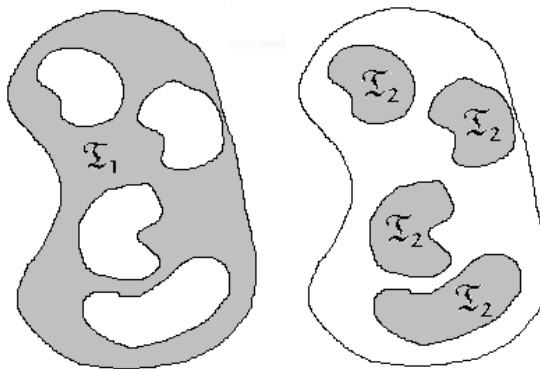
Figure A.1: Sheets used to show Babinet's Principle

within a field, the field behind the screen added together with the field of a plate that forms the complement of the hole, will result in a total field which is the same as when the screen is not present.

To demonstrate Babinet's principle an infinite perfect conducting ground plane (screen), with a zero thickness and a set of holes is taken and placed in free space in the presence of electromagnetic fields. The sources responsible for the electromagnetic fields will be considered to be present in the area where $z < 0$. The field, in the absence of the screen, is responsible for the incident field designated H^i, E^i. However, in the presence of the screen the field becomes the incident field summed with a scattered field H^s, E^s, caused by sources on the screen induced by the incident field. Thus the field in free space is given by:

$$\mathbf{E} = \mathbf{E}^i + \mathbf{E}^s, \mathbf{H} = \mathbf{H}^i + \mathbf{H}^s$$

To find the field in free space where $z > 0$, Love's Equivalence Principle can be used, which states that sources can be added to a closed imaginary region in free-space that satisfies the boundary conditions for the fields at the edges of the closed region. These sources can be constructed using electric and magnetic surface currents which, when added up, satisfy the boundary conditions and have a zero field effect inside the closed region. These equivalent sources of Love's Equivalence Principle can be expressed as in equation (A.1.1) below:

$$\left.\begin{aligned}
\mathbf{M}_s &= -\mathbf{n} \times \mathbf{E}(x, y, z) \\
\rho_m &= \mu \mathbf{n} \cdot \mathbf{H}(x, y, z) \\
\mathbf{J}_s &= -\mathbf{n} \times \mathbf{H}(x, y, z) \\
\rho_e &= \epsilon \mathbf{n} \cdot \mathbf{E}(x, y, z)
\end{aligned}\right\} z > 0 \qquad (A.1.1)$$

where

$$
\begin{aligned}
M_s &= \text{magnetic current density} \\
J_s &= \text{electric current density} \\
\rho_e &= \text{electric charge density} \\
\rho_m &= \text{magnetic charge density} \\
\mathbf{n} &= \text{normal vector}
\end{aligned}
$$

As the screen is depicted as lying on the plane where $z = 0$, $\mathbf{n}$ would be the vector

normal to the screen pointing in the positive z direction.

Since the current and charge densities are known, the vector potential and scalar potential can be calculated to determine the electromagnetic fields. The following equations are used to calculate the vector and scalar potentials:

$$
\begin{aligned}
\mathbf{A} &= \frac{\mu}{4\pi} \iiint_V \mathbf{J}_s \frac{e^{-jkR}}{R} dx \\
\mathbf{F} &= \frac{\varepsilon}{4\pi} \iiint_V \mathbf{M}_s \frac{e^{-jkR}}{R} dv \\
\Phi &= \frac{1}{4\pi\varepsilon} \iiint_V \rho_e \frac{e^{-jkR}}{R} dv \\
\Phi_m &= \frac{1}{4\pi\mu} \iiint_V \rho_m \frac{e^{-jkR}}{R} dv
\end{aligned}
\tag{A.1.2}
$$

Substituting equation A.1.1 into equation (A.1.2) yields the solution for finding the fields. For the calculation of the vector and scalar potential functions, the areas of integration of the screen are divided into two. The area consisting of conductor surrounding the holes is denoted by $\mathfrak{T}_1$ and contains an electric equivalent source, and the area that represents the holes is denoted by $\mathfrak{T}_2$ and contains both an electric and a magnetic equivalent source.

$$
\begin{aligned}
\mathbf{A}(x,y,z) &= \frac{\mu}{4\pi} \iint_{\mathfrak{T}_1+\mathfrak{T}_2} \mathbf{n} \times \mathbf{H}(x,y,z) \frac{e^{-jkR}}{R} dxdy \\
\Phi(x,y,z) &= \frac{\varepsilon}{4\pi} \iint_{\mathfrak{T}_1+\mathfrak{T}_2} \mathbf{n} \cdot \mathbf{E}(x,y,z) \frac{e^{-jkR}}{R} dxdy
\end{aligned}
\tag{A.1.3}
$$

while the field instigated by the magnetic current, which lies over the holes, can be calculated by the following:

$$
\begin{aligned}
\mathbf{F}(x,y,z) &= \frac{1}{4\pi} \iint_{\mathfrak{T}_2} \mathbf{n} \times \mathbf{H}(x,y,z) \frac{e^{-jkR}}{R} dxdy \\
\Phi_m(x,y,z) &= \frac{1}{4\pi} \iint_{\mathfrak{T}_2} \mathbf{n} \cdot \mathbf{E}(x,y,z) \frac{e^{-jkR}}{R} dxdy
\end{aligned}
\tag{A.1.4}
$$

with $R = \sqrt{(x_0 - x)^2 + (y_0 - y)^2 + z^2}$

Using the vector and scalar equations the fields can be found using the following set of equations:

$$
\begin{aligned}
\mathbf{E} &= -\frac{1}{\varepsilon}\nabla \times \mathbf{F} - j\omega\mathbf{A} - \nabla \cdot \Phi \\
\mathbf{H} &= \frac{1}{\mu}\nabla \times \mathbf{A} - j\omega\mathbf{F} - \nabla \cdot \Phi_m
\end{aligned}
\tag{A.1.5}
$$

Dividing the equation of (A.1.4) into its various XYZ components, which are contained exist in (A.1.2) and (A.1.3), yields:

$$
\begin{aligned}
E_x &= \frac{1}{\epsilon_0}\frac{\delta F_y}{\delta z} - j\omega A_x - \frac{\delta \Phi}{\delta x} & H_x &= -\frac{1}{\mu_0}\frac{\delta A_y}{\delta z} - j\omega F_x - \frac{\delta \Phi_m}{\delta x} \\
E_y &= -\frac{1}{\epsilon_0}\frac{\delta F_y}{\delta z} - j\omega A_y - \frac{\delta \Phi}{\delta y} & H_y &= \frac{1}{\mu_0}\frac{\delta A_x}{\delta z} - j\omega F_y - \frac{\delta \Phi_m}{\delta y} \\
E_z &= -\frac{1}{\epsilon_0}\frac{\delta F_y}{\delta x} + \frac{1}{\epsilon_0}\frac{\delta F_y}{\delta y} - \frac{\delta \Phi}{\delta z} & H_z &= \frac{1}{\mu_0}\frac{\delta A_y}{\delta x} - \frac{1}{\mu_0}\frac{\delta A_x}{\delta y} - \frac{\delta \Phi_m}{\delta y}
\end{aligned}
\tag{A.1.6}
$$

Since equation (A.1.6) is derived through Love's Equivalence Principle, where the resulting field from the equivalent sources in the plane $z < 0$ is zero, the sources can be further transformed. That is, in the presence of a perfect conductor the electric conductor equivalence can be applied, in this equivalence the equivalent sources over the area of the conductor are reduced to zero as well as those over the area of the holes. A perfect conducting plane is placed at the boundary, thus making the magnetic source of the holes the only source radiating. The conducting plane creates a mirror function of the radiating magnetic source, thus the conducting screen can be replaced by another magnetic source that adds to the existing magnetic source, rendering it the only source for calculating the field. This property reduces the set of equations to the following:

$$
\begin{aligned}
E_x &= \frac{2}{\epsilon_0}\frac{\delta F_y}{\delta z} & H_x &= -2j\omega F_x - 2\frac{\delta \Phi_m}{\delta x} \\
E_y &= -\frac{2}{\epsilon_0}\frac{\delta F_y}{\delta z} & H_y &= -2j\omega F_y - 2\frac{\delta \Phi_m}{\delta y} \\
E_z &= -\frac{2}{\epsilon_0}\frac{\delta F_y}{\delta x} + \frac{2}{\epsilon_0}\frac{\delta F_y}{\delta y} & H_z &= -2\frac{\delta \Phi_m}{\delta y}
\end{aligned}
\tag{A.1.7}
$$

Equation (A.1.7) will be used to evaluate the screen if the area denoting the holes is smaller than the area denoting the screen. This is similar to the properties of diffraction found in optics where the scattered field is even in the $z-$axis and is expressed:

$$
\begin{gathered}
E_x^s(x,y,z<0) = E_x^s(x,y,z>0) \quad E_y^s(x,y,z<0) = E_y^s(x,y,z>0) \\
H_z^s(x,y,z<0) = H_z^s(x,y,z>0)
\end{gathered}
\tag{A.1.8}
$$

Using the above property of equation (A.1.8) and the observation of the total field that is $E = E^i + E^s$ and $H = H^i + H^s$ it is possible to find an equivalent magnetic source for

expressing the scattered fields in the plane $z < 0$. The equivalent source for the fields in $z < 0$ is:

$$\mathbf{M}_s = \mathbf{n} \times \mathbf{E^s}(x,y,z)$$
$$\rho_m = -\mu \mathbf{n} \cdot \mathbf{H^s}(x,y,z)$$

$$(A.1.9)$$

giving rise to a new set of vector and scalar potential functions but in the $z < 0$ plane, which can be manipulated into:

$$
\begin{aligned}
\mathbf{F}^!_m(x,y,z) &= \frac{\varepsilon}{4\pi} \iint\limits_{\mathfrak{T}_1+\mathfrak{T}_2} \mathbf{n} \times \mathbf{E}(x,y,z<0)\frac{e^{-jkR}}{R}dv \\
&= -\frac{\varepsilon}{4\pi} \iint\limits_{\mathfrak{T}_2} \mathbf{n} \times \mathbf{E}(x,y,z>0)\frac{e^{-jkR}}{R}dv \\
&\quad +\frac{\varepsilon}{4\pi} \iint\limits_{\mathfrak{T}_1+\mathfrak{T}_2} \mathbf{n} \times \mathbf{E^s}(x,y,z<0)\frac{e^{-jkR}}{R}dv \\
&= -\mathbf{F}(x,y,z) - \mathbf{F}^r(x,y,z)
\end{aligned}
$$

$$(A.1.10)$$

$$
\begin{aligned}
\Phi^!_m(x,y,z) &= \frac{1}{4\pi} \iint\limits_{\mathfrak{T}_1+\mathfrak{T}_2} \mathbf{n} \cdot \mathbf{H}(x,y,z<0)\frac{e^{-jkR}}{R}dv \\
&= -\frac{1}{4\pi} \iint\limits_{\mathfrak{T}_2} \mathbf{n} \times \mathbf{E}(x,y,z>0)\frac{e^{-jkR}}{R}dv \\
&\quad +\frac{1}{4\pi} \iint\limits_{\mathfrak{T}_1+\mathfrak{T}_2} \mathbf{n} \times \mathbf{E^s}(x,y,z<0)\frac{e^{-jkR}}{R}dv \\
&= -\mathbf{F}(x,y,z) - \mathbf{F}^r(x,y,z)
\end{aligned}
$$

$$(A.1.11)$$

Now the potential function F^r and Φ^r, are the functions that apply to the back scattering fields in the plane $z < 0$ in the case of a solid ground plane in which the fields must satisfy the boundary conditions, and the fields would be:

$$E^r_x(x,y,0) = -E^i_x(x,y,0) \quad E^r_y(x,y,0) = -E^i_y(x,y,0)$$
$$H^r_z(x,y,0) = -H^i_z(x,y,0)$$

$$(A.1.12)$$

Using the potential functions of (A.1.10) and (A.1.11) to calculate the scattered fields and adding them to the incident fields found in the plane where $z < 0$, yields the following fields:

$$E_x = E_x^0 - \frac{2}{\epsilon_0}\frac{\delta F_y}{\delta z} \qquad\qquad H_x = H_x^0 + 2j\omega F_x + 2\frac{\delta \Phi_m}{\delta x}$$

$$E_y = E_y^0 + \frac{2}{\epsilon_0}\frac{\delta F_y}{\delta z} \qquad\qquad H_y = H_y^0 + 2j\omega F_y + 2\frac{\delta \Phi_m}{\delta y} \qquad\qquad \text{(A.1.13)}$$

$$E_z = E_z^0 + \frac{2}{\epsilon_0}\frac{\delta F_y}{\delta x} - \frac{2}{\epsilon_0}\frac{\delta F_y}{\delta y} \qquad H_z = H_z^0 + 2\frac{\delta \Phi_m}{\delta z}$$

where $H^0 = H^i + H^r$ and $E^0 = E^i + E^r$ is the total field found in $z < 0$ when the ground plane has no holes in it. Now there are two sets of equations of potential functions for finding fields, one set of equations for the plane where $z < 0$ when the screen contains no holes and another set of equations for the plane where $z > 0$. Since E_z, H_x and H_y are continuous across the holes in the ground plane, therefore equations (A.1.7) and (A.1.13) should yield the same answer, and therefore these equations can be combined into:

$$\frac{2}{\epsilon_0}\frac{\delta F_y}{\delta x} - \frac{2}{\epsilon_0}\frac{\delta F_y}{\delta y} = E_z^0 + \frac{2}{\epsilon_0}\frac{\delta F_y}{\delta x} - \frac{2}{\epsilon_0}\frac{\delta F_y}{\delta y}$$

$$-2j\omega F_x - 2\frac{\delta \Phi_m}{\delta x} = H_x^0 + 2j\omega F_x + 2\frac{\delta \Phi_m}{\delta x} \qquad\qquad \text{(A.1.14)}$$

$$-2j\omega F_y - 2\frac{\delta \Phi_m}{\delta y} = H_y^0 + 2j\omega F_y + 2\frac{\delta \Phi_m}{\delta y}$$

From the properties of equation (A.1.12) it is known that:

$$E_z^i(x,y,0) = E_z^r(x,y,0), \quad H_x^i(x,y,0) = H_x^r(x,y,0), \quad H_y^i(x,y,0) = H_y^r(x,y,0)$$

thus equation (A.1.14) becomes:

$$\frac{2}{\epsilon_0}\frac{\delta F_y}{\delta x} - \frac{2}{\epsilon_0}\frac{\delta F_y}{\delta y} = E_z^i$$

$$-2j\omega F_x - 2\frac{\delta \Phi_m}{\delta x} = H_x^i \qquad\qquad \text{(A.1.15)}$$

$$-2j\omega F_y - 2\frac{\delta \Phi_m}{\delta y} = H_y^i$$

and thus the field in the aperture field can be linked to the incident field in the follow-

ing integral equations of the aperture;

$$\iint\limits_{\mathfrak{I}_2} \left[E_x(x,y) \frac{\delta}{\delta x} \left(\frac{e^{-jkr_0}}{r_0} \right) + E_y(x,y) \frac{\delta}{\delta y} \left(\frac{e^{-jkr_0}}{r_0} \right) \right] dxdy \;=\; 2\pi E_z^i(x,y)$$

$$\iint\limits_{\mathfrak{I}_2} \left[j\omega\epsilon_0 E_y(x,y) \left(\frac{e^{-jkr_0}}{r_0} \right) + H_z(x,y) \frac{\delta}{\delta x} \left(\frac{e^{-jkr_0}}{r_0} \right) \right] dxdy \;=\; -2\pi H_x^i(x,y)$$

(A.1.16)

$$\iint\limits_{\mathfrak{I}_2} \left[j\omega\epsilon_0 E_x(x,y) \left(\frac{e^{-jkr_0}}{r_0} \right) - H_z(x,y) \frac{\delta}{\delta y} \left(\frac{e^{-jkr_0}}{r_0} \right) \right] dxdy \;=\; 2\pi H_y^i(x,y)$$

where r_0 refers to a point contained in the plane where $z = 0$, thus $r_0 = \sqrt{(x_o - x)^2 + (y_0 - y)^2}$.

This concludes the analysis of the ground plane with holes in it, where the holes are small and integration over them makes for the fastest solution. When the holes become the larger part of the screen, it is faster to integrate over the conducting screen. The same thought process is applied as with the holes, but instead of using potential functions $\mathbf{F}$ and Φ_m, potential functions $\mathbf{A}$ and Φ are used instead. Thus equation (A.1.7) becomes:

$$E_x \;=\; -2j\omega A_x - 2\frac{\delta\Phi}{\delta x} \qquad H_x \;=\; -\frac{2}{\mu_0}\frac{\delta A_y}{\delta z}$$

$$E_y \;=\; -2j\omega A_y - 2\frac{\delta\Phi}{\delta y} \qquad H_y \;=\; \frac{2}{\mu_0}\frac{\delta A_y}{\delta z}$$

(A.1.17)

$$E_z \;=\; -2\frac{\delta\Phi}{\delta y} \qquad\qquad H_z \;=\; \frac{2}{\mu_0}\frac{\delta A_y}{\delta x} - \frac{2}{\mu_0}\frac{\delta A_y}{\delta y}$$

for the field in the plane $z > 0$ while the field in the plane $z < 0$ can be calculated similar to that of equation (A.1.13) and is expressed as:

$$E_x \;=\; E_x^0 - 2j\omega A_x - 2\frac{\delta\Phi}{\delta x} \qquad H_x \;=\; H_x^0 - \frac{2}{\mu_0}\frac{\delta A_y}{\delta z}$$

$$E_y \;=\; E_y^0 - 2j\omega A_y - 2\frac{\delta\Phi}{\delta y} \qquad H_y \;=\; H_y^0 + \frac{2}{\mu_0}\frac{\delta A_y}{\delta z}$$

(A.1.18)

$$E_z \;=\; E_z^0 - 2\frac{\delta\Phi}{\delta z} \qquad\qquad H_z \;=\; H_z^0 + \frac{2}{\mu_0}\frac{\delta A_y}{\delta x} - \frac{2}{\epsilon_0}\frac{\delta A_y}{\delta y}$$

with the equivalent sources for the problem being:

$$\mathbf{J}_s = -\mathbf{n} \times \mathbf{H^s}(x, y, z)$$
$$\rho_m = -\epsilon \mathbf{n} \cdot \mathbf{E^s}(x, y, z)$$

(A.1.19)

However a slight difference occurs as H_y is now uneven within z plane, on the conducting ground plane. Therefore calculating $\mathbf{F}^!$ and $\Phi^!$ yields that $\mathbf{F}^! = \mathbf{F}$ and $\Phi^! = \Phi$, making equation (A.1.18) valid in both the $z > 0$ and $z < 0$ planes. Since integration is over the conducting sheet the transverse electric fields and normal magnetic fields cannot exist here, so E_x, E_y and H_z fall away and the integration equations for the aperture field become:

$$\iint_{\mathfrak{T}_2} \left[j\omega\mu_0 H_y^s(x, y) \left(\frac{e^{-jkr_0}}{r_0} \right) + E_z^s(x, y) \frac{\delta}{\delta x} \left(\frac{e^{-jkr_0}}{r_0} \right) \right] dxdy = -2\pi E_x^i(x, y)$$

$$\iint_{\mathfrak{T}_2} \left[j\omega\mu_0 H_x^s(x, y) \left(\frac{e^{-jkr_0}}{r_0} \right) + E_z^s(x, y) \frac{\delta}{\delta y} \left(\frac{e^{-jkr_0}}{r_0} \right) \right] dxdy = 2\pi E_y^i(x, y)$$

(A.1.20)

$$\iint_{\mathfrak{T}_2} \left[H_x^s(x, y) \frac{\delta}{\delta x} \left(\frac{e^{-jkr_0}}{r_0} \right) - H_y^s(x, y) \frac{\delta}{\delta y} \left(\frac{e^{-jkr_0}}{r_0} \right) \right] dxdy = -2\pi H_z^i(x, y)$$
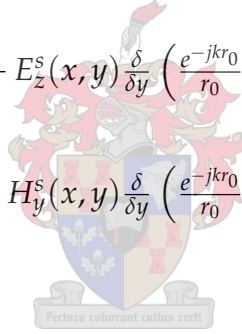
Now to put the equations further in perspective when the two ground planes are complementary, the fields of the plane where the holes are the dominant area will be denoted by E_2 and H_2, and for the screen where the conducting plane is dominant, the fields will be denoted by E_1 and H_1. Since there is an ohmic relationship between electric and magnetic fields in free space, known as the intrinsic free space impedance (η), a normalised weight function is brought in to keep the units intact between the electric field and magnetic fields:

$$\mathbf{E}_1 = \kappa \mathbf{H}_2 \quad \mathbf{H}_1 = \frac{-\kappa}{\eta^2} \mathbf{E}_2$$

(A.1.21)

where κ is the weight function of 1Ω. When equation (A.1.21) is substituted into equation (A.1.16) it gives rise to the following equations:

$$\iint_{\mathfrak{T}_2} \left[H_x(x,y) \tfrac{\delta}{\delta x} \left(\tfrac{e^{-jkr_0}}{r_0} \right) H_y(x,y) \tfrac{\delta}{\delta y} \left(\tfrac{e^{-jkr_0}}{r_0} \right) \right] dxdy = 2\pi H_z^i(x,y)$$

$$\iint_{\mathfrak{T}_2} \left[j\omega\epsilon_0\eta^2 H_y(x,y) \left(\tfrac{e^{-jkr_0}}{r_0} \right) - E_z(x,y) \tfrac{\delta}{\delta x} \left(\tfrac{e^{-jkr_0}}{r_0} \right) \right] dxdy = 2\pi E_x^i(x,y)$$

$$\iint_{\mathfrak{T}_2} \left[j\omega\epsilon_0\eta^2 H_x(x,y) \left(\tfrac{e^{-jkr_0}}{r_0} \right) + E_z(x,y) \tfrac{\delta}{\delta y} \left(\tfrac{e^{-jkr_0}}{r_0} \right) \right] dxdy = -2\pi E_y^i(x,y)$$

$$\text{(A.1.22)}$$

Comparing equation (A.1.20) and (A.1.22) yields the following results:

$$E_x(x,y) = -\kappa H_x^s \quad E_y(x,y) = -\kappa H_y^s \quad E_z(x,y) = \tfrac{\kappa}{\eta^2} H_z^s \tag{A.1.23}$$

The result from (A.1.23) requires adjustment to the potential functions and it gives the following relationship:

$$\begin{aligned} \mathbf{F}(x,y,x) &= \tfrac{\kappa}{\eta} \mathbf{A}(x,y,x) \\ \Phi_m(x,y,x) &= \tfrac{\kappa}{\eta} \Phi \end{aligned} \tag{A.1.24}$$

Thus it is shown that the fields in the plane $z > 0$ are given as:

$$E_1 + \kappa H = E_1^i \quad H_1 - \tfrac{\kappa}{\eta^2} H = H_1^i \tag{A.1.25}$$

This concludes that the incident field on a ground plane can be found by evaluating the fields of the ground plane and the fields of the complementary holes in the ground plane and adding them together.

A.2 Impedance relationship between complementary screens

This is a relationship found by H. G. Booker, [4] and is referred to in various texts, where analysis on a slot is mentioned. The impedance relationship was found between a slot and a dipole using the relationship of fields as derived from the Babinet principle to calculate the voltages and currents on the structures. To illustrate this E_1 and H_1 will be the fields of a dipole and E_2 together with H_2 will denote the fields of the slot. So the following set of equations can thus be used to find the current and voltages:

$$\oint_C \mathbf{H_1}dl = 2 \oint_c \mathbf{H_1}dl = I_1 \quad \oint_S \mathbf{E_1} = V_1$$
$$\oint_C \mathbf{H_2}dl = 2 \oint_c \mathbf{H_2}dl = -I_2 \quad \oint_S \mathbf{E_2} = V_2 \tag{A.2.1}$$

Using the Babinet principle where $\mathbf{E_1} = -\kappa\mathbf{H_2}$ and $\mathbf{H_1} = \frac{\kappa}{\eta}\mathbf{H_2}$ and substituting it into equations (A.2.1) yields the following relationship between the voltages and currents.

$$V_1 = \frac{\eta^2}{\kappa} \oint_C \mathbf{H_2}dl = \frac{\kappa}{2}I_2$$
$$V_2 = \frac{\eta^2}{\kappa} \oint_C \mathbf{H_1}dl = \frac{\eta^2}{2\kappa}I_1 \tag{A.2.2}$$

From this relationship where V_1 and I_1 are the voltages and currents of the dipole and V_2 and I_2 for the slot, it is established that the voltage-current relationship can be derived as:

$$\frac{V_1}{I_1} = \frac{\eta^2 I_2}{4V_2} \tag{A.2.3}$$

Equation A.2.3 can be rewritten to indicate the impedance relationship between a dipole and slot, where the slot impedance will be given as $Z_s = \frac{V_2}{I_2}$ and the dipole impedance is $Z_d = \frac{V_1}{I_1}$, yielding the following equation:

$$Z_s = \frac{\eta^2}{4Z_d}$$
$$Z_s Z_d = \frac{\eta^2}{4}$$
$$= \frac{Z_0^2}{4} \tag{A.2.4}$$

To summarise, the Babinet principle makes it possible to analyse a slot antenna by using an equivalent flat dipole, enabling one to calculate not only the fields of the slot but

also the impedances. Thus, if a slot cut in a ground plane and fed as an antenna, were to be analysed it would be possible to take a flat dipole of similar size and calculate the input impedances of the slot through the relationship and the known impedance of the dipole and that of the intrinsic impedance of free space Z_0. In the following section the above relationship of the impedances between slots and dipoles will be investigated to validate the Feko code for slot analysis using the Babinet Principal.
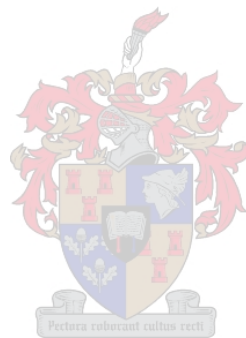
Appendix B

Computational Pitfalls and Limitations

B.1 Physical Limitations

B.1.1 Physical Size

Since Feko does not support computational code that computes a slot or any similar form of geometry that is cut into an infinite ground plane, a method was required to construct and evaluate such geometries with reasonable accuracy. This type of approach would result in a considerable amount of computational time, as a very large plane will have to be defined, which would be much larger than the slot, to achieve the effect of a ground plane of infinite size. The problem that this creates is the large number of triangles for which the currents need solving in Feko. The PM card was used to construct a single plate around the slot, which presented some initial problems which required bridging. One of the first problems that was encountered being the very fine meshing around the slot that was necessary to achieve convergence. This meshing is in the order of $\frac{\lambda}{200}$ and to reduce the number of triangles to under 10000, the ground plane size was made roughly λ in length as well as in width. However, this did not constitute proving the Babinet principle, as slight variations in the size of the ground plane in either the length or width changed the impedance values obtained from Feko. These changes were too significant to validate the computational accuracy of Feko for the analysis on slots.

However, in most texts it is claimed that in evaluation of the far-field effects, it is common to consider that any structure 3λ away from the problem which is being investigated is considered far enough not to have any effect on the problem and to be less sensitive to any changes being made to it. Running some preliminary calculations it was
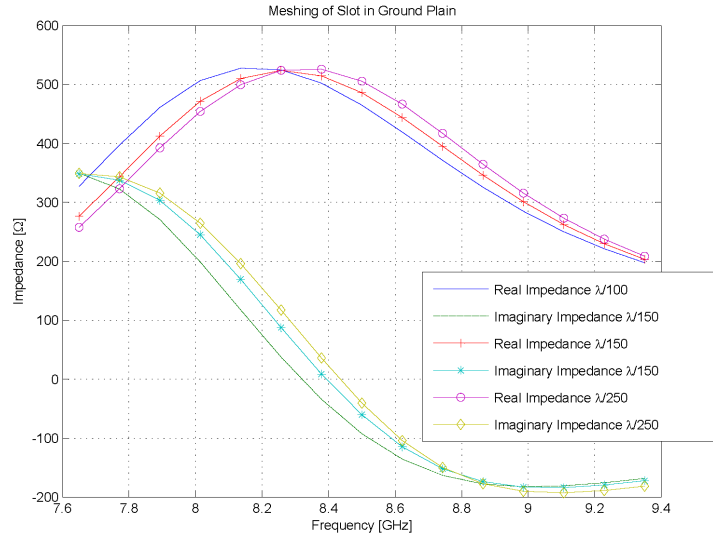
Figure B.1: Meshing problem

established that with a plate with a length of 3λ along the direction of the slot length and 5λ along the width of the slot sufficient results were obtained and the computational accuracy of Feko was validated. The optimal size of the ground plane around the slot was determined by evaluating the magnitude of the current as it flows over the plate as a function of time. The size was then determined by establishing where the currents are small enough along the edges not to influence the calculation too seriously. With these dimensions the Babinet principle was valid for the same slight changes for which it did not hold true on the smaller geometry. However, this was not the only limitation found. The other significant problem encountered was the meshing of such a large geometry, as the slot required a very fine meshing for accuracy, while if the whole plate were to be meshed as finely as the area around the slot, the problem would yield too many triangles to solve in a reasonable amount of time. Thus the plane was divided into two separate plates, an exterior and interior plate. The interior plate has a very fine meshing around the slot which becomes slightly coarser towards the outer regions away from the slot to where it meets the outer plate. While the inner edges of the exterior plate have a similar meshing as the outer edges of the interior plate, to satisfy the Feko segmentation rules for two different geometries touching, the meshing on the outer edges is $\frac{\lambda}{10}$. This yields large triangles on the outside edge compared to those close to the interior plate, and there are therefore still triangles where the transition starts that give warnings on the meshing of the transition area where the ratio of the length to base of the triangle is more than three. However, this does not influence the results significantly, as the current on these segments is quite small and would have little effect on the outcome. Through these steps the total number of triangles for which computation is required is reduced to 5648.

Figure B.1 clearly shows the differences that exist for 3 mesh sizes, being $\frac{\lambda}{100}$ for around the slot, $\frac{\lambda}{150}$ and $\frac{\lambda}{250}$. On a Smith Chart these values appear to be the same, and from figure B.1 either of the results will yield an effective result for the analysis of a slot. However, a mesh larger than $\frac{\lambda}{100}$ would yield data that cannot be considered accurate. The results in figure B.1 for a meshing of $\frac{\lambda}{100}$ already display a slight deviation in the accuracy of the results. The primary factor behind behind the fine meshing for the slot is that the width of the slot is extremely narrow. This fact dictates that a fine meshing is required at the edges of the slot, as the mesh should be roughly 3 times smaller than the width of the slot for accurate calculations, and therefore Feko has efficient accuracy when a good meshing is used.

B.1.2 Complex Geometry

Building a complex geometry for the specific problem of the design yielded some accuracy problems on the segments. This prevented the use of Feko for the original design. The first major problem that was presented by the geometry of a cylindrical cavity with crossed S-shaped slots, was that the architecture of the design required it to have an outer curvature or radius, with some freedom to change the geometry of the inner area. The only card that presented this type of possibilities in Feko was the NU card. The NU card is a geometry card in Feko that is used to define and mesh a NURBS surface from a set of defined points and their weight functions to achieve the correct ratios. Similarly the NU card can be used to define a flat surface with a curved edge. In order to use the NU card for a flat surface, it needs to be defined as a 1 by 2 function, in other words linear in one plane and quadratic in the other.

Using the NU card it is necessary to specify points with certain weights allocated to them, for a flat surface:

Q0	Q1	Q2
P0	P1	P2

P0, P1 and P3 will be points lying in a straight line and each would have a weight function of one. Q0 and Q2 are the points on the curve where the curve starts and ends and the weights of these functions are also one. Point Q1, however, does not have a weight function of one. Q1 is the point where two tangent lines running tangential to the curve and passing through the points Q0 and Q2, will intersect. To find the weight function that will define the radius of the curvature, an imaginary line is connected between points Q0 and Q2, and is joined with point M lying in the centre of the line. Now connect points M and Q1 with another imaginary line, which will intersect the

curve of a certain radius running through points Q0 and Q2 at an imaginary point S. The weight function is now defined as the ratio of the lengths of lines S-M and S-Q1. To find the co-ordinates of these points, Matlab was used to do the calculations and the results pulled into Feko, however countless mesh and segmentation violations were found where the KR card and the NU card segment points did not line up perfectly while trying to define the cavity for the problem.

Trying to solve the problem by dividing it into much smaller segments in an attempt to avoid the problem seemed not to have any effect and the best approach was to try and change the weight functions. This is a hit and run method and was totally discarded, as it was very time consuming to create a small segment for the model and in the end the model was discarded in the analysis.

The cavity analysis approach was then conformed to rectangular cavities and after CADFEKO was released it was possible to build a similar geometry that was analyzed.

B.1.3 Rectangular Cavity

The geometry that was constructed for the rectangular cavity consisted of a top plate, which contained the slots. The side walls and the bottom of the cavity were constructed using the BQ cards. In the calculations of the geometry, it was found that there is strong radiation into the plane behind the cavity with a similar amount of gain as that of the beam that is radiating in the forward direction. Now this should not be the case, as the rear of the cavity is considered to be a part of a ground plane, and should act like a ground plane and therefore radiation behind the cavity should be negligibly small, caused only by small stray currents on the ground plane. The problem with using the BQ card for the back plane of the cavity is that currents flow onto the back of the cavity and are not flowing away or being dissipated as they should. To solve this problem the rear cavity wall was removed and the BO card was introduced to act as a perfect conducting ground plane. This made the necessary difference, especially on the field patterns of the element, as it could clearly be seen that the element was radiating more to the side than to the front.

B.1.4 Symmetry

In reducing the calculation time in Feko, it is possible to use symmetry. Symmetry in Feko can be used as three different types, namely: electrical symmetry; magnetic symmetry and geometrical symmetry. Using electrical and magnetic symmetry, the calcu-

lation time of a problem is considerably reduced as it is no longer necessary to solve for all the currents on the model, since the properties of symmetry dictate that only half the currents need solving and the other half are then added through the plane of symmetry. For magnetic symmetry, the requirements are that the electrical fields should terminate normally onto the plane where the symmetrical plane is to be established. In the calculation Feko will implement an electrical wall to obtain magnetic symmetry and then calculate half the problem on one side of the wall and then mirror the solution around the wall to find the solution. With electrical symmetry the electrical wall is replaced by a magnetic wall, to satisfy the requirements of the magnetic fields terminating normally onto the plane, so that the electrical field can run tangentially to the plane of symmetry. However, it is sometimes impractical to use magnetic or electrical symmetry, for example with a crossed slot configuration there is no symmetry that can be called either electrical or magnetic, as the symmetry wall along the centre axis of one slot would have a totally different effect on the field of the crossing slot. At the centre of the slots the fields will not hold to the conformity that is dictated by the properties of single slot, as the two slots cross each other and the fields would act on each other, breaking any symmetry that might have existed. So the problem is that the symmetry that holds for the one slot clearly does not hold for the other slot. In these circumstances geometrical symmetry is used to construct the geometry without having to define the whole structure. This frees some computational time, however, in comparison with the calculations performed with electrical and magnetic symmetry, it is not a patch on the substrate and integral calculations that need to be done on the entire surface of the model, instead of calculating on half or a quarter of the area the model comprises. Because calculation time of the cross slotted cavity antenna is so long, due to the fine meshing that was used around the slot, a decision was made to reduce the meshing triangles, and to investigate the relative effect of the geometry. Using the relative results, it would be possible to find the coupling effect without serious inaccuracies in the results, since the one of the outcomes of the project is to try and find the coupling effect of the elements on each other.

B.2 Analytical Pitfalls

B.2.1 Array Computation

Building up the array for the calculation was intriguing enough, since this type of array is non uniform, although it has uniform spacing between the elements. However, there is no plane of symmetry, so a single element had to be copied and then shifted

to the correct location on the grid. This is achieved by using the TG card in Feko to produce the elements of the array and this amounts to a large number of triangles. All these triangles push up the calculation time considerably and the objective is to find a solution as fast as possible. The method thought to be most useful is the Multilevel Fast Multiple Method in Feko, using the FM card. The Multilevel Fast Multiple Method technique uses near field type calculations to solve the integral equations and works sufficiently well on large geometries to reduce memory and CPU-time requirements. However, on small geometries the calculation time seemed somewhat longer than normal calculation. There are restrictions involved with the FM card in that it runs a set number of intervals doing calculations, searching for a solution where convergence is found. If the convergence is not obtained, the problem is solved with the results from the interval equations that yielded the least number of errors. However, the results for this project using the FM card were far too inconsistent. The interval equations did not yield a solution and from the results it can be seen that the errors were still too large to yield a correct answer.

It was later established that there are certain rules on segmentation that are required for using the FM card. If these segmentation rules are violated no warning will be given as to those violations that occur in the area where the elements of the array are close to each other. Therefore the meshing in the area where the elements are close together should be evaluated on the grounds of the meshing of a slot, in other words the meshing should be a third of the distance between elements.

B.2.1.1 Beowulf Cluster

Another possibility that was considered to save time on calculation was to use a Beowulf computational Cluster, since it was established that two such clusters existed on the network. One of these clusters that was inquired into, consisted of 8 dual Intel Pentium $2.4GHz$ Celeron processors, with 1 GB of RAM, creating a cluster with 16 nodes. It was not entirely clear as to how the cluster would control the problem. The one technique to solve the problem that could be used was to share the cluster memory for the computation of the problem. The second technique uses all the processors to solve the problem. However, since 1 GB of RAM on a single processor, does not satisfy the RAM requirements, the problem was broken up into blocks. When the problem is broken up into blocks, the other technique for solving the problem over a cluster could be used, this being through parallel computation. Now when the problem is broken up into blocks the Feko out-of-core solving technique is used, which increases the calculation time by $15 - 20\%$ but when running parallel computation of Feko on

a cluster, the computation time of any in-core computation is dramatically reduced by the number of nodes, where a node is any processor that forms part of the cluster. A rough calculation for the time that is saved for in-core parallel calculation, equates to a reduction of 0.8 of the total simulation time, for a single processor, per node. This renders a result showing that a calculation will run $0.8N$ times faster, where N is the number of nodes in the cluster. Due to academic restrictions, parallel licensing could not be obtained for the cluster and due to the uncertainty of the memory requirements of the problem and how it would run over the cluster, it was decided to rather reduce the problem by scaling down on the array size and to consider a smaller array, within the limits of a personal computer.

B.2.2 Feeding Technique

Since a lot of calculation time goes into calculation of the feed currents, it was thought that each slot could be fed from a mutual feed for each element. This means that for the original solution all four feeds of the cross slots would be combined into a single feed. This single feed would then be connected with transmission lines, using the TL card in Feko to connect the feeds with 50Ω loads at the wire segments at the various feed locations. The transmission line length can be defined, which makes it possible to get the necessary phase shifts for the various feeds of the slots. When the calculations were performed on it, it was found that the TL card did not support the functionality that was desired and the calculations had to be continued by doing them with the four separate feeds for each element, as had originally been done.

Appendix C

Matlab Code
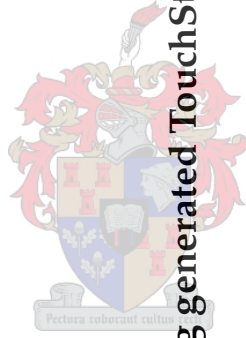
C.1 Loading S-Parameters from Feko using generated TouchStone Output Files

```
function [S,freq,ports]=ldstoneFeko(FileName);

% LDSTONEFEKO(...) is an adaption of original code LDSTONE(...), written by
% Cornell van Niekerk, and loads the measured  S-Parameter data from a text
% file with Touchstone format.  FileName is a text variable containing the
% full path and filename of  the file to be loaded.
%
% format: [S,freq,ports]=ldstone(FileName)
%
% The matrix S containts the loaded S-Parameters in complex format, in a
% three dimensional array where the third dimension would be frequency
% related.
%
% Author : Cornell van Niekerk
% Date   : 2001/01/17
% Adapted: D Voigt
% Date   : 2005/08/15
```

```matlab
% (c)  Cornell van Niekerk
%      Dept. Electrical and Electronic Engineering
%      University of Stellenbosch
%      Stellenbosch
%      South Africa

% Read the header of the Touchstone file by checking for comments
% and the unit identifier line.  If the unit ID line is read,
% scan the contents to determine the format in which the two port
% parameters are stored, as well as the unit of the measured
% frequencies.

nl = 1;
FUnit = 0;

% Establish the number of ports

if (FileName(length(FileName)) == 'p')
    ports = str2num(FileName(length(FileName)-1));
else
    ports = str2num(FileName(length(FileName)-1:length(FileName)));
end

fid = fopen(FileName);

while nl == 1,
    line = fgetl(fid);
    nl = 0;
    if strcmp(line(1),'!') == 1, nl = 1;,end;
    if strcmp(line(1),'#') == 1
        nl = 1;
        if findstr(line,'Hz')  > 0, FUnit = 1E0;, end;
        if findstr(line,'GHz') > 0, FUnit = 1E9;, end;
        if findstr(line,'GHZ') > 0, FUnit = 1E9;, end;
        if findstr(line,'MHz') > 0, FUnit = 1E6;, end;
        if findstr(line,'kHz') > 0, FUnit = 1E3;, end;
```

```
if findstr(line,'MA') > 0, DatFor=1;, end;
if findstr(line,'RI') > 0, DatFor=2;, end;

end;
end;

% Load the N port data and copy it into Matrix S

i=sqrt(-1);
c = 0;
x=0;

while 1;

[vector] = sscanf(line,'%f');
x=x+1;

if (mod(length(vector),ports) == 1 || ports == 1)

    c = c + 1;
    freq(c,1)=vector(1)*FUnit;

for m = 1:ports;
    if DatFor == 1;
        for k = 1:((length(vector)-1)/2);
            mod(x,ports);
            if(ports == 1)
                S(1,k,c)=vector(k*2)*exp(i*vector(k*2+1)/180*pi);
            elseif(ports == 2)
                if(mod(k,2) == 0)
                    if(k == 2)
                        S(k,1,c)=vector(k*2)*exp(i*vector(k*2+1)/180*pi);
                    else
                        S(k-2,2,c)=vector(k*2)*exp(i*vector(k*2+1)/180*pi);
                    end
                else
                    if(k == 1)
                        S(k,1,c)=vector(k*2)*exp(i*vector(k*2+1)/180*pi);
```

```matlab
                    else
                        S(k-2,2,c)=vector(k*2)*exp(i*vector(k*2+1)/180*pi);
                    end
                end
            else
                S(mod(x,ports),k,c)=vector(k*2)*exp(i*vector(k*2+1)/180*pi);
            end;
        end;
    if DatFor == 2;
        for m = 1:((length(vector)-1)/2);
            S(mod(x,ports),k,c)=vector(k*2)  + i*vector(k*2+1);
        end;
    end;
    end;
elseif ( mod(x,ports) ~= 0 )
    for m = 1:ports;
        if DatFor == 1;
            for k = 1:((length(vector))/2);
                S(mod(x,ports),k,c)=vector(k*2-1)*exp(i*vector(k*2)/180*pi);
            end;
        end;
    if DatFor == 2;
        for m = 1:((length(vector))/2);
            S(mod(x,ports),k,c)=vector(k*2-1)  + i*vector(k*2);
        end;
    end;
    end;
else
    for m = 1:ports;
        if DatFor == 1;
            for k = 1:((length(vector))/2);
                S(ports,k,c)=vector(k*2-1)*exp(i*vector(k*2)/180*pi);
            end;
        end;
    if DatFor == 2;
```
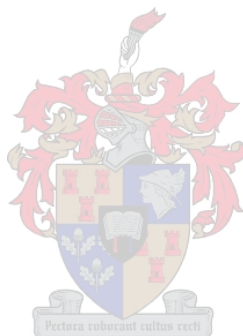
```
        for m = 1:((length(vector))/2);
            S(ports,k,c)=vector(k*2-1) + i*vector(k*2);
        end;
    end;
end
end
line = fgetl(fid);
if ~isstr(line), break, end
end;

% close the file

fclose(fid);
```

## C.2 Loading S-Parameters from MicroWave Office using generated TouchStone Output Files

```
function [S,freq,ports]=ldstoneMWO(FileName);

% LDSTONEMWO(...) loads the measured S-Parameter data from a text file with
% Touchstone format, generated in MicroWave Office.  FileName is a text
% ariable containing the full path and filename of  the file to be loaded,

% format: [S,freq]=ldstoneMWO(FileName)
% The matrix S containts the loaded S-Parameters in complex format, in a
% three dimensional array where the third dimension would be frequency
% related.

% Author : Cornell van Niekerk
% Date   : 2001/01/17
% Adapted: D Voigt
% Date   : 2005/08/28

% (c) Cornell van Niekerk
%       Dept. Electrical and Electronic Engineering
%       University of Stellenbosch
%       Stellenbosch
%       South Africa

% Set the default values of the optional parameters

% Read the header of the Touchstone file by checking for comments
% and the unit identifier line.  If the unit ID line is read,
% scan the contents to determine the format in which the two port
% parameters are stored, as well as the unit of the measured
% frequencies.

nl = 1;
FUnit = 0;

if (FileName(length(FileName)) == 'p')
    ports = str2num(FileName(length(FileName)-1));
else
```
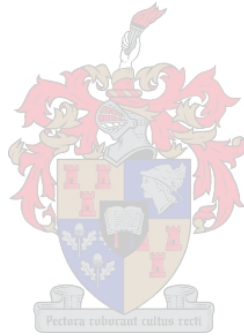
```
        ports = str2num(FileName(length(FileName)-1:length(FileName)));
end

fid = fopen(FileName);

while nl == 1,
    line = fgetl(fid);
    nl = 0;
    if strcmp(line(1),'!') == 1, nl = 1;,end;
    if strcmp(line(1),'#') == 1
        nl = 1;
        if findstr(line,'Hz')  > 0, FUnit = 1E0;,  end;
        if findstr(line,'GHz') > 0, FUnit = 1E9;,  end;
        if findstr(line,'GHZ') > 0, FUnit = 1E9;,  end;

        if findstr(line,'MHz') > 0, FUnit = 1E6;,  end;
        if findstr(line,'kHz') > 0, FUnit = 1E3;,  end;

        if findstr(line,'MA') > 0, DatFor=1;,  end;
        if findstr(line,'RI') > 0, DatFor=2;,  end;

    end;
end;

% Load the two-port data and copy it into Matrix S

i=sqrt(-1);
c = 0;
x = 0;
m = 1;
n = 0;
while 1;

    if (n == ports)
        n = 0;
        if (m == ports)
            m = 1;
        else
            m = m + 1;
```
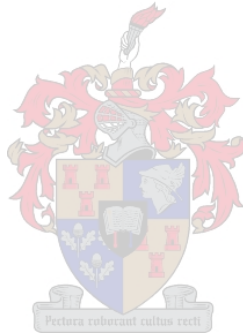
```matlab
        end
    end;
    [vector] = sscanf(line,'%f');
    x=x+1;
    if (length(vector) == 9 || ports == 1)
        c = c + 1;
        freq(c,1)=vector(1)*FUnit;
        for k = 1:(length(vector)-1)/2;
            n = n + 1;
            if DatFor == 1;
                S(m,n,c)=vector(k*2)*exp(i*vector(k*2+1)/180*pi);
            end;
            if DatFor == 2;
                S(m,n,c)=vector(k*2) + i*vector(k*2+1);
            end;
        end;
    else
        for k = 1:(length(vector))/2;
            n = n + 1;
            if DatFor == 1;
                S(m,n,c)=vector(k*2-1)*exp(i*vector(k*2)/180*pi);
            end;
            if DatFor == 2;
                S(m,n,c)=vector(k*2-1) + i*vector(k*2);
            end;
        end;
    end;
    line = fgetl(fid);
    if ~isstr(line), break, end
end;

% close the file

fclose(fid);
```
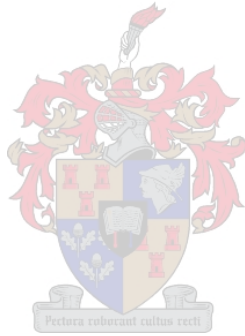
C.3 Generating TouchStone Output Files using S-Parameters to be Imported in MicroWave Office

```
function []=wrtstoneMWO(S,freq,datapath,filename);

% WRTSTONE takes as input a matrix and export it as a Touchtone file
%
% The file can be imported into a commercial circuit simulator.
% The function will check if the data matrix S has 1 or 4 coloms
% and depending on the result, a 1-port or a 2-port Touchstone
% file will be produced.

% Input Parameters:

%    S          Matrix containg S-Parameters
%    freq       Vector containing the frequency values (unit must be Hz)
%    datapath   Define the path to the directory in which the data is saved
%    filename   file to be generated (string)

% format: wrtstone(S,freq,datapath,filename);

% Check for unspecified parameters and provide the default values

% Original Code Supplied by Cornell van Niekerk
% Adapted: Dewald Voigt
% Date   : 2005/08/20

if (nargin < 6), dsp = 0; end;

% Open the specified file for writing.  Any existing file with
% this name will be over written.

fullfilename = fullfile(datapath,filename);
fid=fopen(fullfilename,'w');

% Create the Touschtone file header.

fprintf(fid,'! FILENAME ');fprintf(fid,filename);fprintf(fid,'\n');
fprintf(fid,'# Hz S RI R 50\n');
```
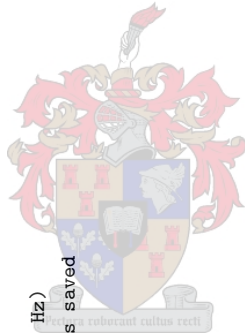
```
% Get the dimensions of the data matrix.  This will determine if a 1 port
% or two port file format should be produced

[a,b]=size(S);

b1 = b / length(freq);

if (b1 == 2),

    % Create the matrix of frequency and S-Parameter data that is to be written to
    % Touchstone text file.

    s11(:,1)=real(S(1,1,:));
    s11(:,2)=-imag(S(1,1,:));
    s21(:,1)=real(S(2,1,:));
    s21(:,2)=imag(S(2,1,:));
    s12(:,1)=real(S(1,2,:));
    s12(:,2)=imag(S(1,2,:));
    s22(:,1)=real(S(2,2,:));
    s22(:,2)=imag(S(2,2,:));

    f=freq;

    A=num2str([f s11(:,1) s11(:,2) s21(:,1) s21(:,2) s12(:,1) s12(:,2) s22(:,1) s22(:,2)],'% 11.4g\t');

end;

% Produce a 1-port Touchstone file

if (b == 1),

    % Create the matrix of frequency and S-Parameter data that is to be written to
    % Touchstone text file.

    s11(:,1)=real(S(:,1));
    s11(:,2)=-imag(S(:,1));

    f=freq;
```

```matlab
A=num2str([f s11(:,1) s11(:,2)],'% 11.4g\t');

end;

if (b1 > 2)
    if (b1 == 3)
        for k = 1:length(freq)
            for m = 1:b1
                for n = 1:b1
                    s(m+(k-1)*b1,(n-1)*2+1) = real(S(m,n,k));
                    s(m+(k-1)*b1,n*2) = imag(S(m,n,k));
                end
            end
        end
        [a,b] = size(s);
        fr = zeros(a,1)+1;
        for K = 1:length(freq)
            fr((K-1)*3+1,1) = freq(K);
        end
        A1=num2str([fr s],'% 11.4g\t')
    end

if (b1 > 3)
    [N,M] = size(S);
    for k = 1:length(freq)
        for m = 1:N
            for n = 1:N/4
                for o = 1:4
                    s((k-1)*N*ceil(N/4)+((m-1)*ceil(N/4)+n),(o-1)*2+1) = real(S(m,(n-1)*4+o,k));
                    s((k-1)*N*ceil(N/4)+((m-1)*ceil(N/4)+n),o*2) = imag(S(m,(n-1)*4+o,k));
                end
                if (mod(N,4) ~= 0)
                    for p = 1:mod(N,4)
                        s((k-1)*N*ceil(N/4)+((m-1)*ceil(N/4)+n+1),(p-1)*2+1) = real(S(m,(n-1)*4+o,k));
                        s((k-1)*N*ceil(N/4)+((m-1)*ceil(N/4)+n+1),p*2) = imag(S(m,(n-1)*4+o,k));
                    end
                    for q = 1:4-mod(N,4)
                        s((k-1)*N*ceil(N/4)+((m-1)*ceil(N/4)+n+1),(p+q-1)*2+1) = 1;
```
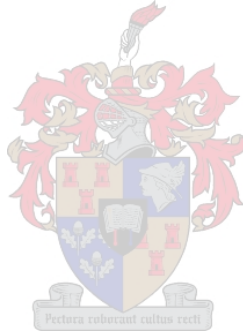
```matlab
                    s((k-1)*N*ceil(N/4)+((m-1)*ceil(N/4)+n+1),(p+q)*2) = 1;
                end
            end
        end
    end
end
[a,b] = size(s);
fr = zeros(a,1)+1;
for K = 1:length(freq)
    fr((K-1)*(N*ceil(N/4))+1,1) = freq(K);
end
A1=num2str([fr s],'% 11.4g\t');
[a,b] = size(A1);

for k = 1:a
    A(k,:) = regexprep(A1(k,:), ' 1\t', ' \t');
end

end
% Write the data to file.

col_number=size(A,2);
row_number=size(A,1);

for i=1:row_number
    line = [(A(i,:))];
    fprintf(fid,[line,'\n']);
end;

% Close the text file and exit the function

fclose(fid);
% Print the filename and data path on the screen for the user

disp(' ')
disp('S-Parameter Touchstone file created')
disp(' ')
```
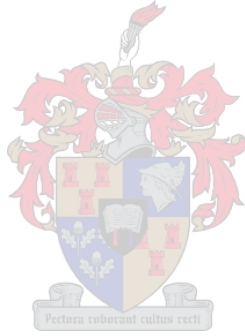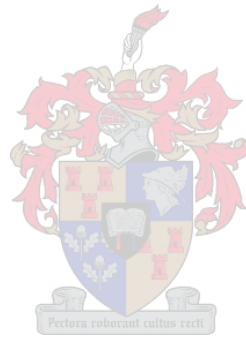
```
disp(['File: ',fullfilename])
disp(' ')
```

C.4 Converting TouchStone files from Feko format to MicroWave Office format

```
function []=Feko2MWOStone(FileName,datapath,filename);

% Feko2MWOSTONE takes as input a TouchStone format file from FEKO
% and transforms it to a TouchStone that can be imported in MWO
% Restrictions are found in the wrtstoneMWO

% Input Parameters:

%    FileName    Define the path and filename for Feko TouchStone File
%    datapath    Define the path to the directory in which the data is saved
%    filename    file to be generated (string)

% format: Feko2MWOStone(FileName,datapath,filename)

[S,freq,ports]=ldstoneFeko(FileName);

wrtstoneMWO(S,freq,datapath,filename);
```
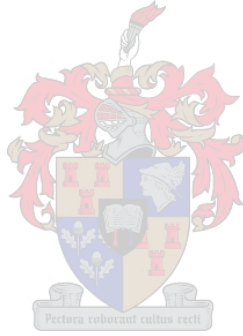
C.5 Computing the Impedance Coupling Matrix from S-Parameters

```
function [Zs] = Zmatrix(S,Z0,freq,ports);

% Zmatrix(...) computes the coupling impedance matrix for a given set of
% S-Parameter

% Input Parameters:

%     S           Matrix containing S-Parameters, S-Parameters needs to loaded
%                 in 3 dimensional array, where one dimension represents the
%                 frequency
%     freq        Vector containing the frequency values (unit must be Hz)
%     Z0          System Impedance
%     ports       Number of Ports

U = eye(ports,ports);

for k = 1:length(freq)
    Zs(:,:,k) = Z0 * inv(U - S(:,:,k))*(U + S(:,:,k));
end

for k = 1:length(freq)
    for p = 1:ports;
        Zs(p,p,k) = Zs(p,p,k)+50;
    end
end
```
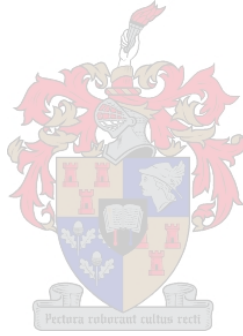
C.6   Computing the Active Input Impedance at the Ports

```
function [Z] = ActiveImpedance(Zmatrix,Z0,V,freq)

% ActiveImpedance(...) Calculates the Active impedances at the ports using
% the coupling impedance matrix and the voltage exitation at every port.

% Input Parameters:

%   Zmatrix           Impedance coupling matrix
%   Z0                System impedance
%   V = [V1, ...., VN] Port excitation

V = V.';

for k = 1:length(freq)
    Y(:,:,k) = inv(Zmatrix(:,:,k));
    I(:,;k) = Y(:,;,k)*V;
    Z(:,;k) = V./I(:,k) - Z0;
end
```
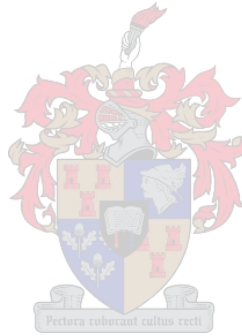
Appendix D

Specification of existing array

Issue 1.18

AERO SATCOM HIGH GAIN ANTENNA HGA-7000

Chelton's new high gain Satcom antenna (HGA) is the business jet operators' gateway to a true office-in-the-sky. Despite the antenna's extremely small size and lightweight, its advanced design and patented steering techniques provide superior performance with full hemispherical coverage.

The Chelton HGA-7000 is fully compatible with ARINC 741 compliant Aero-H/H+ and HSD Satcom systems. It's electronically steered phased-array design and fuselage mounting provides several advantages over conventional mechanically steered, tail-mount Satcom antennas.

- No radome requirement = substantially lower installed cost (and potential fuel savings).
- Can be installed on a much broader range of aircraft (additional fleet coverage and commonality).
- Rugged enough for rotorcraft installation.

The HGA-7000 derives the required positioning information from the aircraft's navigation system. It may also be configured for stand-alone operation with the installation of the optional Chelton Satcom Reference Unit (SRU). This allows the Satcom system to be fully functional without powering the aircraft's navigation system.

Despite its compact dimensions, the HGA-7000 is powerful enough to fully support even the most sophisticated multi-channel Satcom systems installed on Air Transport category aircraft.
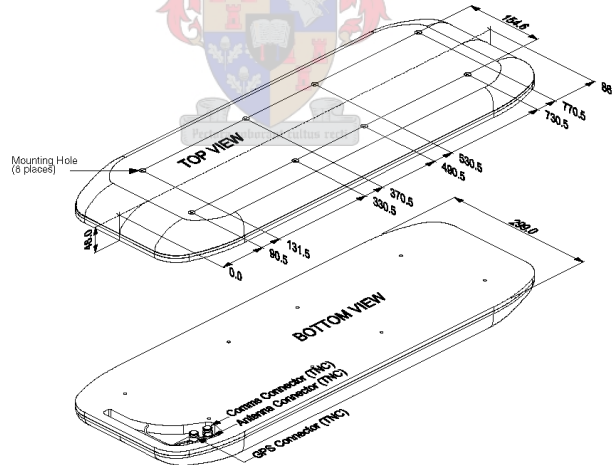

CHELTON

Issue 1.18

HGA-7000 Technical Specifications

TYPE: Electronically-steered, phased array.

SYSTEM COMPONENTS: Antenna, Diplexer LNA (DLNA), Beam Steering Unit (BSU), Connector kit, Optional SRU.

FREQUENCY: 1525 MHz to 1660.5 MHz

COVERAGE: Seamless coverage compliant to Inmarsat SDM.

GAIN: Between 12 and 16 dBiC over 90% of the Inmarsat hemisphere.
10 dBiC over 100% of Inmarsat hemisphere.

MULTIPATH REJECTION: Exceeds 10dB at 5 degrees and 12dB at 20 degrees elevation.

SIDELOBES: 13dB and better over coverage region.

POWER REQUIREMENTS: 28 VDC @ 1.6 amps.

INSTALLATION: Antenna top mounted on aircraft fuselage.
BSU can be mounted up to130 feet from antenna.
Maintenance port for full diagnostics with high level of BITE.

QUALIFICATION: RTCA DO-160D.
(in process) RTCA DO-178B.

DIMENSIONS:

	ANTENNA	BSU	DLNA
Length	33.90" (861 mm)	7.56" (192mm)	11.00" (280 mm)
Width	11.77" (299 mm)	6.38" (162 mm)	7.75" (197 mm)
Height	1.88" (48 mm)	1.95" (49.5 mm)	1.85" (47 mm)
Weight	18.7 lbs (8.5 kg)	3.1 lbs (1.4 kg)	6.5 lbs (2.95 kg)

CHELTON

List of References

[1] W.I. George, "Development of phased array antenna for inmarsat aeronautical applications," in *2005 SA IEEE AP/MMT Confewrence*, Stellenbosch, March 2005.

[2] C. A. Lindberg, "A shallow-cavity uhf crossed slot antenna," *IEEE Transactions on Antennas and Propagations*, vol. AP-17, no. 5, pp. 558–563, September 1969.

[3] F Manshadi, "End loaded crossed slot radiating elements," *IEEE Transactions on Antennas and Propagation*, vol. 39, no. 8, pp. 1237–1240, August 1991.

[4] H.G Booker, "Slot aerials and their relation to complementary wire aerials (babinet's principle)," *Journal IEE*, vol. 93, no. IIIA, pp. 620–626, 1946.

[5] Dennis Roddy, *Microwave Technology*, chapter 10, pp. 405–449, Prentice Hall Englewood Cliffs, 1986.

[6] H. E. King and J. L. Wong, "A shallow ridged-cavity crossed-slot antenna for the 240 to 400-mhz frequency range," *IEEE Transactions on Antennas and Propagation*, vol. Succinct Paper, pp. 687–689, September 1975.

[7] Constantine A Balanis, *Antenna Theory Analysis and Design*, John Wiley & Sons INC, second edition edition, 1997.

[8] Janis Galwjs, "Excitation of slots in a conducting screen above a lossy dielectric half space," *IRE Transactions on Antennas and Propagation*, vol. 10, pp. 436–443, July 1962.

[9] James R. Melcher Hermann A. Haus, *Electromagnetic Fields and Energy*, vol. Vol 1, Pentice Hall Inc, 1988.

[10] Edward A Wolff, *Antenna Analysis*, John Wiley & Sons Inc, 1966.

[11] Stuart A. Long, "A mathematical model for the impedance of the cavity backed slot antenna," *IEEE Transaction on Antennas and Propagation*, vol. AP-25, no. 6, pp. 829–833, November 1977.

[12] Gabrel M. Rebeiz Thomas M. Weller, Linda P. B. Katehi, "Single and double folded-slot antennas on semi infinite substrates," *IEEE Transactions on Antennas and Propagation*, vol. 43, no. 12, pp. 1423–1428, December 1995.

[13] V. V. Liepa Thomas B. A. Senior, "A planar creeping wave," *IEEE Transactions on Antennas and Propagation*, vol. 17, pp. 378 – 379, May 1969.

[14] Takahashi Masayuki Kiyomichi Arraki, Hideatsu Ueda, "Numerical analysis of circular disk microstrip antennas with parasitic elements," *IEEE Transactions on Antennas and Propagation*, vol. AP-34, no. 12, pp. 1390–1394, December 1986.

[15] John Manges James T Aberle, David Pozar, "Phased arrays of probe-fed stacked microstip patches," *IEEE Transactions on Atennas and Propagation*, vol. 42, no. 7, pp. 920–927, July 1994.

[16] Akihide Sakitani Shigeru Egashira, Eisuke Nishiyama, "Stacked microstrip antenna with wide band and high gain," *IEEE International Antenna and Propagation Symposium Digest*, vol. 28, pp. 1132 – 1135, May 1990.

[17] Akihide Sakitani Eisuke Nishiyama, Shigeru Egashira, "Stacked circular polarized microstrip antenna with wide band and high gain," *IEEE International Antenna and Propagation Symposium Digest*, vol. 30, pp. 1923 – 1926, July 1992.

[18] JT Aberle, "On the use of metallized cavities backing microstrip antennas," *IEEE International Antennas and Propagation Symposium*, vol. 29, pp. 60–63, June 1991.

[19] Amos E. Gera, "A simplified computational procedure for the analysis of planar arrays," *IEEE Transactions on Antenna and Propagation*, vol. AP-32, no. 6, pp. 647–651, June 1984.

[20] David M Pozar, *Microwave Engineering*, John Wiley & Sons, INC, second edition edition, 1998.

[21] Arlon T Adams John L Luzwick, Eugene C Ngai, "Analysis of a large linear antenna array of uniformly spaced thin wire dipoles parallel to a perfect conducting plane," *IEEE Transactions on Atenna Propagation*, vol. AP-30, no. 2, pp. 230–234, March 1982.

[22] David M Pozar, "Analysis of finite phased arrays of printed dipoles," *IEEE Transactions on Antenna and Propagation*, vol. AP-33, no. 10, pp. 1045–1053, October 1985.

[23] Leon Peters Jr. Charles E. Ryan Jr, "A creeping-wave analysis of the edge-on echo area of disks," *IEEE Transactions on Antennas and Propagation*, vol. 16, pp. 274 – 275, March 1968.

[24] Kai Chang Ming-yi Li, Kenneth A. Hummer, "Theoretical and experimental study of the input impedance of the cylinderical cavity-backed rectangular slot antennas," *IEEE Transaction on Antenna and Propagation*, vol. 39, no. 8, pp. 1158–1166, August 1991.

[25] Robert Stratman Elliott, *Antenna Theory and Design*, Prentice Hall Inc.Engeland Cliffs, 1981.